MICRONEEDLES FOR TRANSDERMAL DRUG DELIVERY IN HUMAN SUBJECTS

A Dissertation
Presented to
The Academic Faculty

by

Jyoti Gupta

In Partial Fulfillment
of the Requirements for the Degree
Doctor of Philosophy in the
School of Chemical & Biomolecular Engineering

Georgia Institute of Technology
August 2009

MICRONEEDLES FOR TRANSDERMAL DRUG DELIVERY IN HUMAN SUBJECTS

Approved by:

Dr. Mark R. Prausnitz, Advisor
School of Chemical & Biomolecular Engineering
Georgia Institute of Technology

Dr. Victor Breedveld
School Chemical & Biomolecular Engineering
Georgia Institute of Technology

Dr. Peter J. Ludovice
School Chemical & Biomolecular Engineering
Georgia Institute of Technology

Dr. Ajay K. Banga
Department of Pharmaceutical Sciences
Mercer University

Dr. Eric I. Felner
Department of Pediatric Endocrinology
Emory University

Date Approved: June 26, 2009

To my Parents,

for their love, support, and encouragement

ACKNOWLEDGEMENTS

My PhD journey has been a long and exciting experience and would definitely not have been possible without the support and inspiration of so many people. I would like to take this opportunity to thank all of them.

I would like to thank my thesis advisor, Dr. Mark Prausnitz, for giving me the opportunity to join his group and for his invaluable advice and support over the last five years. His passion for conducting meaningful research and his high scientific standards have been an excellent source of motivation. I would also like to thank him for always being readily accessible to answer my questions (even if it is after 6:30 PM!), for ensuring I always had access to the resources I need to conduct my research, for his patience and flexibility, and for allowing me to seek numerous growth opportunities.

I would also like to thank Dr. Eric Felner for collaborating with me over the last several years and for introducing me to the the challenges facing diabetes patients. I'd like to thank him for his dedication, mentorship, and patience while spending countless hours, even weekends, helping and supervising my insulin, lidocaine, and saline delivery experiments.

I would like to specially thank all my other thesis committee members, Dr. Ajay Banga, Dr. Victor Breedveld, and Dr. Peter Ludovice for their valuable intellectual support and guidance.

I thank Dr. Donald Denson for his help with the design and execution of my lidocaine delivery studies.

I would also like to take this opportunity to specially thank Donna Bondy for all her help and support over the last five years. Donna's excellent ability to keep track of all the IRB protocols, deadlines, and renewals has been invaluable to the success of my research and clearly, none of my studies could have been performed without her help. I'd also like to thank her for helping with my numerous strange purchase orders, especially just before a study.

I would also like to specially thank my current and past labmates for their help over the past several years: I would like to thank Dr. Harvinder Gill for teaching me how to cut and polish solid microneedles; Dr. Wijaya Martanto and Dr. Jason Jiang for helping me to learn glass needle fabrication; Dr. Vladimir Zarnitsyn for his valuable discussions; Samantha Andrews for assisting with my impedance studies and Samir Patel for helping solve my numerous computer/virus issues. I would also like to thank all other current and former lab members: Ying Liu, Yoo Chun Kim, James Norman, Leonard Chu, Chris Edens, Josh Hutcheson, Dr. Jeong Woo Lee, Dr. Seong-O Choi, Dr. Robyn Schlicher, Dr. Yeu Chun Kim, Dr. Prerona Chakravarty, Dr. Sean Sullivan, Dr. Daniel Hallow, Dr. Jung-Hwan Park, Dr. Ping Wang and Dr. Young Bin Choy for their helpful discussions, support, and friendship.

I would also like to thank my undergraduate and high school research students whose work has been invaluable to the success and speed of my research: Sara (Sohyun) Park for helping fabricate microneedles and assisting with my saline study, Brian Bondy for assisting with data extraction, and Erika Gemzer for helping fabricate microneedles.

I thank Richard Shafer for teaching me how to use the lasers. I would like to thank Brad Parker and Jeff Andrews for their help and patience in preparing my

numerous devices. I would also like to the administrative staff at the School of Chemical and Biomolecular Engineering and at the Institute of Bioengineering and Biosciences for helping me with departmental/building paperwork and room reservations. I would also like to thank the staff members at Emory Children's Center for assisting with the insulin study, especially Maureen McGrath, Jane McCurdy, and Megan Consendine.

I would also like to thank all the subjects who participated in my studies. Their willingness to volunteer has been invaluable to my research as this thesis would not be possible without their participation.

I thank all my friends who have supported me over the past several years. I would also like to thank my mentors, Dr. Bailey Lipscomb and Dr. Stanley Weinrich, who have offered valuable advice before and during my PhD studies and continue to do so. I would also like to thank all my teachers over the past 25 years, as it is their teachings and support that has bought me this far.

I would like to thank my sister for her support and encouragement throughout my life and for always setting a good example for me to follow.

Lastly, but most importantly, I would like to thank my parents for all the love, support, and encouragement they have given me in every thing I do.

TABLE OF CONTENTS

LIST OF TABLES

LIST OF FIGURES

LIST OF SYMBOLS AND ABBREVIATIONS

Ag = Silver

AgCl = Silver chloride

A_{MN} = Area of microneedle array

ANOVA = Analysis of variance

AUIC = Area under insulin curve

BSA = Bovine serum albumin

Cl = Drug clearance rate

C_{max} = Peak concentration on a concentration versus time curve

$\triangle C_{patch}$ = Change in drug concentration of drug patch

CMC = Carboxymethylcellulose

D = Diffusion coefficient

DNA = Deoxyribonucleic acid

EMLA = Eutectic mixture of local anesthetic

GAG = Glycosaminoglycans

GI = Gastrointestinal

HCl = Hydrochloric acid

IV = Intravenous

J = Flux

k_a = Absorption rate constant

k_{el} = Elimination rate constant

L = Length of microchannel created by microneedle in the stratum corneum

MEMS = Microelectromechanical systems

MN = Microneedle

NTX = Naltrexone

NTXOL = Naltrexol

p = Probability value

PD = Phramacodynamic

PG = Proteoglycan

PK = Pharmacokinetic

PLGA = Poly (lactic-co-glycolic acid)

PVP = Polyvinylpyrrolidone

ρ = Electrical resistivity

SC = Stratum Corneum

SD = Standard deviation

t_{max} = Time to peak concentration (C_{max})

TD = Transdermal

TEWL = Transepidermal water loss

U = Units of insulin

USP = United States pharmacopeia

VAS = Visual analog scale

V_{dist} = Volume of drug distribution

Z = Electrical impedance

SUMMARY

Over the past decade, microneedles of various geometries and materials have been developed as a minimally invasive alternative to painful hypodermic needles to deliver modern biotherapeutics such as proteins, peptides, DNA, and vaccines. Previously, several *in-vitro* and *in-vivo* animal studies have been conducted to show that microneedles increase skin permeability to a wide range of macromolecules and hydrophilic molecules which cannot cross the skin using conventional transdermal patches. However, only a limited number of studies have been performed to study microneedle-based drug delivery in human subjects. Since the ultimate clinical application of microneedles cannot be realized until it is studied in human subjects, this thesis performed some of the first-in-humans microneedle studies to understand the applications of microneedle treatment in human subjects.

This first aim of this thesis sought to characterize the skin repair responses to microneedle insertion by determining the microneedle and skin condition parameters that affect the duration of enhanced skin permeability using impedance spectroscopy. The study demonstrated for the first time that skin occlusion significantly slowed down skin barrier recovery following microneedle treatment; however, the skin barrier rapidly resealed in the absence of occlusion. This was because skin occlusion blocked the transdermal water gradient within the SC, which is the key signal necessary to facilitate skin barrier repair. The study also revealed that microneedle geometry played a significant role in the skin resealing process in the presence of occlusion such that skin treated with longer, increased number, and larger cross-sectional area needles recovered

more slowly under the effect of occlusion. Further, analysis of pain scores revealed that increasing the number of needles and needle cross-sectional area led to slower barrier recovery without significantly affecting pain. This study also led to the development and validation of a pharmacokinetic model to predict transdermal drug delivery *in-vivo* using skin impedance measurements as the input without any fitted parameters.

The second part of this thesis studied the effect of microneedle insertion and infusion parameters on the flow conductivity of skin. The study showed for the first time that microneedle-based delivery within the dermis typically led to a decrease in flow conductivity with increasing fluid volume *in-vivo*. This was due to fluid flow against the dense fibers within the dermis and also due to further compaction of this dense structure through compression at the needle tip. Microneedle retraction, lower infusion flowrates, and the addition of hyaluronidase helped reduce the skin's resistance to flow. Further, analysis of pain scores during infusion demonstrated that microneedles can be used to deliver up to 800 µl of fluid at moderate to high flow rates with significantly less pain than hypodermic needle insertion. Delivery of 1 mL of fluid can be attained with less pain than hypodermic needles at either low flow rates, shallow depths, or through the addition of hyaluronidase.

The third aim of this thesis studied the efficacy of microneedles for systemic drug delivery effects by delivering insulin to Type 1 diabetes subjects and comparing results to a subcutaneous catheter control. This study was carried out in three steps. The study first determined the optimum microneedle insertion depth for effective insulin delivery by inserting microneedles to different depths within the skin ranging from 1 mm to 5 mm. The 1 mm depth led to the fastest insulin absorption and was then used to determine if

intradermal microneedle-based insulin delivery can be used to reduce postprandial glucose levels by delivering a bolus of insulin prior to consumption of a standardized meal. Upon determining that insulin delivery at 1 mm was effective in reducing glucose levels, a more in-depth study involving additional subjects was performed at a depth of 900 μm. This phase of the study demonstrated that intradermal insulin delivery led to faster pharmacokinetics with higher peak insulin concentrations and faster times to reach these peaks while causing tighter glycaemic control. This was due to the rapid absorption of insulin as a result of the microneedles targeting the rich capillary network of the papillary dermis. The study also showed that microneedles caused less pain and irritation than catheters and were preferred by all study subjects.

The last aim of this thesis studied the efficacy of microneedles for delivery of local therapeutics by delivering lidocaine for local anesthesia. Lidocaine was delivered to the volar forearm skin and the back of the hand of healthy adult subjects to compare the pain and efficacy of microneedle injection with that of traditional hypodermic needle injection. The study results were the first to demonstrate that microneedle-based lidocaine delivery was less painful than and as effective as hypodermic needles in terms of anesthesia onset time, area and depth of analgesia, and lack of pain associated with an intravenous catheter insertion. Further, greater than 77% of the subjects preferred microneedle treatment over hypodermic needles and greater than 82% of the subjects considered microneedles to be not painful.

Overall, these results are among the first to demonstrate the clinical application of microneedles in human subjects. The research in this thesis is translational in nature and

provides key results necessary to facilitate the transfer of microneedles from the laboratory to clinical practice.

CHAPTER 1: INTRODUCTION

Drugs are conventionally delivered to the body either orally via pills or by means of injections using hypodermic needles. While these methods have historically been effective, they each have their own advantages and limitations. Oral delivery is painless, however, many modern therapeutics such as proteins, peptides, and DNA based compounds cannot be delivered orally as they lose their activity either by enzymatic degradation in the gastrointestinal tract (GI) or by first-pass effects of the liver or they are poorly absorbed across the intestinal epithelium leading to low bioavailability (Swarbrick and Boylan 2002). These modern drugs are therefore delivered by means of injections using hypodermic needles which can effectively deliver drugs without losing activity. However, hypodermic needles require administration expertise and are often painful and cause fear and anxiety among many people leading to poor patient compliance (Hamilton 1995; Nir, Paz et al. 2003; Deacon and Abramowitz 2006). Further, hypodermic needles are generally used to deliver a large bolus of drug to the body and do not allow for sustained drug delivery.

Transdermal drug delivery, which refers to the penetration of drugs across the skin, is an attractive alternative to deliver these modern biotherapeutics, as it is painless, can be self-administered, avoids degradation in the GI tract and first-pass effects of the liver, and can allow for sustained drug delivery over extended periods of time (Prausnitz and Langer 2008). Additionally, the large surface area of the skin makes it an appealing route for drug delivery (Prausnitz 2001). Transdermal patches have been developed to deliver drugs across the skin; however they can only be applied to a limited number of

drugs that are small enough and lipophilic enough to permeate through outermost barrier layer of the skin at therapeutic rates. Consequently, micron-dimension needles called microneedles, which are long enough to pass the skin's barrier, but short enough to avoid stimulating nerve endings have been developed to increase skin permeability to large and hydrophilic molecules while minimizing pain.

Over the past decade, microneedles of various materials, geometries, and delivery mechanisms have been developed (Prausnitz, Gill et al. 2008). Several studies have been conducted in *in-vitro* skin models and *in-vivo* in animals to show that microneedles enhance skin permeability to a large number of drugs. However, only a limited amount of research has been conducted in human subjects and several key questions regarding the safety, efficacy, and patient acceptance of microneedles in clinical applications still remain to be answered. An ideal microneedle drug delivery system would be one that: **i)** is safe by maintaining skin permeability only during the desired period of drug delivery, **ii)** can create sustained or bolus delivery profiles, **iii)** can deliver therapeutic volumes/doses of drug quickly with minimal discomfort, **iv)** has rapidly responsive pharmacokinetics and pharmacodynamics, **v)** causes minimal pain and irritation, and **vi)** is simple, inexpensive, and well-accepted by patients. This thesis seeks to answer some of the questions pertaining to the safety, efficacy, and usability of microneedles for clinical applications in human subjects.

Therefore, the **objective** of this thesis was to perform the first-in-humans microneedle studies to: **a)** characterize skin repair responses to solid microneedle insertion to determine the extent of increased skin permeability coupled with predictions of pharmacokinetics of drug delivered through premeabilized skin, **b)** determine the

effect of hollow microneedle-based infusion parameters on flow conductivity of skin and pain and thereby identify barriers to fluid flow into the skin from hollow microneedles, **c)** assess the safety and efficacy of systemic therapeutic effects through measurement of pharmacokinetic parameters, pain, irritation, and user preference for microneedle-based insulin delivery in type 1 diabetes subjects, and **d)** assess the safety and efficacy of local therapeutic effects though delivery of lidocaine to the skin.

CHAPTER 2: BACKGROUND

2.1. Skin Anatomy

Human skin is a complex, multilayered tissue that serves the function of preventing water loss from the body and protecting the body against microorganisms and other exogenous materials by acting as a permeability barrier to the environment (Schaefer and Redelmeier 1996). The skin is the largest functional organ in the body and its structure can be categorized into four main layers: the stratum corneum (SC), the viable epidermis (the stratum corneum and viable epidermis together make up the epidermis), the dermis, and the hypodermis (or subcutaneous fat layer) (Williams 2003).

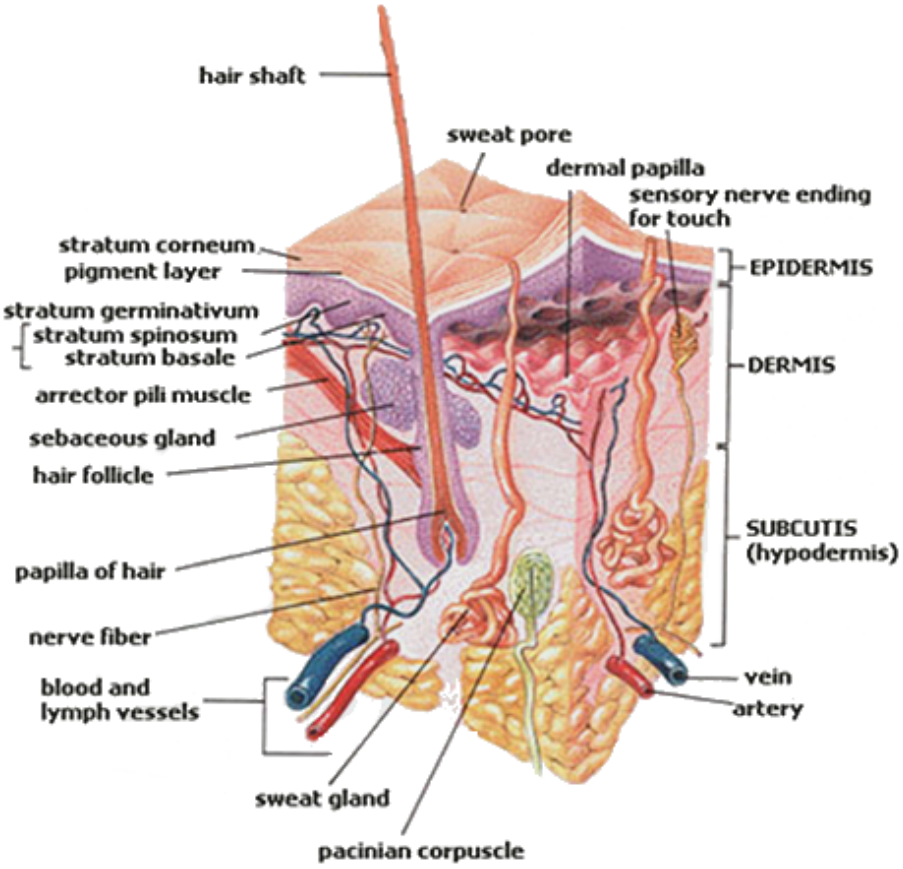

Figure 2.1: Structure of human skin (http://en.wikipedia.org/wiki/Skin).

The outermost superficial layer of the skin is called the stratum corneum (SC) and is between 10-20 μm thick. Although the SC is the thinnest layer of the skin, it is this outermost layer that forms the main skin barrier and is responsible for preventing molecules from entering and leaving the body through the skin. The stratum corneum is a thin two-compartment membrane consisting of dead, polyhedral, keratinized cells without any nuclei called corneocytes embedded in a lipid matrix. The corneocytes are approximately 40 μm in diameter and 0.5 μm thick (Schaefer and Redelmeier 1996). The intercellular lipid matrix consists of ceramides, free fatty acids, cholesterol, and cholesterol sulphate and is the only continuous medium in the stratum corneum. The most important feature of these lipids is that they are structured into ordered lipid bilayers (Guy and Hadgraft 2003). In fact, the SC is commonly described as a "brick and mortar" model in which 15-20 corneocyte layers are embedded in a mortar of more than 100 lipid bilayers (Williams 2003). The corneocytes disrupt the continuous intercellular lipid phase and create a tortuous diffusional pathway by increasing the intercellular path length by 50 to 100 fold (Schaefer and Redelmeier 1996). It is this unique ordered organization of the hydrophilic keratin cells within the hydrophobic, lipid environment that makes the stratum corneum an extremely efficient biological barrier to foreign molecules, including drugs delivered via transdermal delivery systems. The stratum corneum has an acidic pH which helps provide antimicrobial resistance and in addition to proteins (70% - alpha and beta keratin) and lipids (15%), it also contains water (15%) (Fluhr and Elias 2002).

Below the stratum corneum lies the viable epidermis which has a thickness ranging between 50 and 100 μm. The stratum corneum and the viable epidermis together form the epidermis. The epidermis consists of 70% water and keratinizing epithelial cells

responsible for synthesis of the SC. The epidermis does not contain any blood vessels and hence molecules permeating across the epidermis must cross the dermal-epidermal layer to enter the body's systemic circulation. Melanocytes, Langerhans cells, and Merkel cells are also present in this layer (Williams 2003).

Directly below the epidermis lies a thicker region called the dermis. The dermis is a non-homogeneous, anisotropic, viscoelastic layer (Grebenyuk 1994). This thick layer (1 - 2 mm) forms the bulk of the skin and consists of a vast network of fibrous, filamentous, and amorphous connective tissue. The dermis can be sub-divided into two layers: the superficial papillary dermis where collagen fibers are packed in thin bundles the deeper, thicker, and denser reticular dermis formed by an entangled mass of collagen bundles (Irion 2002). The papillary dermis is highly vascularized and consists of a rich bed of blood capillaries and lymphatic vessels which are found immediately below the epidermis (Monteiro-Riviere 1991; Pettis, Harvey et al. 2002). The reticular dermis is relatively less vascularized. The overall vasculature nature of the dermis offers a rich blood flow of approximately 0.05 mL/min/mg which is effective for the removal of molecules (including drugs) that have passed the outer layers of the skin, allowing for transport of drug molecules from the dermal-epidermal layer to the systemic circulation (Williams 2003). The lymphatic system also reaches the dermal-epidermal layers and can also help remove drug molecules that have passed the upper skin layers (Pettis, Harvey et al. 2002; Williams 2003). Figure 2.2 depicts the vasculature network within the skin.

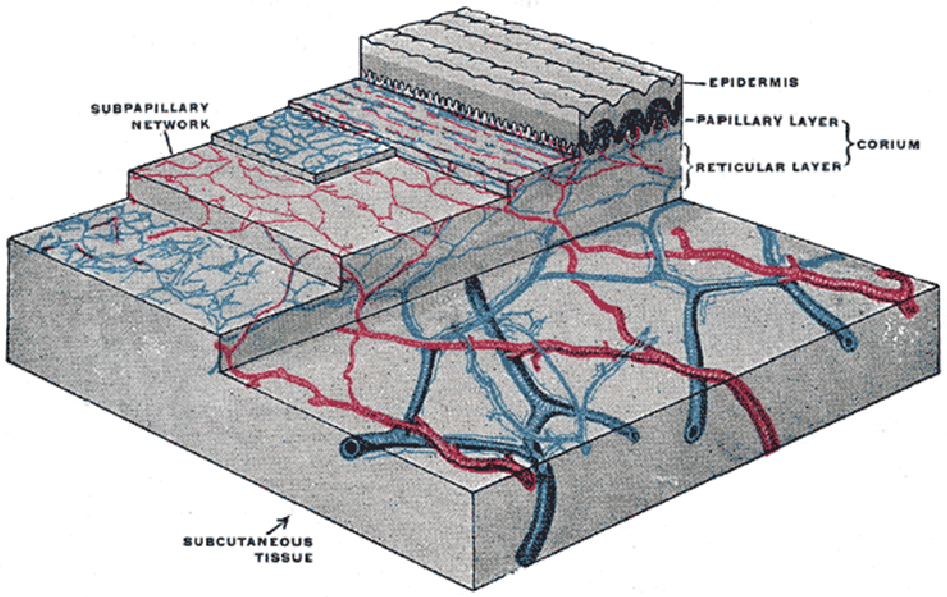

Figure 2.2: Vasculature network in the skin (modified from Gray's Anatomy of the Human Body, Fig 942: http://www.bartleby.com/107/234.html).

The connective tissue in the dermis is primarily made up collagenous fibers which form a scaffold running through the dermis. Elastic connective tissue is also present and provides elasticity for the shape of the skin and is also associated with hair follicles and vascular networks (Schaefer and Redelmeier 1996). Several proteins such as elastin and fibrillin are associated with these fibers. All these structures prevent tissue failure by withstanding deformation and dissipating energy. As mentioned previously, the skin is viscoelastic in nature. This is predominantly due to the dermis. The typical stress-strain curve for human skin represents a biphasic response that consists of linear low- and high-strain regions (Seehra and Silver 2006). In the low strain region, the skin behaves elastically and this behaviour is dominated by elastic fibers which act to recover small strains in the dense collagen network. In the high-strain region, as the tissue is strained, the collagen fibrils become aligned and absorb and store the strain energy. The high-

strain response includes a viscous component associated with energy dissipation of the applied load through viscous sliding of collagen fibrils in the extracellular matrix (Seehra and Silver 2006). The elastic component is due to the axial stretching of the collagen structure (a triple helix) and energy storage, which is important in ensuring shape recovery after skin deformation (Seehra and Silver 2006).

Proteoglycans (PG), which are large brush-shaped macromolecules that are constructed of carbohydrates that are often sulfated, known as glycosaminoglycans (GAGs) attached to a protein core are also present in the dermis. These structures bind up to 1000 times their weight in water and are responsible for the water-retaining capacity of the dermis. The collagen fibers and proteoglycans (including GAGs) in the dermis are responsible for the resistance of the dermis to fluid flow (Swartz and Fleury 2007). All these connective tissue structures in the dermis determine the tensile strength and elasticity of the skin and provide physical support for the extensive nerve and vascular networks in the skin. Fibroblasts, endothelial cells, mast cells, and sensory nerve endings are also present in this layer (Schaefer and Redelmeier 1996).

The hypodermis lies beneath the dermis and is made up of a network of adipocytes. The hypodermis typically has a thickness on the order of a few millimeters and plays an important role in energy storage and metabolism and also provides insulation and protection from injury. The hypodermis also contains an extensive circulatory network (Schaefer and Redelmeier 1996) as well as nerve fibers.

2.2. Skin Repair

As indicated above, the SC contains about 15% water, while the underlying epidermis contains 70% water leading to a water gradient across the stratum corneum

from 70% at the deepest SC layers to ambient humidity at the outer surface of the SC (Wertz and Michniak 2004). Although the SC is an excellent water barrier, it is not entirely impermeable and under normal conditions water from the deeper hydrated skin layers diffuses at a slow rate through the SC and evaporates at the surface. This outward diffusion of water through the skin is called transepidermal water loss (TEWL) (Levin and Maibach 2005). Any breach in the stratum corneum barrier leads to a significant increase in TEWL as the water now diffuses through the barrier perturbation instead of following the tortuous SC intracellular pathway (Figure 2.3). This increased TEWL flux is the main signal for recovery of the SC barrier structure and function (Grubauer, Elias et al. 1989).

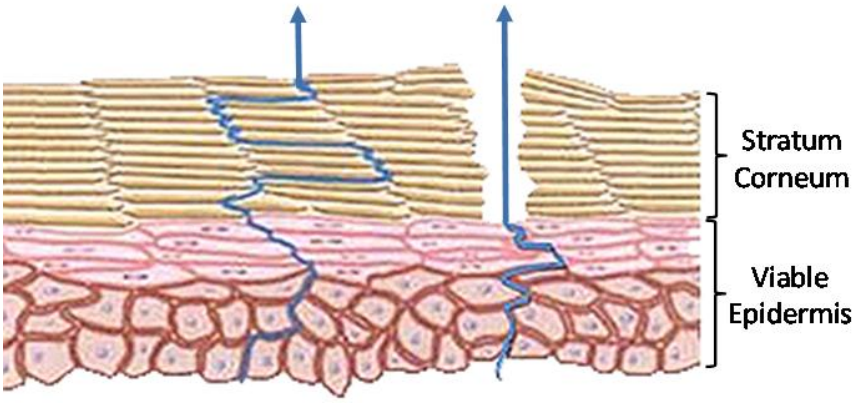

Figure 2.3: TEWL across intact skin is slow and requires diffusion across the tortuous intercellular pathway. A breach in the stratum corneum increases TEWL (modified from http://www.pg.com/science/skincare/Skin_tws_toc.htm).

Upon disruption of the stratum corneum barrier, the TEWL rises and triggers barrier recovery. The first step in the skin repair response is the rapid secretion of organelles called lamellar bodies which are rich in polar lipids and catabolic enzymes. These epidermal lamellar bodies serve as carriers of precursors of the stratum corneum lipids. The increased lamellar body secretion leads to an upregulation of skin lipid

enzymes leading to increased synthesis of the SC lipids (cholesterol, ceramides, and fatty acids) from the lamellar body polar lipids. The re-accumulated lipids are then organized into ordered lipid bilayers, thereby restoring the SC barrier function (Elias and Feingold 2006). The skin repair process continues with a burst in DNA synthesis which is also necessary for normalizing the skin barrier function (Proksch, Feingold et al. 1991). The degree of lipid and DNA synthesis depends on the degree of barrier perturbation (i.e: greater the damage, greater the synthesis).

2.2.1. Effect of Occlusion

Occlusion refers to covering of the skin by a membrane that is impermeable to air or moisture. As described above, disruption of the SC barrier leads to an increase in TEWL. However, if an occlusive membrane is placed on the damaged skin surface, then the membrane acts as an artificial barrier and the recovery of the SC is retarded as the TEWL signal for barrier recovery is blocked. This consequently hinders lamellar body secretion and lipid and DNA synthesis (Grubauer, Elias et al. 1989; Proksch, Feingold et al. 1991; Menon, Feingold et al. 1992). Further, the decrease in transepidermal water loss leads to an increase in SC hydration, thereby swelling the corneocytes, promoting uptake of water into the intercellular lipid domains and subsequently disrupting lipid order (Warner, Boissy et al. 1999). The swollen corneocytes expand until they interconnect forming a continuous pore pathway which can enhance skin permeability (Elias, Tsai et al. 2002).

2.3. Transdermal Drug Delivery Systems

Since the approval of the first transdermal drug delivery patch system 30 years ago, transdermal delivery has proven to be a successful and painless delivery route for

local and systemic drug effects. However, today, there are only a handful of such conventional transdermal patch systems available on the market. This is because transdermal patches require drug molecules to pass through the stratum corneum barrier by passively diffusing through the tortuous intercellular lipid pathway between the SC corneocytes before entering the body. This pathway, however, only allows drugs with low molecular mass (<500 Da), high lipophilicity (oil soluble), and small dosage requirements (daily dose ≤ 20 mg) to permeate through the SC barrier (Finnin and Morgan 1999; Prausnitz, Mitragotri et al. 2004). Therefore, there is a need for transdermal delivery systems that have the ability to increase skin permeability to macro and hydrophilic molecules. Consequently, several chemical and physical methods have been developed to increase skin permeability by reversibly disrupting or reorganizing the stratum corneum structure to allow for increased transport of large molecules across the skin in an effective and minimally invasive manner.

Chemical enhancers use surfactants, fatty acids, water, or solvents to increase skin permeability (Barry 2001; Williams and Barry 2004). These enhancers work by disrupting the bilayer structure of the SC by either increasing hydration of the intracellular keratin, inserting amphiphilic molecules into the layers to disrupt the ordered molecular packing or by extracting intracellular lipids to created nano-scale defects in the stratum corneum (Prausnitz and Langer 2008).

A physical method of enhancing the rate of transdermal drug delivery is iontophoresis. Iontophoresis uses an electric field to move charged or uncharged molecules across the skin by electrophoresis, electro-osmosis, or transiently increased skin permeability. This process has the ability to increase transdermal delivery rates for

large and hydrophilic molecules in a minimally invasive manner (Nair, Pillai et al. 1999; Pillai, Nair et al. 1999; Prausnitz, Mitragotri et al. 2004). Another physical method of increasing skin permeability is electroporation which applies short, high voltage pulses to create nanometer sized disruptions in the skin allowing hydrophilic and macromolecules to permeate the skin (Prausnitz, Edelman et al. 1995; Prausnitz 2001). Application of low frequency ultrasound by means of a process called sonophoresis has also been found to premeabilize skin to a large number of drugs due to cavitation and formation of acoustic micro-jets that impact the stratum corneum and disrupt the lipid bilayers (Mitragotri and Kost 2000; Prausnitz, Mitragotri et al. 2004). Thermal ablation, whereby micron-sized holes are generated in the skin by the application of electrical energy which is converted to thermal energy has also demonstrated increased skin permeability to a number of large molecules (Smith and Tomlinson 2008). Application of a high-frequency alternating current through densely spaced micro-electrodes placed on the skin surface also create permeable micro-channels in the skin by means of radiofrequency ablation (Banga 1998; Banga 2009). A mechanical method of increasing skin permeability includes micro-dermabrasion which uses a stream of fine aluminum-oxide crystals to disrupt and remove the stratum corneum (Barry 2001). Jet injectors are another mechanical system which puncture the skin without the use of needles by firing liquid or solid particles across the skin at a very high velocity (Arora, Prausnitz et al. 2008). This system allows large quantities of drugs to be administered rapidly without depending on diffusion across the SC.

While all of these methods overcome the limitation of conventional transdermal patches by breaching the skin's barrier to allow for increased permeability to

macromolecules, each of them has its own limitations which hinder its clinical application. Chemical enhancers, although painless to apply are known to cause skin irritation and skin toxicity (Prausnitz, Mitragotri et al. 2004) leading to safety concerns. Electrical transdermal delivery devices are minimally invasive, however, they all require a power source which makes the device cumbersome, bulky and expensive (Prausnitz, Gill et al. 2008). Further, most of these devices require special training to administer and poorly designed iontophoresis systems have been known to cause skin irritation and burns (Houck and Sethna 2005; Zempsky 2008). Further, while these systems reversibly disrupt the stratum corneum barrier and increase permeability, in some cases, the barrier typically takes on the order of several hours or days to recover, thereby creating risk for entry of unwanted foreign molecules into the body long after drug delivery has been completed (Farinha, Kellogg et al. 2006). Micro-dermabrasion also employs an expensive bulky device and needs to be performed carefully as excessive abrasion may damage the skin. Jet injectors can allow for bolus delivery of large drug doses, however the high drug velocity can cause pain and bruising and the device cannot be used for sustained drug delivery (Bremseth and Pass 2001).

Therefore, there remains a need for an ideal transdermal drug delivery system that **a)** is safe by maintaining skin permeability only during the desired period of drug delivery, **b)** can create sustained or bolus delivery profiles, **c)** can deliver therapeutic volumes/doses of drug quickly with minimal discomfort, **d)** has rapidly responsive pharmacokinetics and pharmacodynamics, **e)** causes minimal pain and irritation, and **f)** is simple, inexpensive, and self-administrable.

Consequently, micron dimension needles called microneedles have been developed to reversibly increase skin permeability by creating micron-sized channels in the skin allowing for increased transdermal drug transport of small and large drug molecules in a minimally invasive manner (Prausnitz 2004). These microneedles are long enough to breach the skin's barrier to allow for drug transport, yet are short enough to avoid stimulating the nerves, thereby reducing pain. Additionally, microneedles do not require any power supply and are relatively simple to use.

2.4. Microneedles

The concept of microneedles was first proposed in the 1970s (Gerstel and Place 1976) to provide a minimally invasive route for transporting drugs into the skin by combining the benefits of hypodermic needle injections and transdermal patches while eliminating the shortcomings associated with both techniques. However, this concept was not realized in practice until more recently when the microelectronics industry provided the micro-electronic mechanical system (MEMS) tools required to make structures of micron sized dimensions (Prausnitz 2004). Microneedles are typically hundreds of microns long, 1 to 50 μm wide at the tip, and approximately 50 - 300 μm at the base. They can be solid or hollow and can be fabricated as single needles or multi-needle arrays (Figure 2.4) (Prausnitz 2005).

Over the past decade, microneedles of various geometries and materials have been developed. Depending on the microneedle design, microneedles can be applied by four different delivery strategies (Prausnitz, Gill et al. 2008):

a) "Poke and patch" – this was the first microneedle concept to be developed and involves inserting (poking) an array of solid microneedles into the skin to create

transport pathways followed by the application of a drug loaded transdermal patch over the channels. The creation of these micron-dimension channels enhances delivery of large and hydrophilic molecules which would not be able to traverse an intact SC barrier via passive diffusion.

b) "Poke and flow" – this method is analogous to hypodermic delivery, however, instead of inserting needles deep into the subcutaneous or intramuscular region, this method uses hollow microneedles to deliver liquid drug formulations to the dermal capillaries via pressure driven convection.

c) "Coat and poke" – this method involves coating drug molecules onto the microneedles. The coated needles are inserted into the skin and the drug coating is dissolved off the needles into the skin.

d) "Poke and release" – this delivery method involves fabrication of biodegradable polymer microneedle structures with drug encapsulated inside the needle. The needles are then inserted into the skin and the polymer either degrades or dissolves, releasing the encapsulated drug into the skin. This technique generates no biohazardous sharp waste allowing for elimination of contamination due to needle-sticks and potential needle reuse. Depending on the type of polymer used, the delivery process can be controlled from on the order of a few seconds to several days.

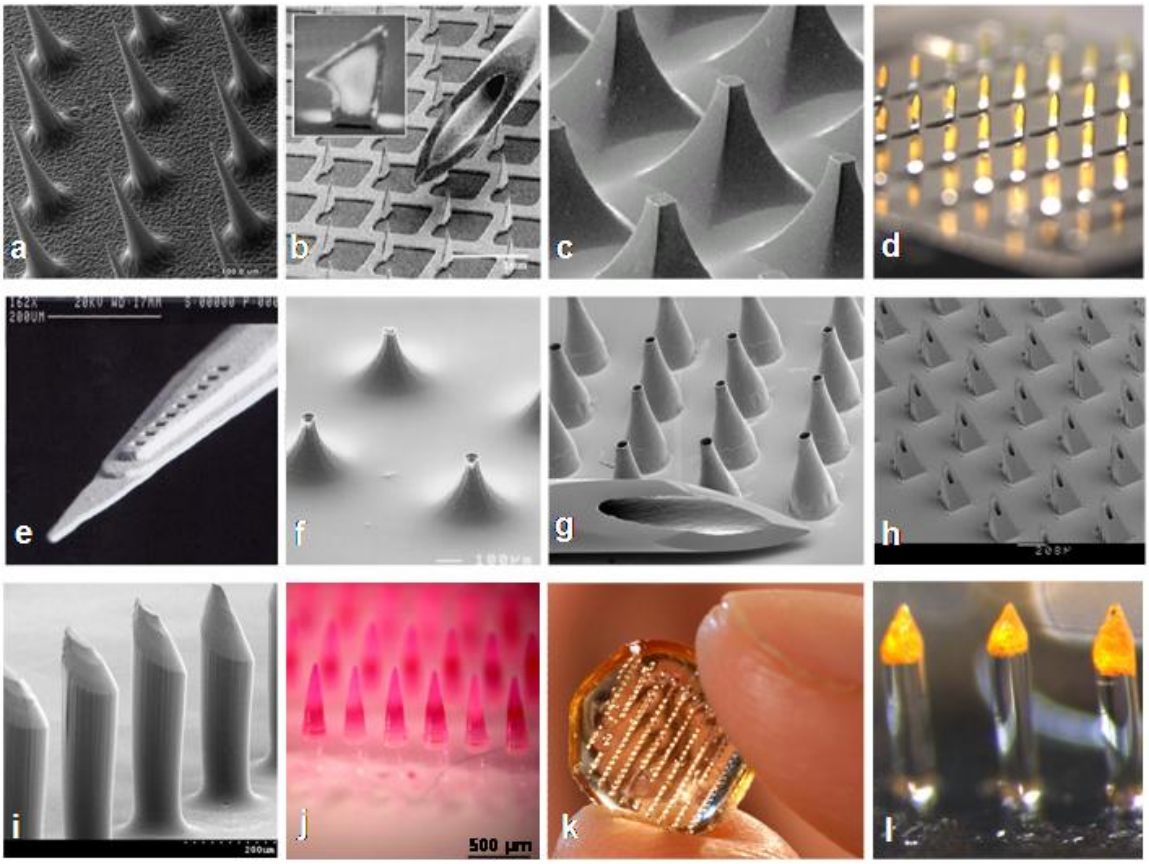

Figure 2.4: *Solid Microneedles:* a) solid silicon microneedles (150 µm tall) (Henry, McAllister et al. 1998); b) solid microneedles of a microprojection array (300 µm tall) etched from a titanium sheet (Matriano, Cormier et al. 2002); c) solid microneedles of a microenhancer array (200 µm tall) etched from a silicon wafer (Mikszta, Alarcon et al. 2002); d) stainless steel microneedle coated with Vitamin B2 (750 µm tall) (Gill 2007). *Hollow Microneedles:* e) in-plane hollow single needle with multiple ports (30 μm^2 ports) (Brazzle, Mohanty et al. 1999); f) Hollow silicon microneedles (200 µm tall) (Stoeber and Liepmann 2000b); g) Hollow metal microneedles (500 µm tall) (Davis, Prausnitz et al. 2003); h) Hollow silicon microneedles (350 µm tall) (Gardeniers, Luttge et al. 2003). *Polymer Microneedles:* i) solid polyglycolic acid (PGA) biodegradable microneedles (600 µm tall) (Park, Allen et al. 2005); j) array of polyvinyl pyrrolidone (PVP) microneedles (750 µm tall) encapsulated with sulforhodamine (Sullivan, Murthy et al. 2008); k) array of 200 poly-lactide-co-glycolide (PLGA) microneedles (Park, Allen et al. 2006); l) bevel-tip PLGA microneedles (600 µm) encapsulating calcein within their tips (Park, Allen et al. 2006).

2.4.1. In-Vitro Microneedle Delivery

The initial microneedle studies were carried out *in-vitro* in animal and human cadaver models. The first studies to determine that microneedles can be used to increase skin permeability of macromolecules were carried out using solid silicon microneedles by Henry et al. (Henry, McAllister et al. 1998) and McAllister et al. (McAllister, Wang et al. 2003). Using the poke and patch approach they showed that microneedles increased the permeability of human cadaver skin to calcein, insulin, bovine serum, albumin, and latex nanospheres as large as 10 nm in diameter by several orders of magnitude, in some cases as high as 10,000-fold. Other studies using the same approach have also been carried out to show increased permeability of human skin *in-vitro* to lipid-polycation plasmid DNA using silicon microneedles (Chabri, Bouris et al. 2004) and to BSA and calcein using polyglycolic acid (PGA) polymer needles (Park, Allen et al. 2005). Increased permeability of rat skin to calcein was demonstrated using silicon microneedles (Teo, Shearwood et al. 2005). Polycarbonate microneedles were also used to deliver calcein to rat cadaver skin and results showed that longer needles and increased needle density led to increased permeability (Oh, Park et al. 2008).

Hollow microneedles of various lengths ranging from 600 to 800 μm have been studied to demonstrate the distribution of calcein and fluorescently labeled insulin within the epidermis and dermis *in-vitro* in hairless rat skin (Wang, Cornwell et al. 2006). Further, 200 μm long hollow microneedles have been shown to deliverer blue ink and fluorescent lucifer yellow dye to a depth of 100 μm under the skin (~ dermal-epidermal junction) of chicken thigh (Stoeber and Liepmann 2000a; Stoeber and Liepmann 2000b). Hollow microneedles have also been inserted into human cadaver sclera to deliver

nanoparticles on the order of 280 nm (Jiang, Moore et al. 2009). Hollow microneedle studies in human cadaver tissues have demonstrated that the primary resistance to fluid flow to skin via microneedles resides within the skin and not the microneedles. These studies have shown than insertion of hollow microneedles into the skin or sclera followed by retraction leads to an increase in fluid flow into tissue as microneedle insertion causes tissue compaction while retraction allows the skin to recoil to its original state (Wang, Cornwell et al. 2006; Martanto, Moore et al. 2006a; Jiang, Moore et al. 2009). Further, addition of drug spreading enzymes such as hyaluronidase to the drug formulation has also demonstrated an increase in fluid flow into tissue through hollow microneedles (Martanto, Moore et al. 2006a; Jiang, Moore et al. 2009).

Coated microneedles have also been studied in human cadaver sclera to show rapid delivery of sulforhodamine and BSA in less than 30 seconds (Jiang, Gill et al. 2007). Further, insertion of microneedles coated with vitamin B, calcein, and 1 μm barium-sulfate microparticles into porcine cadaver skin has shown rapid dissolution of the drug from the needle into the dermis within a matter of seconds (Gill and Prausnitz 2007). A variation of the coat and poke method whereby the needle base substrate is coated with drug matrix instead of the needles themselves has demonstrated controlled delivery of calcein and BSA from a chitosan coated substrate reservoir in rat skin (Xie, Xu et al. 2005).

Poly-lactide-co-glycolide (PLGA) microneedles (750 μm long) using the poke and release approach have been shown to deliver calcein just below the dermal-epidermal junction in a controlled release manner to human cadaver skin (Park, Allen et al. 2006). Depending on the encapsulation formulation, these needles could control delivery times

ranging from hours to months. Further, carboxymethylcellulose (CMC) microneedles demonstrated delivery of sulforhodamine to porcine dermis in both a bolus release (minutes) and sustained release (hours) manner by encapsulating just the needles and both the needles and substrate with the model drug respectively (Lee, Park et al. 2008). Polyvinylpyrrolidone (PVP) microneedles have also shown to rapidly deliver BSA into porcine cadaver skin on the order of a minute whereas PVP copolymerized with methacrylic acid can lead to slow delivery over a couple of hours (Sullivan, Murthy et al. 2008).

2.4.2. In-Vivo Microneedle Delivery

2.4.2.1. Animals

Over the past decade, microneedles have been studied extensively *in-vivo* in animals for delivery of peptides, proteins, genetic material, and vaccines among many other molecules. Solid microneedles have been used to deliver peptides like insulin to diabetic hairless rats by inserting a microneedle array into the rat skin at a high velocity followed by deposition of a solution of insulin on top of the array. Delivery over a period of four hours caused blood glucose levels to drop as much as 80% (Martanto, Davis et al. 2004). Hollow microneedles have also shown reduction in plasma glucose levels during basal insulin delivery in rats using silicon and glass microneedles (Gardeniers, Luttge et al. 2003; McAllister, Wang et al. 2003; Wang, Cornwell et al. 2006; Nordquist, Roxhed et al. 2007). Rapidly dissolving dextrin-based insulin loaded microneedles also led to a reduction in blood glucose levels in mice (Ito, Hagiwara et al. 2006). The same dextrin microneedles have been used to deliver proteins such as erythropoietin, in mice and a polysaccharide drug, viz. low molecular weight heparin in rats (Ito, Yoshimitsu et al.

2006; Ito, Murakami et al. 2008). Self dissolving chondroitin sulfate microneedles encapsulated with insulin have also been shown to reduce blood glucose levels in dogs (Ito, Ohashi et al. 2008). CMC microneedles too have demonstrated successful delivery of peptides through administration of human growth hormone to rats (data not published). Further, peptide delivery was accomplished via desmopressin-coated microneedles which were inserted into hairless guinea pig skin and showed bioavailability as high as 85% (Cormier, Johnson et al. 2004).

Small molecules such as diclofenac and pilocarpine have been delivered via hollow microneedles to rat skin (Gardeniers, Luttge et al. 2003) and through coated microneedles to rabbit eyes, respectively (Jiang, Gill et al. 2007). Lin et al. (Lin, Cormier et al. 2001) successfully delivered genetic material (oligonucleotides) in hairless guinea pigs by poking the skin with solid microneedles followed by covering the skin with an oligonucleotide loaded gel.

Microneedles have also been used for vaccination in animals and have shown dose-sparing of vaccine and an immune response that is at least as good as conventional intramuscular or subcutaneous vaccination. This is because microneedles target the highly immunogenic dendritic cells in the dermis and epidermis. Studies have demonstrated solid microneedle-based delivery of vaccines against hepatitis B, anthrax, and Japanese encephalitis in animals leading to a strong immune response (Mikszta, Alarcon et al. 2002; Dean, Alarcon et al. 2005; Mikszta, Dekker et al. 2006). Microneedles coated with ovalbumin, a model antigen also led to strong immune response and suggested dose-sparing in hairless guinea pigs (Matriano, Cormier et al. 2002; Widera, Johnson et al. 2006). More recently, microneedles coated with different

strains of inactivated influenza virus demonstrated complete protection of mice against the virus (Koutsonanos, del Pilar Martin et al. 2009; Zhu, Zarnitsyn et al. 2009). Hollow microneedles also showed dose-sparing and strong immune response in rats using three different types of influenza vaccines (Alarcon, Hartley et al. 2007). These hollow needles were also used to vaccinate mice and rabbits against anthrax and non-human primates against Japanese encephalitis respectively (Dean, Alarcon et al. 2005; Mikszta, Sullivan et al. 2005).

In-vivo animal studies have also been carried out to demonstrate the increased permeability of skin after microneedle treatment as characterized by transepidermal water loss. Solid microneedle treatment of hairless guinea pig skin showed that microneedles enhanced skin permeability over a 48 h time period (Banks, Gill et al. 2005). Further, in another study, treatment of skin with hollow microneedles showed that transepidermal water loss increased immediately after needle insertion, but then returned to normal within a few minutes (Gardeniers, Luttge et al. 2003).

2.4.2.2. Humans

While extensive studies have been carried out using microneedles in living animals, only a few studies have been carried out in human subjects. Coated microneedles developed by a company called Zosano Pharmaceuticals have been used to successfully deliver parathyroid hormone and desmopressin to human subjects (Padmanabhan, Phipps et al. 2008). Hollow microneedles (200 μm long) have been used to deliver very small volumes (1 μL) of methyl nicotinate to human subjects. More recently, 1.5 mm long hollow microneedles developed by Becton Dickinson have been used for influenza vaccination and led to a stronger immune response than intramuscular

injection in elderly subjects (Holland, Booy et al. 2008) and a comparable immune response in younger subjects (Beran, Ambrozaitis et al. 2009). The same needles have also been used to deliver sterile saline to human subjects and confirmed fluid delivery in the dermis with less insertion pain than hypodermic needles (Laurent, Bonnet et al. 2007). Influenza vaccine delivery has also been carried out in human subjects by using arrays containing four hollow microneedles (450 μm long) developed by Nanopass (Van Damme, Oosterhuis-Kafeja et al. 2009). Biodegradable, 500 μm long maltose microneedles encapsulated with ascorbate-2-glycoside have been inserted in the skin of human subjects and found to be dissolved in the epidermis and dermis within 5 min with no adverse skin reactions and without causing pain on insertion (Miyano, Tobinaga et al. 2005). Other studies have also evaluated pain associated with microneedle insertion. Kaushik et al., Gill et al., and Haq et al. demonstrated that pain caused by inserting solid microneedles into skin was significantly less than that of a conventional hypodermic needle (Kaushik, Hord et al. 2001; Gill, Denson et al. 2008; Haq, Smith et al. 2009). Few studies have also been carried out in human subjects where transepidermal water loss was used to demonstrate that microneedle insertion leads to an increase in skin permeability (Mikszta, Alarcon et al. 2002; Bal, Caussin et al. 2008; Haq, Smith et al. 2009). Lastly, microneedles have been used to extract interstitial fluid from the volar forearm skin of human subjects in a painless manner for the purpose of glucose monitoring (Wang, Cornwell et al. 2005).

2.5. Skin Electrical Impedance

Electrical impedance is the resistance of a material to the flow of an alternating current. The skin's electrical impedance is therefore defined as the skin's opposition to

flow of alternating current. Skin impedance is generally modeled as an equivalent circuit consisting of two parallel resistor/capacitors in series. One parallel RC combination represents the stratum corneum, while the other represents the deeper tissue layers (Yamamoto and Yamamoto 1976a; Burnette and DeNuzzio 1997). The skin's capacitance is mainly due to the dielectric properties of the lipid-protein components of the epidermis while the skin's resistance is associated primarily with the stratum corneum layer (Burnette and DeNuzzio 1997). The high electrical resistance of the stratum corneum is attributed to the multilamellar structure of the lipids between the corenocytes (Pliquett and Prausnitz 2000). In fact, the stratum corneum is the predominant contributor to the skin's resistance (Yamamoto and Yamamoto 1976b). Although the SC is in series with the viable epidermis and dermis, these deeper layers do not act as a barrier to electric current and their resistance is negligible (Yamamoto and Yamamoto 1976a; Pliquett and Prausnitz 2000). This has been demonstrated through studies which showed that removal or puncturing of the stratum corneum leads to a significant decrease in skin impedance, ultimately approaching a very low constant value beyond which further skin removal or puncturing does not affect resistance (Lawler, Davis et al. 1960; Edelberg 1971; Yamamoto and Yamamoto 1976a). Studies have also demonstrated that the resistance in the SC is not homogenous; the resistance is highest in the uppermost layers of the SC and decreases as one moves lower into the stratum corneum (Burnette and DeNuzzio 1997). As a result, skin electrical impedance is a good indicator of the skin barrier integrity. Consequently, since skin permeability depends on the integrity of the stratum corneum, skin electrical impedance is a good indicator of skin permeability. *In-vitro* studies have shown that there is a strong linear relationship between skin

impedance and skin permeability, with a decrease in impedance corresponding to an increase in permeability (Karande, Jain et al. 2005).

Disruption of the SC barrier and/or an increase in skin hydration leads to a decrease in skin's electrical impedance. As described previously, any breach in the skin barrier leads to diffusion of water from the deeper skin layers across the stratum corneum, thereby increasing the water content of the SC. Occlusion too increases the hydration of the SC. This increased water content leads to an increase in the dielectric constant of the SC, allowing ions to move more freely, thereby reducing the skin's resistance to current flow (Burnette and DeNuzzio 1997). Additionally, the keratin protein chains in the SC have a dipole moment; therefore an increase in hydration causes the keratin to become more flexible and responsive to an electric field (Burnette and DeNuzzio 1997) ultimately leading to reduction in skin impedance.

2.6. Single-Compartment Pharmacokinetic Model

Compartmental analysis is used to determine what happens to a drug as a function of time once it has been delivered to the body. The primary assumption behind this type of analysis is that the human body can be divided into one or more compartments where the drug resides in a dynamic state for a period of time. A compartment is a hypothetical space, bound by an unspecified membrane across which drugs are transferred and it is an open system where drug passes freely into and out of the system (Allen, Popovich et al. 2005). *In-vivo* absorption of drugs across the skin is generally modeled using single-compartment pharmacokinetics (Roberts and Anissimov 2005). This model depicts the body as one compartment having a certain volume of distribution (V_d). V_d is a theoretical volume in which the drug must be distributed to achieve the desired concentration of drug

measured in blood or plasma. This volume of distribution is a constant that is determined by the drug properties as well as factors such as age and state of disease. This model assumes that the drug is confined to the blood (or plasma) and then eliminated (Allen, Popovich et al. 2005).

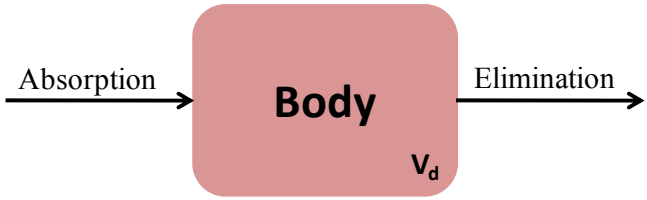

Figure 2.5: Single-compartment pharmacokinetic system (Fisher and Peattie 2007).

For transdermal systems, the drug is absorbed into the compartment at a certain rate given by (Fisher and Peattie 2007):

$$Absorption: \frac{dA}{dt} = -k_a A \qquad (2.1)$$

where k_a is the absorption rate constant and A is the drug present at the absorption site which disappears with time and depends on the initial dose delivered and the volume of distribution. The drug is eliminated from the body at a rate given by:

$$Elimination: \frac{dE}{dt} = k_{el} C \qquad (2.2)$$

where k_{el} is the elimination rate constant, E is the eliminated drug and C is the concentration of the drug in the body (compartment). The drug concentration in the compartment is given by:

$$Body: \frac{dC}{dt} = k_a A - k_{el} C \qquad (2.3)$$

These three differential equations define single-compartment pharmacokinetics and can be used to calculate pharmacokinetic parameters such as time to maximum concentration of drug in body, t_{max}; the peak drug concentration, C_{max}, and the area under the plasma/blood concentration versus time curve, AUC, which represents the total amount of drug absorbed in the body.

2.7. Diabetes and Insulin Delivery

Diabetes Mellitus is the fourth leading cause of death by disease in the world. With an estimated 246 million current cases of diabetes worldwide and a forecasted increase to almost 380 million cases by 2025, it is becoming one of the most prevalent non-communicable diseases in the world (International Diabetes Foundation). Diabetes if not managed effectively can be fatal. Consequently, a significant amount of money is being spent to manage this disease. It is estimated that the annual healthcare costs associated with treating and preventing diabetes and its complications worldwide were at least US$ 232 billion in 2007 (Diabetes Atlas – Economic Impacts). Moreover, intangible costs such as reduced quality of life and reduced life expectancy are immeasurable and significant.

Diabetes is a metabolic disease that affects how the body uses glucose (blood sugar). Glucose is the main source of energy for the cells that make up muscles and other tissues. Food is one of the major sources of glucose. During digestion, sugar (glucose) is absorbed into the bloodstream. In healthy patients, glucose then enters the cells with the help of insulin. Insulin is a hormone secreted by the pancreas and acts as a key to unlock cells, allowing glucose to enter. As glucose enters the cells, blood glucose levels drop and consequently insulin secretion from the pancreas also drops. Diabetes can be

classified into two categories: type 1 diabetes, whereby the body's own immune system attacks the pancreas making it lose its ability to produce insulin, and type 2 diabetes, which is caused by insulin resistance and subsequent insulin deficiency. If the body does not produce/absorb enough insulin, the blood sugar levels continue to rise and can be fatal. As a result, diabetes is generally characterized by a rise in blood glucose levels known as hyperglycaemia which is associated with long-term damage, dysfunction, and failure of various organs, especially the eyes, kidneys, nerves, heart, and blood vessels (American Diabetes Association, 2003).

Type 1 diabetes affects 5-10% of all diabetes patients and is typically diagnosed in children and adolescents. These patients are dependent on insulin and require daily delivery of external insulin in order to survive. Diabetes management involves tight control of blood glucose levels as close as possible to levels found in normal subjects (between 80 – 120 mg/dL before a meal). Since insulin cannot be administered orally due to degradation and loss of activity in the gastrointestinal tract, these patients self-administer insulin subcutaneously several times a day using hypodermic needle in order to control blood glucose levels. However, the kinetics of the injected insulin are far from the natural rise and fall of insulin levels within the body and hence, inaccurate dosing can often lead to hypo- or hyper-glycaemic conditions (Tyagi 2002). In order to more closely mimic the natural insulin secretion behaviour, insulin pumps have been developed which allow for flow of insulin into the patient's body at set basal rates throughout the day and bolus injections for meal time requirements using a subcutaneous catheter (Webb 2006). Although this method provides some time controlled release of insulin, the device is fairly bulky and inconvenient, and the insertion of subcutaneous catheters is quite painful

resulting in omission of insulin doses, anxiety, and poor patient compliance, especially among young patients which can lead to serious complications (Mollema, Snoek et al. 2001; Hanas 2004). Moreover, the pharmacokinetics of the insulin itself is far from ideal, as the rate of insulin absorption is slow and it takes several minutes before the drug begins to take effect. As a result, patients have minimal flexibility in their meal-time lifestyle.

Several insulin analogues have been developed to improve insulin pharmacokinetics; however, there still remains room for improved analogues that have improved pharmacokinetics and pharmacodynamics. With regards to insulin delivery devices, jet injectors are currently available; however, they are associated with pain and are not commonly recommended, except for patients who fear needles or who have severe lipoatrophy (Cefalu 2004; Warrell, Cox et al. 2005). Exubera, a form of inhalable insulin marketed by Pfizer was introduced in 2006 as the first insulin delivery route alternative to subcutaneous insulin since 1922. However, it was withdrawn the following year as it had low bioavailability, high cost, a bulky design, and unknown health risks (Bailey and Barnett 2007; Barnett 2008). Other methods such as buccal, nasal, oral, and other transdermal methods such as iontophoresis, thermal and radio-frequency ablation, and sonophoresis are still being studied, however with limited success (Cefalu 2004).

Therefore, in order to improve diabetes management so as to increase patient compliance, reduce complications, and enhance quality of life for diabetes patients there is a need for more convenient and less-painful insulin delivery devices with improved pharmacokinetics.

2.8. Lidocaine Delivery

Lidocaine is an amino amide type local anesthetic commonly used in topical, infiltration, nerve block, ophthalmic, epidural, and intravenous (IV) regional anesthesia. By blocking the fast sodium channels in the cell membrane, lidocaine alters the depolarization in neurons. With sufficient blockade, the ionic fluxes required for the initiation and conduction of impulses are inhibited and the cell membrane will not depolarize, thereby, not transmitting an action potential, leading to its anesthetic effects. Lidocaine is generally used in the form of lidocaine hydrochloride and is available in several forms such as injected local anesthetic, dermal patch, oral gel or liquid, and topical gel or liquid (Lidocaine Hydrochloride Package Insert, 2001).

One of the most common applications of lidocaine is for regional anesthesia during needle insertion for venipuncture or intravenous cannulation, as this process can be painful, uncomfortable, and frightening, especially for children and can often lead to needle phobia (Lysakowski, Dumont et al. 2003; Migdal, Chudzynska-Pomianowska et al. 2005). In a study performed by Cummings et al. (Cummings, Reid et al. 1996), placement of IV lines was ranked as the second highest source of worst pain in children only after disease-related pain. Painless topical anesthetics such as eutectic mixture of local anesthetics (EMLA) have been shown to provide effective local anesthesia for venipuncture and intravenous catheterization, however, effective analgesia requires application of the topical formulation for 30 to 90 minutes prior to needle insertion, thereby limiting its usefulness in busy ambulatory health care settings (Lander, Hodgins et al. 1996; Eichenfield, Funk et al. 2002). Consequently, physicians continue to use hypodermic needles to inject lidocaine prior to IV placement due to its rapid onset;

however, though quite rapid, this procedure is painful as compared to EMLA. As a result, several alternative transdermal delivery systems are being studied for lidocaine delivery for local dermal anesthesia. Needle free jet injectors have been used in clinical applications for pre IV placement treatment, however, the jet injection procedure itself is painful and the procedure has also been found to be cost prohibitive (Lysakowski, Dumont et al. 2003). Lidocaine delivery using iontophoresis, sonoporation, and electroporation have been found to provide effective topical anesthesia of the skin and underlying tissue for pain free venipuncture and IV placement within 5-15 minutes of treatment in children (Zempsky, Anand et al. 1998; Wallace, Ridgeway et al. 2001; Katz, Shapiro et al. 2004). Devices using these methods have been marketed, however, most of them have had poor patient/physician uptake and some have subsequently been withdrawn due to poor sales. Just earlier this year, Zingo, a new lidocaine jet-injection system marketed by Anesiva was discontinued (Anesiva Annual Report, 2008) and previously a sonoporation device company, Sontra, also suffered poor sales. Iontophoresis devices such as LidoSite developed by Vyteris too have suffered poor market acceptance causing the company to de-emphasize its focus on iontophoresis based lidocaine delivery (Vyteris Annual Report, 2008). This is presumably due to the cost, complexity, and slower onset of these systems in comparison to conventional hypodermic needle-based lidocaine delivery. Therefore, there continues to remain a need for a simple, pain-free, cost-effective, and rapid onset local anesthesia device.

CHAPTER 3: METHODS

3.1. Microneedle Fabrication

3.1.1. Solid Microneedles

Solid microneedles were fabricated by laser cutting stainless steel sheets (Trinity Brand Industries, SS 304, 75 μm and 125 μm thick; McMaster-Carr, Atlanta, GA) using previously published methods (Martanto, Davis et al. 2004; Gill and Prausnitz 2007). The microneedles designs were first drawn according to their geometry specifications in AutoCAD (Autodesk, Cupertino, CA) and then cut in-plane using an infrared laser (Resonetics Maestro, Nashua, NH). The arrays were then cleaned, bent out of plane at 90 degrees, and electropolished as described previously (Gill and Prausnitz 2007) followed by sterilization in a steam autoclave (Steris Amsco Renaissance 3033 Prevac Steam Sterilizer; Steris Corporation, Mentor, OH). The microneedle arrays had an overall footprint size of 12 mm by 12 mm. Figure 3.1 shows an example of a solid microneedles used in this thesis.

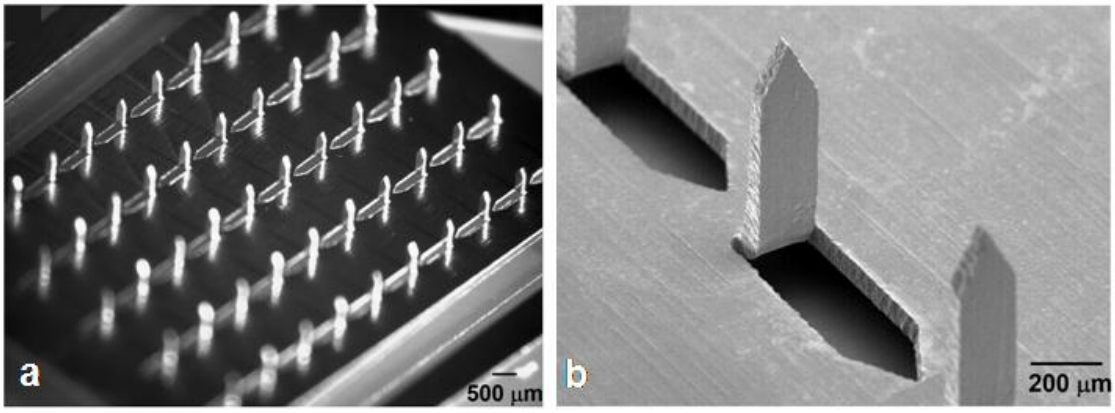

Figure 3.1: Solid stainless steel microneedles. a) Brightfield micrograph of a 50 microneedle array, and b) scanning electron micrograph of a section of the 50 microneedle array.

3.1.2. Hollow Microneedles

Hollow microneedles (Figure 3.2a) were fabricated by pulling fire-polished type I borosilicate glass pipettes (BF150-86-15, Sutter Instrument, Novato, CA) with a micropipette puller (P-97, Sutter Instrument). Programmable puller parameters of Pull = 40, Velocity = 10, Heat = 580, Time = 150, and P = 500 allowed reproducible production of microneedles with tip properties strong enough to insert into skin without breakage. The pulled needles were then beveled at a 30° angle using a beveler (BV-10 beveler, 104D fine bevel plate, Sutter Instrument) producing hollow microneedles with an oval-shaped opening. Due to this oval shape, the effective radius of the needle opening was determined by averaging the lengths of the long and short axes of the needle tip opening. The effective tip radii of the microneedles used in this thesis were between 60 and 80 μm. The microneedles were then cleaned in an ultrasonic deionized water bath (SW-34, Sonicwise Ultrasonics, San Diego, CA) for 2 min by bubbling air through the needles dipped in water via an air filled syringe (10 mL, Becton Dickinson, Franklin Lakes, NJ) and tubing (2C5685, Baxter, Deerfield, IL) connected to the non-tip needle end. The needles were placed in an autoclavable micropipette storage bell jar (World Precision Instruments, Sarasota, FL) and dried for 2 h in an oven at 180°C (VC-300, Grieve Corp., Round Lake, IL) followed by steam sterilization in an autoclave (Scientific Series 3021-S, AMSCO Erie, PA).

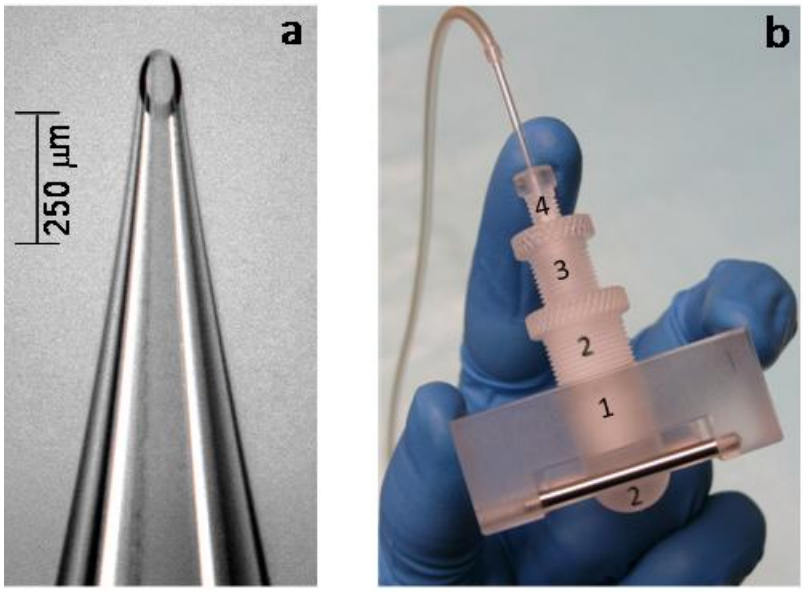

Figure 3.2: a) Hollow borosilicate glass microneedle, b) custom rotary microneedle insertion device.

3.2. Hollow Microneedle Insertion Device

To insert the hollow microneedles into the skin of human subjects safely and accurately, a custom rotary device was fabricated by modifying previously used designs (Wang, Cornwell et al. 2005). As seen in Figure 3.2b, the device consisted of 4 parts positioned concentrically within each other so as to allow the glass microneedle to pass through. The rectangular block (piece 1) allowed the user to hold and stabilize the device on the skin's surface. The ball-shaped end of piece 2 helped minimize skin deflection during microneedle insertion. Only the microneedle length protruding beyond the convex-surface was inserted into skin. Piece 3 was threaded into piece 2 and these parts together served as the depth-controlling structures. The threads were calibrated such that each 360° turn of piece 3 moved the microneedle tip 800 µm in its axial direction. Graded markings on pieces 2 and 3 allowed the microneedle to be precisely "drilled" into

the skin at the desired depth with ±10 μm accuracy. The fourth and final piece served as a set-screw that helped keep the needle firmly within the device. A rubber gasket (Pipette seal PS-15, Warner Instruments, Hamden, CT) was placed between pieces 1 and 2 to ensure the needle was secured tightly within the device. The non-tip end of the needle extended beyond piece 1 and was connected to tubing. The microneedle was inserted into skin at a 90° angle by placing the convex end of the device on the skin followed by carefully inserting the microneedle to the desired depth into the skin.

3.3. Assessment of Pain

All experiments in this thesis involved asking study subjects to assess the pain associated with microneedle insertion and fluid infusion. These pain scores were measured using a Visual Analog Scale (VAS) consisting of a 100 mm ruler with "No Pain" written on the left end and "Worst Imaginable Pain" on the right end. There were no other markings visible to the subject. In order to measure pain, subjects were asked to slide a marker along the ruler to correspond with his or her pain. An un-blinded observer recorded the pain score in millimeters by reading a number corresponding to the marker position on the opposite side of the ruler.

3.4. Resealing of Human Skin Barrier *In-Vivo*

3.4.1. Study Subjects

Ten healthy adult human subjects (3 female, 7 male, age: 24-52) with no history of dermatological disease were recruited to participate in this study. Both the left and right volar forearms of all subjects were used in the study. Subjects were asked to refrain from application of any topical formulations or soaps on their arms, as well as to avoid any vigorous physical activity or extreme temperature showers one day prior to and

throughout the duration of the experiment. In order to obtain hourly skin impedance data over a period of 48 hours after treatment, subjects were divided into two groups of five individuals each. The first group provided data for time points 1-11 and 23-35 h post treatment and the second group generated data for time-points 12-22 and 36-48 h post treatment. Both groups also provided data for time-points -1, -0.5, and 0 (immediately after treatment) h. Subjects remained in the study room throughout each data collection period. Prior to commencing skin impedance data collection on each study day, subjects were asked to rest in the controlled environment study room for 1 h in order to acclimate to the experimental conditions of 40% relative humidity and room temperature of 21°C. The study was approved by the Georgia Tech Institutional Review Board and all subjects provided informed consent prior to participation. The experiments were conducted in accordance with the Declaration of Helsinki protocol.

3.4.2. Experimental Design

Five different solid microneedle geometries with varying microneedle length, number of needles, and base cross-sectional area were fabricated (Table 3.1).

Table 3.1: Parameters of the five different microneedle geometries and two other experimental controls studied

Design	Length *(l)* μm	Thickness *(t)* μm	Width *(w)* μm	Number of Microneedles	
A	750	75	200	50	
B	750	75	200	10	
C	500	75	200	50	
D	1500	75	200	10	
E	750	125	500	50	
F	Hypodermic Needle (26 Gauge)				
G	No Treatment				

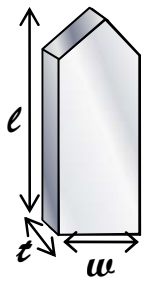

A total of 11 sites (left arm: 6 and right arm: 5) were identified on the volar forearms of all ten subjects and were outlined with a pen. The six sites on the left arm received treatment with microneedles having geometries A, B, and C, three of which were occluded and the remaining three were non-occluded. Of the five sites on the right arm, four received occlusive and non-occlusive treatments with microneedle geometries D and E. At all sites, the microneedles were inserted into the skin manually by pressing the array into the skin for approximately 15-20 s using the thumb of a study investigator. The application took place such that the microneedles were inserted perpendicular to the surface of the skin. In the occasional event that the microneedles did not successfully insert into the skin as characterized by high impedance measurements after insertion, the sites were then treated as no-treatment, negative control sites (G).

The last site on the right arm received non-occlusive treatment using a 26-gauge hypodermic needle (treatment F) inserted 5 mm deep into the skin (Becton Dickinson, Franklin Lakes, NJ) and served as the positive control. This site was studied only in the absence of occlusion, because hypodermic needle treated sites are traditionally left un-occluded in clinical practice. To control the insertion depth, the protective needle cap covering the hypodermic needle was cut such that only 5 mm of the hypodermic needle was protruding from the cap.

The location and order of treatments on the marked skin sites were not randomized and remained consistent among all subjects. Further, neither the investigators nor the subjects were blinded to the treatments and all personnel were aware of the treatment being administered and its corresponding location during the study. The treatment sites were arranged such that the reference electrode was at the center of the

volar forearm surrounded by the sites with approximately 5 mm spacing between the reference and the treatment electrodes. Figure 3.3 shows the experimental set-up on the left volar forearm of a subject.

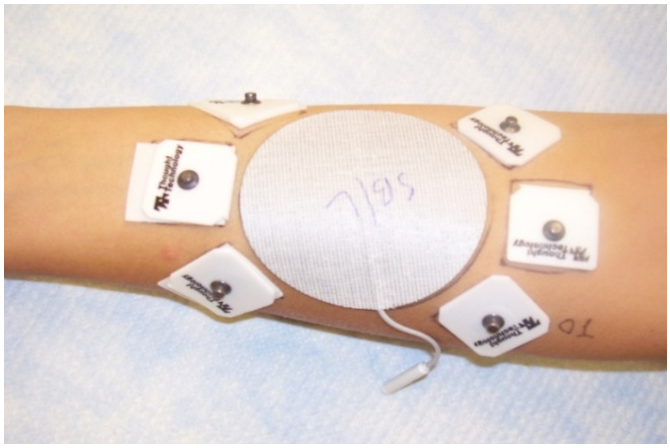

Figure 3.3: Experimental set-up of the left volar forearm of a human subject: a large, highly conductive, gelled reference electrode surrounded by dry Ag/AgCl measurement electrodes placed on treatment sites. Impedance measurements were made by periodically connecting reference and measurement electrodes to an impedance meter by applying low frequency alternating current.

3.4.3. Experimental Procedure

Prior to commencing the study, all subjects were allowed to acclimate to the study environment conditions for a period of 1 h, after which the treatment sites were gently wiped with 70% isopropyl alcohol swabs (BD Alcohol Swabs; Becton Dickinson). The experimental measurement procedure then commenced with a baseline pre-treatment skin impedance recording of the t = -1 h reading for all sites by placing the reference and treatment electrodes on their respective sites. Each reading required approximately 30 s to obtain. After data collection, the reference and non-occluded site electrodes were removed. The occluded sites remained covered with the measurement electrode (25 mm x 25 mm); an occlusive tape (3M Blenderm Surgical Tape; 3M Healthcare, St. Paul, MN)

was added to further occlude the sites. Pre-treatment skin impedance measurements were repeated 30 min later at t = -0.5 h.

At t = 0 h, the occlusive coverings were removed and all sites were administered their respective treatments. Subjects were asked to rate the pain they felt during insertion using the VAS pain scale. Electrodes were immediately placed on the sites and impedance measurements were recorded (the occluded sites were covered again). Measurements were taken on the two subject groups to generate impedance data up to 48 h post treatment. After the 42nd hour reading, all occlusive dressings were removed and all sites remained non-occluded for the last 6 h. At the end of each study day, the occluded sites were further covered with a waterproof dressing (Nexcare Absolute Waterproof Premium Adhesive Pad, 3M Healthcare) and with an occlusive film of polyvinylidene chloride (Saran Wrap; SC Johnson, Racine, WI) which was secured with waterproof tape (Nexcare Absolute Waterproof First Aid Tape; 3M Healthcare) to ensure complete occlusion when subjects went home for the night.

3.4.4. Electrodes and Impedance Measurement

Ag/AgCl dry electrodes (Thought Technology T-3404; 25 mm x 25 mm total area; 10 mm active electrode diameter; Stens Corporation, San Rafael, CA) were used as the measurement electrodes for the treatment sites. A large electrode with a highly conductive gel (Superior Silver Electrode with PermaGel, 70 mm total and active electrode diameter; Tyco Healthcare Uni-Patch, Wabasha, MN) was used as the reference electrode to keep the impedance contribution of the reference site at a negligibly low value. Impedance measurements were made by connecting lead wires to the reference and measurement electrodes, the opposite ends of which were connected to an impedance

meter (EIM-105 Prep-Check Electrode Impedance Meter; General Devices, Ridgefield, NJ) applying a low frequency (30 Hz) alternating current modified with a 200 kΩ resistor (Ack Electronics, Atlanta, GA) in parallel to allow for measurement of skin impedance values greater than 200 kΩ. Due to the parallel resistor modification, the impedance meter readout was converted to the actual measured skin impedance (Z) by using the formula:

$$Z = \frac{1}{\left(\frac{1}{R_{meter}} - \frac{1}{R_p} \right)} \tag{3.1}$$

where R_{meter} is the meter readout, R_p is the resistance of the resistor in parallel as measured by a multimeter.

3.4.5. Statistical Methods

One- and two-way repeated measures ANOVA were performed using NCSS 2007 (NCSS, Kaysville, UT). Analysis of the occluded and non-occluded data over all time points and for all needle geometries was performed using the general linear model (GLM) ANOVA using Minitab 15 (Minitab Inc., State College, PA). Tukey's post-hoc pairwise comparisons were performed to compare which factor levels led to significant differences. Comparisons of goodness of fit between experimental naltrexone delivery concentrations (Appendix B) and impedance-based predicted concentrations were performed using the χ^2 test with 12 degrees of freedom (12 experimental measurement points). In all cases, a value of $p < 0.05$ was considered statistically significant.

3.5. Flow Conductivity in Human Skin During Microneedle Infusion

3.5.1. Study Subjects

Ten healthy adult subjects (1 female, 9 male) were recruited to participate in this study. Subjects with diseased or abnormal skin and/or known hypersensitivity to hyaluronidase enzyme were not included in the study. The study was approved by the Georgia Institute of Technology and Emory University Institutional Review Boards and all subjects provided informed consent prior to participation. The study was carried out in accordance with the Declaration of Helsinki protocol and was performed at Emory University under the supervision of a physician.

3.5.2. Experimental Design

This was a non-randomized, single-blinded study. A total of 9 sites were identified on the volar forearms of subjects (left: 5, right: 4) and were marked as T1 thorough T9. Sites T1-T4 were infused with sterile saline at a flow rate of 0.3 mL/min using hollow microneedles (described in section 3.1.2) at various depths ranging from 500 μm (intradermal) to 4 mm (subcutaneous). Site T5 was treated with a 26-gauge intradermal bevel hypodermic needle (Becton Dickinson) and was inserted into the skin using the standard Mantoux technique for intradermal delivery of sterile saline at 0.3 mL/min. For site T6, the hollow microneedle was first inserted to a depth of 1 mm into the skin and then retracted back to 500 μm after approximately 5 seconds and then infusion was carried out at that depth. Sites T7 and T8 involved microneedles inserted 750 μm into the skin followed by infusion of sterile saline at flow rates of 1 mL/min (fast) and 0.1 mL/min (slow), respectively. The last site T9 involved microneedle-based

delivery of hyaluronidase into the skin at 750 µm and 0.3 mL/min. Table 3.2 summarizes all 9 treatment sites from this study.

Table 3.2: Experimental conditions for the 9 treatment sites

		Insertion Depth					
		500 µm	**750 µm**	**1 mm**	**4 mm**	**26G Intradermal**	**Insert 1mm/retract to 500 µm**
Flow Rate (mL/min)	**0.1 (low)**		T8				
	0.3 (medium)	T1	T2	T3	T4	T5	T6
	1 (high)		T7				
	Hyaluronidase (0.3 mL/min)		T9				

3.5.3. Experimental Set-up

Figure 3.4 depicts the experimental apparatus for this experiment. A syringe pump (NE-1000, New Era Systems, Farmingdale, NY) housing a 10 mL syringe (Becton Dickinson) was connected to the hollow microneedle by means of flexible infusion tubing (Mallinckrodt - three way stopcock with 12 in pressure tube, Tyco Healthcare, Pleasanton, CA and 2C5685, Baxter, Deerfield, IL). A digital manometer (DigiMano, Netech, Hicksville, NY) was placed in-line to measure the pressure associated with infusion. The hollow microneedle was housed in the custom rotary drilling device described in section 3.2. Needle insertion and retraction were controlled via the graded markings on the microneedle device.

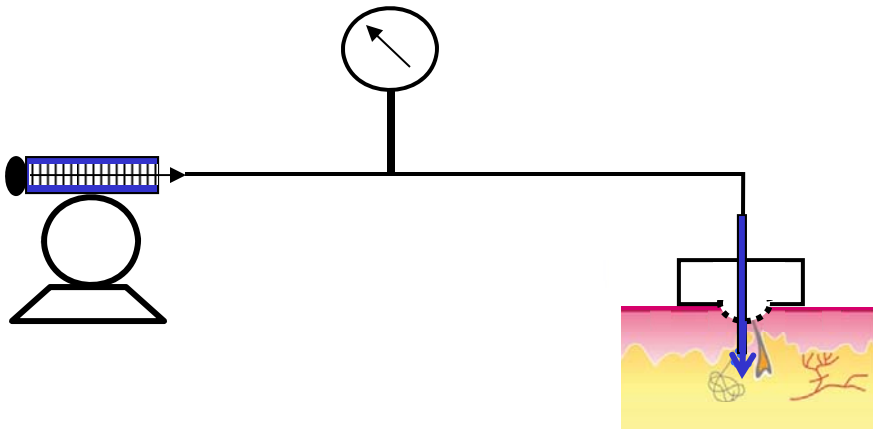

Figure 3.4: Experimental apparatus set-up: an in-line manometer was placed between the microneedle and syringe to measure the pressure during fluid infusion into skin.

A digital video-camera (PV-GS380 MiniDV Camcorder, Panasonic, Secaucus, NJ) was used to capture continuous readings on the manometer and the movements of the syringe plunger. The video-camera data was converted to 1-second interval image files by using the batch capture feature in Adobe Premiere Elements 4.0 (Adobe, San Jose, CA). The pressure readings were obtained for every second from the corresponding captured image files and the volume delivered was determined by measuring the displacement of the plunger every 200 μL in pixels (Adobe Photoshop CS3, Adobe).

3.5.4. Injection Solutions

Sterile saline (0.9% sodium chloride injection, USP, Hospira, Lake Forest, IL) was used for the saline delivery procedures in this study. Hyaluronidase delivery was achieved by using Hylenex recombinant solution (Baxter, Deerfield, IL).

3.5.5. Experimental Procedure

After obtaining informed consent and ensuring subjects met the study inclusion/exclusion criteria, the subject was seated and asked to place his/her arms

beneath a curtain barrier such that the subject was unable to see the experimental procedure. The subject's forearms were wiped with 70% isopropyl alcohol (Becton Dickinson) swabs followed by marking of an outline of the treatment sites with a fine black marker using a custom made stencil to ensure consistent spacing and location of the treatment sites among subjects. The skin sites were then imaged using an ultrasound skin imaging device that allowed visualization of the different layers of the skin in a non-invasive manner (DermaScan C, Cortex Technology, Denmark). The sites were once again wiped with isopropanol swabs ensuring that the marker outline was not erased. The subject was then informed that the first treatment procedure was about to begin. Treatments were carried out in a non-randomized order from T1 to T9. The needle/microneedle was inserted into the skin and the subject was asked to indicate the pain associated with needle insertion by using the VAS pain scale. The pain score was recorded and the scale marker was moved back to the zero position by the study investigator. The syringe pump was then turned on and infusion began as per the flow rate corresponding to the treatment site. Continuous pressure and volume measurements were taken via continuous video imaging of the manometer and syringe. Upon infusion of 0.2 mL of fluid, the subject was again asked to rate the pain associated with infusion using the VAS scale. Keeping the VAS marker in the same position as the 0.2 mL score, the subject was asked to slide the maker in either direction upon infusion of 0.4, 0.6, 0.8, and 1 mL respectively. Upon delivery of 1 mL of fluid, the pump was stopped. The needle was slowly removed from the skin and then the subject was asked to rate the overall delivery procedure as causing "no pain", "no pain to mild pain", "mild pain", "mild to moderate pain", "moderate pain", "moderate to severe pain", "severe pain" or

"worst possible pain". The treatment site skin layers were re-imaged using the ultrasound Dermascan device. The treatment procedure was then repeated for the remaining sites at their corresponding depths and flow rates using the appropriate injection solution.

3.5.6. Statistical Methods

Comparisons between two treatment conditions were carried out using Student's t-test. Comparisons between three or more conditions were carried out using one- and two- way ANOVAs for one and two factors respectively. Tukey's post-hoc pairwise comparisons were performed to compare which factors levels led to significant differences. In all cases $p < 0.05$ was considered significant. NCSS 2007 (NCSS), Minitab (Minitab Inc.), and Microsoft Excel 2007 were used to perform the analyses.

3.6. Insulin Delivery to Type 1 Diabetes Subjects Using Hollow Microneedles

3.6.1. Study Subjects

Five subjects with type 1 diabetes (1 female, 4 male; age 11-44), who were managed with an insulin pump and were in good glycaemic control were recruited to participate in this study. In order to be included in the study, subjects were required to have type 1 diabetes for at least 2 years, be using a conventional Food and Drug Administration-approved insulin pump with lispro insulin for the past year, have mean hemoglobin A1c levels ≤8% for the past year and a body mass index within the 85th percentile for their age. Subjects were excluded if they had type 2 diabetes, acanthosis nigricans, a clinically significant major organ system disease, were on glucocorticoid therapy, had an insulin requirement of ≥150 U/day, an illness on the day of the study, or were pregnant or breast-feeding. The demographics of the study subjects are shown in Table 3.3.

Table 3.3: Demographics of study subjects

Parameter	*Subject 1*	*Subject 2*	*Subject 3*	*Subject 4*	*Subject 5*
Age (years)	43	38	11	19	18
Race	Caucasian	Caucasian	Caucasian	Caucasian	Caucasian
Gender	Female	Male	Male	Male	Male
Mean HbA1c[a] (%)	6.5	6.2	6.9	6.3	6.9
Weight (kg)	63.5	78.0	45.2	80.8	72.6
BMI (kg/m^2)	23.3	25.5	19.7	26.6	21.8
Time since diagnosis (years)	30.0	28.5	5.5	10.75	14.5
Duration of pump use (years)	12.2	7.5	3.9	7.4	5.0
Length of pump catheter (mm)	9.0	9.0	9.0	9.0	9.0
Mean insulin per day (units)	40.0	45.0	36.0	80.0	52.0
ICR (units/g)	1:7.5	1:10	1:7.5	1:5	1:7.5

BMI, body mass index; ICR, insulin to carbohydrate ratio.
[a]Mean hemoglobin A1c over the past year.

This study was performed in the Diabetes Clinic at the Emory Children's Center at Emory University (Atlanta, GA) in accordance with the Declaration of Helsinki protocol. The study was approved by the Institutional Review Board at Emory University. All subjects provided informed consent (or written assent for subjects under age 18 along with parental consent) to participate in the study.

3.6.2. Microneedle Insertion

Hollow microneedles with a bevel angle of 30° and effective tip radii between 60 and 80 μm were fabricated and sterilized as described in section 3.1.2. The microneedles were inserted at a 90° angle into the abdominal skin at various depths ranging from 900 μm to 5 mm using the custom-made rotary drilling device described in section 3.2. The microneedle was connected to a 3-mL syringe (Becton Dickinson) by means of a flexible intravenous extension set tubing (2C5685, Baxter). The syringe was further connected to a syringe pump (NE-1000, New Era Systems) that controlled the insulin delivery flow

rate at 1 mL/min. The microneedles were removed from the skin immediately after insulin delivery was completed.

3.6.3. Insulin

Humalog insulin (lispro, Eli Lilly, Indianapolis, IN) was used in this study. The control treatments used a 100-U insulin formulation, whereas the microneedle treatments used a 50-U insulin, which was prepared by diluting 100-U insulin with sterile diluent for Humalog (Eli Lilly).

3.6.4. Experimental Design

The study was an open-label, within-subjects, controlled design. This study was conducted in three phases. The first phase was carried out in subject 1 in the absence of a meal to determine the optimum microneedle insertion depth for intradermal insulin delivery. The second phase was performed on subject 2 using the optimum depth obtained from Phase 1 and included consumption of a standardized meal immediately after insulin administration. Unequal insulin doses were given for the microneedle and control treatments as post-prandial (after a meal) insulin bioavailability following intradermal-microneedle insertion was initially unknown. Guided by the results of phase 2, the third phase was carried out in all 5 subjects and included consumption of a meal after insulin administration and equal insulin doses for both microneedle and control treatments. The protocols for each phase are described as follows.

3.6.5. Phase 1: Effect of Microneedle Insertion Depth

This phase was conducted to determine the minimum microneedle insertion depth for effective bolus insulin delivery through a microneedle device in fasting subjects. The

study was carried out in Subject 1 and included four study visits. The first visit served as the control visit (subcutaneous insulin catheter: 9 mm) and the subsequent three visits served as the study visits (microneedle: 5 mm, 3.5 mm, and 1 mm insertion depths, respectively). Prior to each visit, the subject underwent overnight fasting for a minimum of 10 h. In an effort to minimize the amount of insulin on board, subjects turned their pumps off 2 h prior to insulin delivery. Capillary glucose measurements were then taken every 30 min using a glucose meter (FreeStyle Lite™, Abbott Laboratories, Abbott Park, IL) until blood glucose levels remained stable or were at the onset of rising. An intravenous catheter was then placed in the subject's antecubital fossa, and a 10-mL blood sample was drawn. The specimen was collected in a sterile vacuum blood collection tube (BD Vacutainer Plus plastic serum tube 367820, Becton Dickinson) followed by centrifugation at 1,300 g (Vanguard V6500, Hamilton Bell, Montvale, NJ), separation, and immediate freezing at –4°C. A capillary glucose measurement was also taken at this time.

The abdominal insulin administration site was then wiped with 70% isopropyl alcohol (Becton Dickinson). This was followed by administration of an insulin bolus into the subject's abdomen either by inserting a subcutaneous insulin catheter (9 mm, Paradigm Quick-set, Medtronic MiniMed, Northridge, CA) connected to a conventional insulin pump (Paradigm, Medtronic MiniMed) in the case of the control treatment or through a microneedle connected to a programmable syringe pump at the rate of 1 mL/min for the study treatment. The insulin dose was determined based on the subject's blood glucose level, individual insulin requirement, and type of delivery device. After insulin delivery, the pumps were immediately shut off, and the subject received no basal

insulin during the experiment. Capillary glucose level measurements and blood draws were collected periodically at 30 min, 45 min, 60 min, 75 min, 90 min, and every 30 min thereafter until blood glucose levels returned to normal. All samples were assayed for plasma glucose and free insulin concentrations (Esoterix, Calabasas Hills, CA).

The first phase of the study did not involve the consumption of any food after insulin delivery, and the subject fasted throughout the study. If at any time the subject developed severe hypo-glycaemia (capillary glucose <70 mg/dL) or severe hyper-glycaemia (capillary glucose >300 mg/dL), felt ill, or desired to withdraw from testing, the study was discontinued. The subject was asked to qualitatively describe and compare the pain associated for each of the four delivery procedures.

3.6.6. Phase 2: Effect of Microneedle-Based Insulin Delivery on Postprandial Glucose Levels (unequal control and microneedle insulin doses)

This phase was carried out in Subject 2 and involved three study visits: the first served as the control visit (subcutaneous insulin catheter: 9 mm) and the last two as the study visits (microneedle: 1 mm). The protocol for this study was identical to that in phase 1; however, the subject consumed a standardized mixed meal comprising 75 g of carbohydrates, 12 g of protein, and 14 g of fat immediately following the insulin bolus. Capillary glucose levels and blood draws were collected according to the same schedule as phase 1. The subject was asked to qualitatively describe and compare the pain associated with both the delivery procedures. The insulin delivery sites were imaged (PowerShot SD400, Canon, Tokyo, Japan) periodically before and after the insulin bolus for the control and first microneedle visit. Figure 3.5 shows a hollow microneedle next to the conventional catheter used in this study.

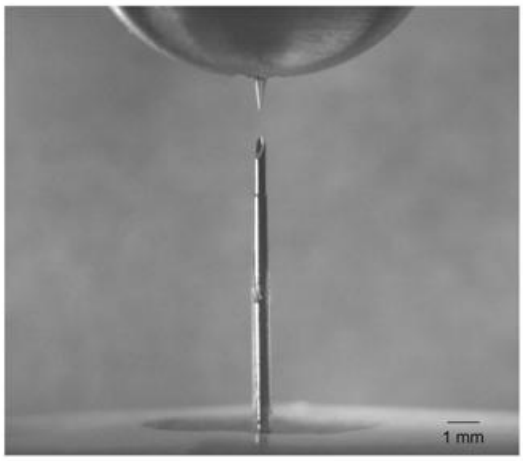

Figure 3.5: A 1-mm hollow microneedle in a holder (above) compared to a 9-mm infusion catheter (below).

3.6.7. Phase 3: Effect of Microneedle-Based Insulin Delivery on Postprandial Glucose Levels (equal control and microneedle insulin doses)

This phase was carried out in all five subjects and consisted of two visits per subject. The first visit was the control visit where a bolus dose of U-100 insulin based on the subject's glucose level and insulin-to-carbohydrate ratio was administered to the subject's abdomen using a 9-mm catheter and the insulin pump. During the second visit, the same insulin dose was administered using U-50 insulin and a 900-µm long microneedle connected to a syringe pump set at 1 mL/min.

Prior to each visit, subjects underwent overnight fasting and were required to turn off their insulin pumps 45 min before the start of the study. At the start of the study, a blood draw was taken from the antecubital fossa and a capillary blood measurement was also made. This was followed by insulin bolus administration to the abdomen skin by one of the two treatment methods and immediate consumption of the same standardized meal as in phase 2. Capillary glucose measurements and venous blood draws were taken

periodically every 15 min for the first 2 hours and every 30 min thereafter up to a total of 3.5 h or until the subject became hypo- or hyper-glycaemic as described above.

3.6.8. Pain Scores and Skin Irritation

Subjects were asked to rate the pain associated with microneedle and catheter insertion and insulin infusion using the VAS pain scale. Subjects were also asked to give their treatment preference among the two delivery procedures. Erythema and edema scores were recorded using the Draize Dermal Irritation Scoring System (Table 3.4) at every blood collection time point (Bonnette, Rodabaugh et al. 2002).

Table 3.4: Draize dermal irritation scoring system for erythema and edema

Score	Erythema Description	Edema Description
0	• No erythema	• No edema
1	• Very slight erythema (barely perceptible)	• Very slight edema (barely perceptible)
2	• Well-defined erythema	• Slight edema (edges of area well defined by definite raising)
3	• Moderate to severe erythema	• Moderate edema (raised ~ 1 mm)
4	• Severe erythema (beet-redness) to slight, eschar formation	• Severe edema (raised more than 1 mm and extending beyond the area of exposure)

3.6.9. Calculation of Pharmacokinetic Parameters

Phase 3 pharmacokinetic (PK) parameters t_{max} and C_{max} were directly determined from the plasma free insulin level assay data. The area under the insulin curves were calculated from the plot of plasma free insulin levels versus time graph using the trapezoidal rule:

$$AUIC = \sum_{n=1}^{n} \left(\left(\frac{C_{n-1} + C_n}{2} \right) - C_0 \right) (t_n - t_{n-1}) \qquad (3.2)$$

where C_0 is the initial plasma free insulin concentration at t = 0, t_n corresponds to a particular blood collection time point and t_{n-1} corresponds to the time point immediately before it. Similarly, C_n corresponds to the plasma concentration at t_n and C_{n-1} to the concentration at t_{n-1}.

Using the above PK parameters and the single-compartment model described in section 2.6, the absorption (k_a) and elimination (k_{el}) rate constants were calculated using the following method. The solution to the differential equation (equation 2.3) describing the drug concentration in the body for a single-compartment model is given as follows:

$$C(t) = \left(\frac{k_a A_0}{k_{el} - k_a} \right) \left(e^{-k_a t} - e^{-k_{el} t} \right) \tag{3.3}$$

where A_0 is given by the insulin dose delivered divided by the volume of distribution of insulin ($A_0 = \text{Dose}/V_{dist}$). The time when the maximum insulin concentration occurs in the body, t_{max} is given by:

$$t_{\max} = \frac{\ln\left(\frac{k_{el}}{k_a} \right)}{k_{el} - k_a} \tag{3.4}$$

and the corresponding peak insulin concentration, C_{max} is given by the following equation:

$$C(t_{\max}) = A_0 \left(\frac{k_{el}}{k_0} \right)^{\frac{k_{el}}{k_a - kel}} \tag{3.5}$$

Using the above three equations, the experimental plasma free insulin concentrations, and the experimental t_{max} and C_{max} values, the unknown values for k_a and k_{el} were calculated.

3.6.10. Statistical Methods

All phase 3 pharmacokinetic parameters, rate constants, and pain scores are reported as mean ± SD. Statistical significance comparisons for phase 3 results were performed using a two-tailed Student's t-test with $p < 0.05$ being considered significant. Microsoft Excel 2007 was used to perform all t-tests.

3.7. Local Anesthesia Using Hollow Microneedles in Human Subjects

3.7.1. Study Subjects

Fifteen healthy adult human subjects (11 male, 4 female; age: 22-56) participated in this study. Subjects having diseased or abnormal skin, known diseases affecting nerve function or perception of pain, allergies to lidocaine, and poorly accessible veins on the dorsum (back) of their hand were excluded from the study. The study was approved by the Emory University Institutional Review Board and all subjects provided informed consent prior to participation. The study was carried out in accordance with the Declaration of Helsinki protocol. The study was conducted at Emory University under the supervision of a physician.

3.7.2. Endpoints

The following end points were measured: a) pain associated with microneedle and hypodermic needle-based lidocaine injection, b) area of skin numbness at t = 0, 7.5, and 15 min after lidocaine injection, c) depth of skin numbness at t = 0, 7.5, and 15 min after lidocaine injection, d) efficacy of injection based on pain associated with administration of an intravenous catheter (IV) immediately after lidocaine delivery, e) onset of anesthesia based on results from b, c, and d, and f) preferred treatment method among microneedle and hypodermic needle injection.

3.7.3. Pain Scores

Pain scores were measured to assess the pain associated with microneedle and hypodermic needle-based lidocaine injection and to determine the efficacy of lidocaine anesthesia by measuring pain associated with administration of the IV catheter. Pain scores were measured using the VAS pain scale. Immediately after lidocaine injection and after IV insertion, subjects were asked to slide a marker along the VAS ruler to correspond with his or her pain as described in section 3.3.

3.7.4. Lidocaine

A 2% preservative-free injectable lidocaine hydrochloride solution (Hospira) was used for all injection procedures in this study.

3.7.5. Microneedle Fabrication and Injection

Hollow microneedles with a bevel angle of 30^{o} and tip radii between 60 and 80 μm were fabricated as described in section 3.1.2. The microneedles were inserted at a 90^{o} angle into the skin to a depth of 500 μm using the custom rotary drilling device. The microneedle was connected to a 3-mL syringe (Becton Dickinson) by means of a flexible IV extension set tubing (2C5685, Baxter). The syringe was further connected to a syringe pump (NE-1000, New Era Systems) which controlled the lidocaine delivery flow rate at 300 μl/min. The microneedles were removed from the skin immediately after infusion.

3.7.6. Hypodermic Needle Injection

A 26-gauge 3/8 inch intradermal bevel needle (Becton Dickinson) connected to a 1 mL syringe (Becton Dickinson) was used as the positive control lidocaine injection

method. The needle was inserted at a small angle (Mantoux method), almost parallel to the skin, into the intradermal space by an experienced anesthesiology personnel and lidocaine was injected within a period of approximately 3-5 s. Figure 3.6 shows a hollow microneedle compared to a 26-gauge hypodermic needle.

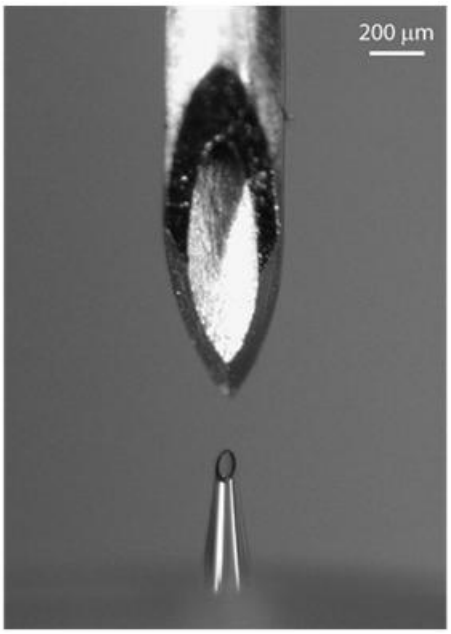

Figure 3.6: The bevel opening of a 26-gauge intradermal bevel hypodermic needle (top) compared to the entire length of a 500 μm long microneedle (bottom). As seen in the image, the entire microneedle (bevel + shaft) is short enough to sit inside the bevel of the hypodermic needle.

3.7.7. Study Design

This study was a randomized, within subjects, controlled, single-blinded design and was carried out in two phases. One phase was carried out on the forearm while the other was carried out on the dorsum (back) of the hand. The forearm phase was carried out to assess the pain associated with microneedle-based injection and to determine the efficacy of injection by measuring the area and depth of numbness. The phase on the dorsum of the hand was carried out to further assess the pain associated with

microneedle-based injection and to determine the efficacy of injection by assessing pain associated with subsequent intravenous catheter insertion. All subjects received treatments with both devices on their forearms and on the dorsum of their hands and each subject served as his or her own control. The sequence of these two phases (forearm or dorsum) was randomized among subjects. The study was controlled using hypodermic needle-based lidocaine injection. Within each phase, the procedure sequence (i.e.: microneedle or hypodermic needle) and the treatment forearm/hand (i.e.: left or right) was also randomized among subjects. The subjects were blinded throughout the study by placing their arms under a curtain barrier.

3.7.8. Forearm Protocol

The volar forearm insertion site was identified and marked 7 cm from the midpoint of the antecubital fossa. The site was then wiped with 70% isopropanol swabs (Becton Dickinson) followed by injection of 200 μl of lidocaine using a microneedle or hypodermic needle as per the randomization schedule. The subject was asked to rate the pain associated with injection using the VAS scale. The subject was then asked if he/she considered the procedure to be painful. The area of numbness was then measured via a pin-prick test by gently tapping the blunt stylet of a 25-gauge 3.5 inch spinal needle (Becton Dickinson) on the skin starting from the insertion point and extending radially outward in four directions until the subject felt a sensation (Figure 3.7).

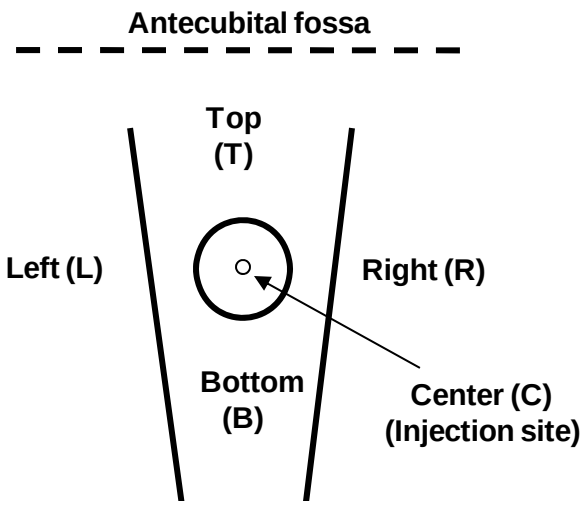

Figure 3.7: Schematic of the volar forearm insertion site and measurement map. Position C depicts the injection site located 7 cm from the middle of antecubital fossa. The area of numbness was measured by conducting a pin-prick test starting from position C and extending radially outward towards the top, bottom, left, and right. The depth of numbness was measured by inserting a 26-gauge 3/8 inch needle into the skin at point C until the subject indicated presence of sensation.

The depth of numbness was measured by inserting a 26-gauge 3/8 inch (Becton Dickinson) hypodermic needle into the skin at the site of lidocaine injection until the subject indicated that he/she felt a sensation (up to a maximum of 9.5 mm). The procedure took approximately 2 min to complete and was carried out immediately after lidocaine injection (t = 0 min) and again at 7.5 min and 15 min after injection. The lidocaine injection followed by pain and efficacy assessment was then repeated on the opposite forearm using the other injection method. At the end of both treatment procedures, subjects were asked to rank their preference between the microneedle and hypodermic needle injections by indicating if they preferred the first or second injection procedure.

3.7.9. Dorsum of Hand Protocol

A site near a vein accessible for venipuncture was identified and wiped with isopropanol swabs. Lidocaine (100 μl) was then injected using a microneedle or a hypodermic needle as per the randomization schedule to generate a skin wheal. The subject was then asked to rate the pain associated with lidocaine injection using the VAS scale and indicate if the procedure was painful. A 22-gauge IV catheter (Optiva, Smiths Medical, Carlsbad, CA) was then inserted through the wheal into the vein until a small amount of blood was drawn, upon which the IV catheter was immediately removed. The site was wiped with an isopropanol swab and covered with an adhesive bandage. The subject was asked to rate the pain of inserting the IV catheter and indicate if the procedure was painful. The procedure was then repeated on the opposite hand using the other injection method. At the end of both treatments, the subject was asked to indicate the preferred treatment method between the first and second treatment.

3.7.10. Local Skin Reaction

Immediately following lidocaine delivery and 1 h post delivery, the injection sites were visually examined for skin irritation (not using the Dermal Draize scale).

3.7.11. Statistical Methods

All data are expressed as mean ± SD. VAS pain scores between hypodermic and microneedle-based lidocaine delivery were compared using Student's t-test. Venous cannulation pain scores following the two treatment methods were also compared via Student's t-test. In all cases, p-value < 0.05 was considered significant. Differences in the radii of numbness (top, bottom, left, and right) for the two treatment methods over all three time points were compared using a repeated measures three-way ANOVA. The

total area and depth measurements for the two devices were compared over the three time points using a repeated measures two-way ANOVA. All comparisons were performed using NCSS (NCSS), Minitab (Minitab Inc.), and Microsoft Excel 2007 software.

CHAPTER 4: RESULTS & DISCUSSION

4.1. Resealing of Human Skin Barrier *In-Vivo*

4.1.1. Introduction

As described in chapter 2, microneedles can be fabricated as single or multi-needle arrays having hollow channels or solid structures that can be coated with or encapsulate with drug. Hollow microneedles actively deliver drug to the dermis through convective flow, similar to the mechanism of a hypodermic needle. Solid microneedles also deliver drug actively by either inserting drug-coated needles or drug-encapsulated needles into the skin. In each of these active delivery cases, from a safety standpoint it is desirable for the micro-channels to close soon after needle removal to prevent permeation of undesired toxic substances or pathogenic microbes that may lead to infection at the treatment site.

Solid microneedles can also deliver drugs via passive diffusion by creating micro-channels to increase skin permeability followed by the application of a drug-loaded patch on top of the channels (Henry, McAllister et al. 1998; Wermeling, Banks et al. 2008). To achieve sustained delivery, from an efficacy standpoint, it is desirable for these micro-pathways to stay open as long as the drug patch is on the skin. However, it is also desired for the holes to close immediately after patch removal to prevent site infection.

To achieve prolonged drug delivery using solid microneedles, it is essential to determine the extent and duration of the skin's increased permeability because as with any skin wounds or abrasions, the holes created in the skin reseal over time due to the skin's natural repair mechanisms. Upon disruption of the stratum corneum barrier,

lamellar body secretion is immediately initiated followed by synthesis of lipids, which are necessary to restore and maintain the SC barrier (Grubauer, Elias et al. 1989; Menon, Feingold et al. 1992). Because the kinetics of SC repair depend on the degree of barrier perturbation (Schaefer and Redelmeier 1996), it is also important to study SC repair following treatment with microneedles of various geometries. Further, because the presence of a drug-loaded patch on the treatment site covers (occludes) the skin, it is also necessary to study the effect of occlusion on skin resealing after microneedle treatment.

Previous *in-vivo* studies performed in hairless guinea pigs have shown that microneedles enhanced skin permeability over a 48 h time period as characterized by transepidermal water loss (Banks, Gill et al. 2005). Other studies have also been carried out in human subjects using transepidermal water loss to show that microneedle insertion leads to an increase in skin permeability, but the kinetics of repair were not examined (Bal, Caussin et al. 2008; Haq, Smith et al. 2009). Thus, no kinetic studies have been performed to determine the "window" of increased permeability following microneedle treatment and how it can be modulated.

In this chapter, we perform the first human experiments to analyze the recovery of skin's barrier properties after microneedle insertion and determine the duration of increased skin permeability as a function of microneedle geometry and skin occlusion. We also study the role of occlusion to influence the expected safety and efficacy of microneedle treatment as well as the relationship between pain and skin recovery time. Lastly, we use the results from this study to develop a model to predict the transdermal drug delivery of a drug (naltrexone) *in-vivo* and compare the prediction to experimental observations.

Several non-invasive biophysical tools such as transepidermal water loss, infrared spectroscopy and electrical impedance spectroscopy have been evaluated to determine the *in-vivo* integrity of the SC barrier and the permeability of the skin (Curdy, Naik et al. 2004; Fluhr, Elsner et al. 2005). While TEWL is the most commonly used evaluation tool, this method requires areas studied under occlusion to be un-occluded during the measurement procedure. Because this study specifically tested the effects of occlusion, we employed electrical impedance spectroscopy as our measurement tool so as to allow the occluded treatment sites to remain occluded throughout the experimental period.

The skin's electrical resistance lies predominantly in the stratum corneum and any break in the integrity of the barrier leads to a decrease in skin impedance (Yamamoto and Yamamoto 1976a; Yamamoto and Yamamoto 1976b), thereby making impedance spectroscopy a useful tool to determine skin barrier integrity after microneedle insertion. Previous studies have demonstrated that there is a strong correlation between skin impedance and skin permeability with a decrease in skin impedance corresponding to an increase in skin permeability (Karande, Jain et al. 2005). Additionally, impedance spectroscopy is a non-invasive and safe measurement tool that is often used in dermatology for the assessment of skin diseases and in the cosmetic industry to study the effect of cosmetics on skin (Burnette and DeNuzzio 1997).

Microneedles are known to increase skin permeability to a wide range of molecules by creating microchannels in the skin. In this study, we quantify that effect using impedance spectroscopy and determine the lifetime of transdermal transport pathways by testing the hypothesis that increasing microneedle length, number, and base

cross-sectional area in conjunction with occlusion leads to an increase in skin resealing time that can exceed one day.

4.1.2. Effect of Microneedle Design on Initial Skin Impedance Drop

As described in section 3.4, the left and right volar forearms of 10 healthy adult human subjects were used in this study. Five different microneedle geometries (Table 3.1) with varying length, number, thickness, and width (Designs A-E) were studied under occlusive (impermeable to air and moisture) and non-occlusive conditions and compared to positive (F, hypodermic needle) and negative (G, no treatment) controls. A total of 11 sites (5 occluded, 6 non-occluded) were identified and marked. Figure 3.1 shows a microneedle array used in this study and Figure 3.3 depicts the treatment sites on the arm. Pre-treatment impedance measurements were taken at the beginning of the study, after which the marked sites on each subject were administered their respective treatments at time t = 0 h, followed by hourly skin impedance measurements. The impedance values were then normalized with respect to their corresponding positive control hypodermic needle (F) impedance to account for inter-subject variability.

To determine the effect of microneedle design on the initial drop in skin impedance as compared to that caused by a 26-gauge hypodermic needle, the average normalized skin impedance Z_{norm} for each of the treatment conditions (A-G) at time t = 0 h was analyzed (Figure 4.1). The impedance values for the microneedle (A-E) and hypodermic needle (F) sites were all significantly lower than that of the no treatment control (G) (repeated measures one-way ANOVA; $p < 0.05$), however, there were no significant differences among treatments A-F (repeated measures one-way ANOVA; $p > 0.05$). Since *in-vivo* intact human skin is generally characterized by relatively high

impedance and the skin's electrical resistance is attributed primarily to the stratum corneum, these low impedances indicate that the SC barrier was compromised with increased permeability to drug molecules. Further, though we anticipated that more needles and needles with larger cross-sectional area would make more/bigger holes, which would lead to lower initial impedance at t = 0 h, comparisons between geometries A and B, and A and E revealed no significant difference in initial impedances. However, we hypothesize that larger changes in needle width and number of needles would make a significant difference.

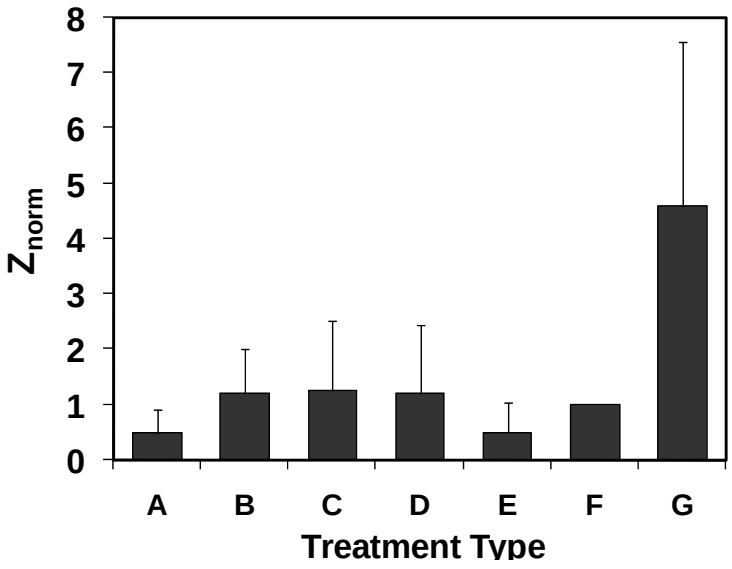

Figure 4.1: Comparison of normalized (relative to hypodermic needle (F) positive control) average skin impedance (Z_{norm}) values at time = 0 h (immediately after treatment) for the different treatment conditions. A significant reduction in skin resistance upon treatment with microneedles (A-E) and hypodermic needle (F) was observed in comparison to the intact skin negative control (G). There was no significant difference among treatments A-F. Graphs expressed as mean ± SD.

4.1.3. Kinetics of Skin Barrier Recovery: Effect of Occlusion

To determine the duration of the increased skin permeability caused by microneedles, skin impedance profiles for all microneedle geometries were measured and

analyzed in the presence and absence of occlusion over a 48 h experimental study period. The impedance data for each subject were normalized with respect to their corresponding t = 0 positive control (F) and the average normalized impedance was plotted over time for both the occluded and non-occluded cases as shown in Figure 4.2. From these data, the kinetics of skin resealing can be determined as a function of microneedle geometry and skin occlusion.

Analysis of the effect of occlusion on skin resealing was performed in two ways. First, the impedance profiles for the occluded and non-occluded sites were compared up to the 42 h time point (at which point occlusion was removed from all occluded sites). As can be seen from Figure 4.2, the impedance values for both the occluded and non-occluded cases dropped significantly from their pre-treatment values immediately after needle insertion and then increased over time indicating skin barrier recovery. However, the speed of this recovery depended on the occlusive condition of the skin and on microneedle design. Comparison of the occluded and non-occluded cases over all time-points indicated that skin recovery was significantly faster in the absence of occlusion (GLM ANOVA followed by Tukey's post-hoc pairwise comparison; $p < 0.05$).

Second, the data for the occluded sites (Figure 4.2a) were analyzed before and after removal of occlusion at the 42nd hour. This evaluation revealed that upon removal of occlusion after the 42nd hour, the skin impedance immediately increased within one hour (two-way ANOVA followed by Tukey's post-hoc pairwise comparison; $p < 0.05$), confirming that skin recovery was significantly faster in the absence of occlusion.

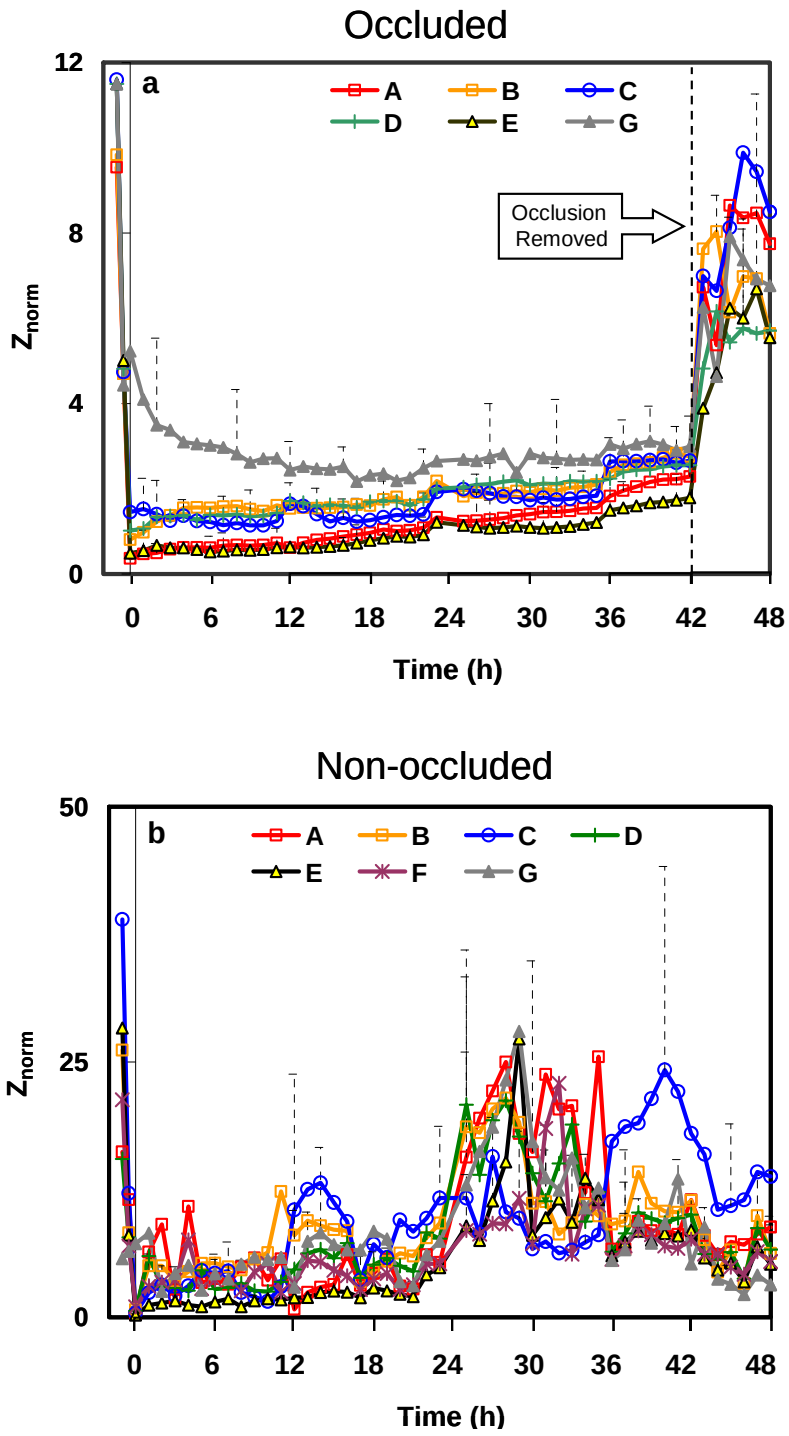

Figure 4.2: Normalized (relative to hypodermic needle (F) positive control impedance at t = 0) average skin impedance (Z_{norm}) profile over the course of a 48 h time period for different skin treatments (Table 3.1). Profile (a) under occlusion and (b) without occlusion. Occlusion led to a slower recovery of skin impedance on the order of several hours to days for all treatment conditions when compared to non-occluded sites. Upon removal of occlusion, skin impedance rapidly increased. Graphs expressed as mean ± SD; n = 5 for t > 0, n = 10 for t ≤ 0.

We hypothesize that this slow barrier recovery under occlusion is due to the reduced transepidermal water loss under occlusive skin conditions. Previous studies have shown that stratum corneum barrier repair is regulated by the formation of a water gradient in the skin caused by increased transepidermal water loss through the compromised skin barrier (Grubauer et al. 1989). Occluding the skin with a vapour impermeable membrane introduces an artificial skin barrier and eliminates this gradient. As a result, the secretion of lamellar bodies and lipid synthesis, which are essential to repair and regulate the SC barrier, are significantly retarded, leading to prolonged barrier recovery (Grubauer, Elias et al. 1989; Menon, Feingold et al. 1992). Additionally, under occlusion, the skin becomes significantly hydrated. Hydration is the primary variable influencing the skin's impedance, with increased SC hydration leading to a reduction in skin impedance (Burnette and DeNuzzio 1997; Curdy, Naik et al. 2004).

This switch-like behaviour where microneedle-generated channels remain open under occlusion but close rapidly after removal of occlusion gives insight into the safety and efficacy of solid microneedle-based passive-delivery systems described earlier. This finding suggests that a drug-loaded occlusive patch can be applied to the skin immediately after solid microneedle treatment to enable prolonged drug delivery, followed by rapid skin resealing and termination of delivery upon patch removal. Additionally, the fast resealing of microneedle holes in the absence of occlusion reduces the chance of infection at the insertion site, which should increase safety of non-occlusive active-delivery microneedle systems such as hollow, drug-coated, and drug-encapsulated microneedles.

Figure 4.2a also shows that the no-treatment negative control line (G) gradually decreased during the first 10 to 12 h and then remained relatively constant for the remainder of the study until occlusion was removed. This reduction in impedance was due to the increased hydration of the skin under occlusion as described above. The non-occluded negative control on the other hand did not show this reduction in impedance, but rather, showed an erratic noisy behaviour (Figure 4.2b). This was also true for the non-occluded treated sites once they recovered (A-F). While the underlying reason for the erratic behaviour is not known, this could be due to a measurement artifact. For intact skin with high impedance, even a small change in the barrier or its hydration can have a large effect on the impedance values. In contrast, compromised skin with low impedance is relatively insensitive to such small changes.

4.1.4. Kinetics of Skin Barrier Recovery: Effect of Microneedle Design

This study also hypothesized that increasing microneedle length, number, thickness, and width leads to an increase in skin barrier recovery time. In order to test this hypothesis and to determine the time for the channels created by microneedles to recover, the impedance profiles for each treatment type were compared with that of the no-treatment negative control (G). The skin resealing time (Table 4.1) was determined as the time at which there was no significant difference between the treatment and negative control sites shown in Figure 4.2. This comparison controlled for the effects of hydration due to occlusion (in the case of the occluded sites) and thereby identified effects of the treatment itself.

Table 4.1: Skin resealing time and pain as a function of needle design and skin occlusion

	Time (h)[a]	
Design	**Occluded**	**Non-Occluded**
A	30	2
B	3	2
C	22	2
D	18	2
E	40	2
F	n/a	2

[a]Time to achieve non-significant difference of skin impedance from negative control.

Analysis of the occluded data revealed that the window of increased permeability showed strong dependence on microneedle geometry (Table 4.1). The non-occluded data on the other hand revealed that for all needle treatment conditions (A-F), the skin impedance increased rapidly and within 2 h of treatment, skin was resealed with no dependence on needle geometry.

To further elucidate the effect of microneedle geometry parameters on skin resealing under occlusion, we compared the resealing times based on changes in length, number, and cross-sectional area of microneedles as seen in Figure 4.3. Doubling the microneedle length while keeping other parameters constant led to a 6-fold increase in skin recovery time as revealed by comparison of geometries B (750 μm length) and D (1500 μm length). Further, comparing geometries C (500 μm length) and A (750 μm length) indicated that a 50% increase in microneedle length, while holding other parameters constant, led to approximately 35% increase in skin resealing time. Both these comparisons confirmed the hypothesis that increasing microneedle length increases skin barrier recovery time under the effect of occlusion.

The number of microneedles also affected skin resealing time with a 5-fold increase in number of needles corresponding to a 10-fold increase in barrier recovery time demonstrated by comparing geometries B (10-needle array) and A (50-needle array) (Figure 4.3). Further, a 4-fold increase in cross-sectional area led to a 33% increase in recovery time as revealed by comparing geometries A (w = 200 μm, t = 75 μm) and E (w = 500 μm, t = 125 μm). Under occlusion, microneedles with geometry E had the longest skin resealing time of 40 h. These results validated that increasing microneedle number and cross-sectional area led to an increase in barrier recovery time under occlusion.

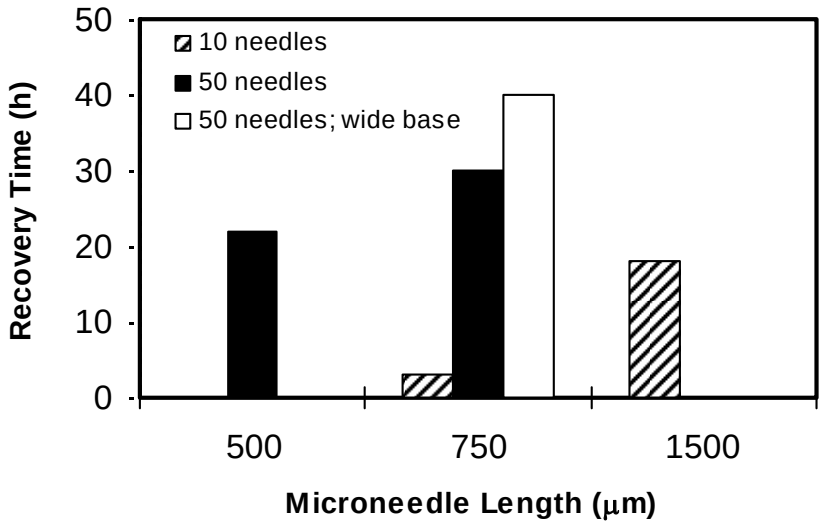

Figure 4.3: Comparison of skin barrier recovery time under occlusion based on microneedle length, number of microneedles, and cross-sectional area. Geometry E with 50 microneedles having length 750 μm, width 500 μm, and thickness 125 μm had the slowest recovery at 40 h under occlusion.

In the small array (10 needles), increasing needle length (geometry B vs. D) and increasing number of needles (geometry B vs. A) both dramatically increased recovery time. In the large array (50 needles), increasing needle length (geometry C vs. A) and increasing needle cross-sectional area (geometry A vs. E) both had much smaller effects

on recovery time. This suggests that very minor injury from a small number of short needles (geometry B) can be quickly repaired, but injury beyond some threshold exceeded by increasing needle length and/or number of needles significantly slows the repair process from a few hours to on the order of one day.

4.1.5. Relationship Between Microneedle Design, Recovery Time, and Pain

Overall, under occlusion, skin recovery depended on microneedle length, number, and cross-sectional area with length and number having the most sensitive effects. While these parameters have strong effects in increasing skin recovery time, they also have a significant effect on pain. We therefore hypothesized that microneedles causing increased recovery time also cause increased pain, because both are secondary measures of tissue injury. To test this hypothesis, we asked the subjects to report the VAS pain scores felt during each microneedle insertion. The pain scores for each subject were then normalized with respect to their corresponding hypodermic needle positive control (F) (Figure 4.4). All pain scores with the exception of geometry D were significantly different from the hypodermic needle F. Increasing the base cross-sectional area (A to E) led to the longest recovery time with no increase in pain.

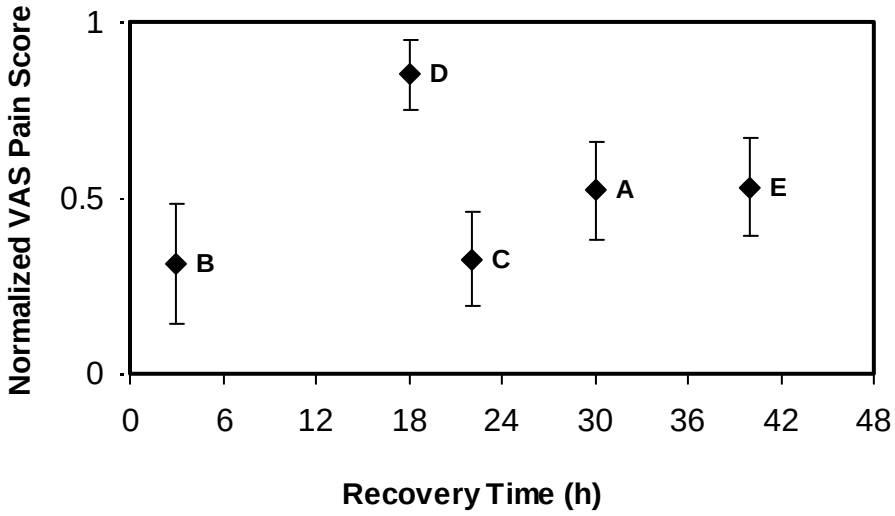

Figure 4.4: Normalized VAS insertion pain scores (with respect to hypodermic needle (F) positive control) for the 5 microneedle geometries as a function of recovery time under occlusion. VAS scores expressed as mean ± SD of occluded and non-occluded treatments, since pain was measured irrespective of skin condition; i.e. n = 20 for A-E and n = 10 for F.

Overall, all microneedle geometries with the exception of D were significantly less painful than the hypodermic needle control, F (one-way ANOVA followed by Tukey's post-hoc pairwise comparison; $p < 0.05$), and all microneedle geometries with the exception of D were not significantly different from each other (one-way ANOVA followed by Tukey's post-hoc pairwise comparison, $p > 0.05$). This finding is consistent with previous measurements of pain caused by microneedles, which showed that microneedle length is the most important factor (Gill, Denson et al. 2008). This finding also indicates that although varying microneedle length, number and area all affected skin resealing time, only microneedle length affected pain, over the range of parameters considered. These observations are inconsistent with our proposed hypothesis and suggest that aspects of tissue injury caused by microneedles that affect pain are different from those which affect resealing time. This could be explained because pain is

influenced by a direct interaction between microneedles and sensory nerve fibers, whereas resealing time is influenced by damage to the stratum corneum, which is devoid of nerves. The finding that skin resealing time and pain are not directly coupled presents opportunities for design of microneedle devices that cause prolonged skin permeability (under occlusion), but still cause little or no pain. It appears that using larger numbers of needles with larger cross-sectional area, rather than long needles, can accomplish this goal (e.g., geometry E).

4.1.6. Skin Impedance to Predict Transdermal Drug Delivery

In order to determine if the skin impedance results in this study can be used to predict transdermal drug delivery following microneedle-based poke and patch treatment, we compared our data to a study carried out in collaboration with the University of Kentucky to deliver naltrexone to human subjects after treatment with the same microneedles used in this study (Appendix B). Two microneedle arrays with geometry A were inserted four times each into the forearm of six healthy subjects to create a total of 400 micro-channels per subject. A naltrexone gel patch was then placed over the treated area and covered by an occlusive dressing for 72 h. Data from that study show that plasma naltrexone concentration increased over the first few hours and then held relatively steady for the remaining 72 h study (Figure B.1). As a first comparison, our study found that the resealing time for microneedle geometry A was 30 h, which contrasts with the finding shown in Appendix B that naltrexone concentration remained elevated for at least 72 h. This result, however, can be explained by the fact the naltrexone study inserted arrays of microneedle geometry A a total of 8 times into the skin (i.e., 400 micro-channels), whereas our prediction of skin resealing is based on a

single insertion (i.e., 50 micro-channels). Given the strong dependence of skin resealing on the number of microneedles seen when comparing a 10-needle array to a 50-needle array, increasing from 50 needles to, effectively, 400 needles could further increase resealing time. In addition, our impedance data measured the time taken for the SC barrier to repair, whereas the naltrexone delivery study measured the kinetics of plasma naltrexone levels. Plasma drug levels are influenced not only by SC permeability, but also by drug diffusion through the skin and into the bloodstream and by drug elimination from the bloodstream, which in the case of naltrexone has a half-life of 4.4 h, and from a possible drug depot within the skin often associated with transdermal delivery.

To provide a more detailed comparison between the naltrexone data and our predictions of drug delivery based on skin impedance measurements, we developed a single-compartment pharmacokinetic model to predict plasma naltrexone concentration over time. In order to do this, we first sought to estimate a relationship between the permeable area of skin available for drug transport after microneedle treatment and skin impedance. To do this, we assumed that the channels created by microneedles have a cylindrical geometry and then correlated the total pore size to skin impedance using the following relation:

$$A_{permeable} = \frac{\rho L}{Z} \tag{4.1}$$

where $A_{permeable}$ is the total permeable area of all micro-channels created by an array, ρ is the electrical resistivity of interstitial fluid in the skin (~78 Ω-cm (Trajanoskil, Schaupp et al. 1996)), L is the length of the diffusional pathways in the stratum corneum (~15 μm, which is the average thickness of the SC (Prausnitz and Langer 2008)), and Z is the

absolute skin impedance measured during the study. We then determined a relationship between flux across skin and skin impedance using Fick's first law of diffusion according to which the theoretical transdermal flux ($J_{Theoretical}$) of a drug-loaded patch across skin treated with microneedles can be described as:

$$J_{Theoretical} = K_p \, \Delta C_{patch} \tag{4.2}$$

where ΔC_{patch} is the difference in drug concentration in the patch and in the body (~160 mg/mL (Appendix B)), and K_p is the permeability of skin treated with microneedles defined by:

$$K_p = f \times \frac{D}{L} \qquad \text{(McAllister, Wang et al. 2003)} \tag{4.3}$$

In this equation, D is the diffusion coefficient for naltrexone at infinite dilution in water as determined via Stokes-Einstein equation (= 4.6×10^{-6} cm^2/sec, using a molecular diameter of 9.15 A for naltrexone (Iyer, Barr et al. 2007)), L is the length of the micro-channel created by the microneedle in the stratum corneum, and f is the fractional skin area containing holes from microneedles and can be expressed as $A_{permeable}/A_{MN\text{-}array}$, where $A_{permeable}$ is given by equation 4.1 developed above and $A_{MN\text{-}array}$ is the area of the microneedle array for which impedance measurements were taken. Using these relations, the theoretical transdermal flux ($J_{Theoretical}$) of a drug loaded patch across skin treated with microneedles is given by:

$$J_{Theoretical} = \frac{\rho D \Delta C_{patch}}{Z(t) A_{MN-array}} \tag{4.4}$$

Using the above relation, we developed a single compartment pharmacokinetic model to predict the plasma concentration of naltrexone (c) over time (t) as follows:

$$\frac{dc}{dt} = \frac{N \rho D \Delta C_{patch}}{V_{dist} Z(t)} - \frac{Cl\ c(t)}{V_{dist}} \qquad (4.5)$$

where N is the area of microneedles arrays in the clinical naltrexone study divided by the area of arrays in this impedance study (i.e. 8/1), V_{dist} is the apparent volume of distribution for naltrexone (~1350 L (Pagliaro and Pagliaro 1998)), Z(t) is the absolute skin impedance measured in this study, and Cl is the total body clearance of naltrexone (~3.5 L/min (Pagliaro and Pagliaro 1998)). This equation indicates that the rate of change of the naltrexone plasma concentration is equal to the rate of absorption of naltrexone (first term on right hand side of equation) minus the rate of elimination (second term on right hand side of equation). The absorption term containing impedance was obtained by multiplying the Flux (equation 4.4) by the area of the arrays used in the naltrexone study and dividing by the volume of distribution. The elimination term was simply defined as the elimination rate constant ($k_{el} = Cl/V_{dist}$) multiplied by the naltrexone concentration as commonly used in pharmacokinetic analysis (Davidian and Giltinan 1995). Therefore, all parameters in this model are based on properties of the drug and skin and the model does not contain any fitted parameters. Figure 4.5 shows a plot of the experimental (from Appendix B) and predicted (from equation 4.5) plasma naltrexone concentrations over a 30 h period.

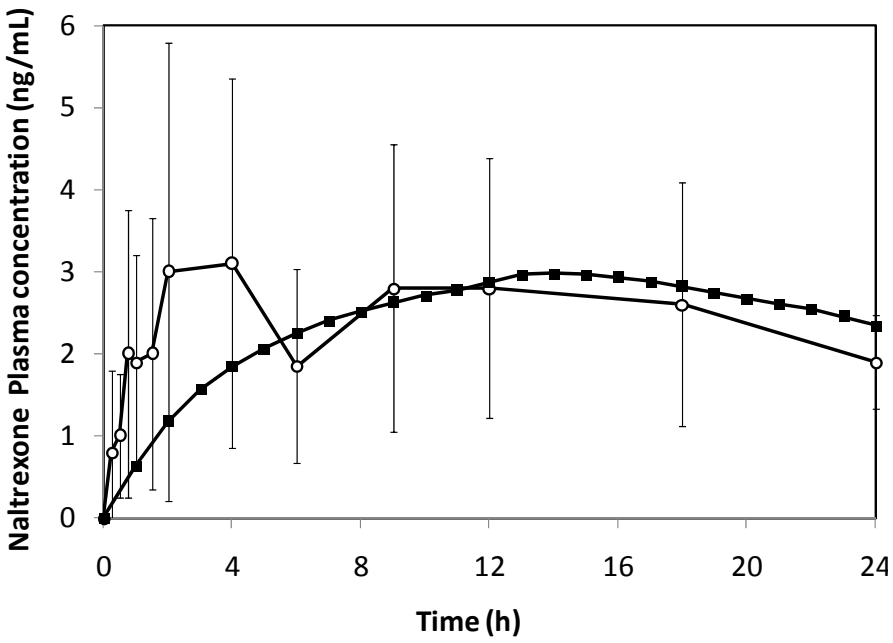

Figure 4.5: Plasma concentrations of naltrexone from (○) experimental study involving delivery of naltrexone to human subjects, and from (■) theoretical prediction using equation 4.5 for 30 h. The predicted data are in agreement with the experimental results. Experimental data are expressed as mean ± SD n = 6.

As seen in the figure, both graphs saw an initial increase in naltrexone concentrations and then remained relatively steady. The concentration profile plotted for the experimental data is an average of the six subjects who participated in the study and hence the peak concentration and the time to peak concentration in this graph are not representative of the true peak values. The real peak concentration from the naltrexone delivery experiment was found to be 4.5 ± 2.5 ng/mL and the time to this peak was 8.8 ± 7.6 h. The predicted naltrexone profile led to a peak concentration of 3 ng/mL at 13 h. A χ^2 test to compare the experimental plasma concentrations of naltrexone and the predicted concentrations from Equation 4.5 revealed that the predicted data is in agreement with the experimental observations ($\chi^2 = 5.16 < \chi^2_{\text{critical value}} = 21.06$). These results indicate that

skin impedance can be used to predict drug concentrations in the body after microneedle-based delivery to within the accuracy of the experimental data.

4.1.7. Conclusions

This study validated the hypothesis that increasing microneedle length, number, and cross-sectional area in conjunction with occlusion leads to an increase in skin resealing time that can exceed one day. Results indicated that occlusion significantly retards skin barrier recovery after microneedle treatment. However, skin rapidly reseals in the absence of occlusion. The study also revealed that the initial degree of skin permeabilization created by microneedles is relatively insensitive to the length, number, or cross-sectional area of the microneedles. However, these parameters do play a significant role in the SC resealing process. Longer, increased number, and larger cross-sectional area needles recovered more slowly under the effect of occlusion. Analysis of pain scores demonstrated that only increasing microneedle length increased pain, which suggests that the duration of increased skin permeability can be extended without increasing pain through increasing the number of microneedles rather than their length. Overall, this study demonstrated that microneedles can be used to increase skin permeability over timescales ranging from as little as 2 h to as long as 40 h. This study also validated that skin impedance measurements can be used to predict transdermal flux *in-vivo*.

The findings of this study have implications for both passive and active microneedle delivery systems. From an efficacy standpoint, piercing skin with microneedles can provide increased skin permeability to facilitate drug delivery from a transdermal patch over a period of almost 2 days. However, increased skin permeability

can be quickly reversed in the absence of occlusion due to the rapid skin resealing that occurs under these conditions. This simple dependence of skin permeability on skin occlusion provides an inherent safety feature that allows skin to reseal rapidly after removal of microneedles at the end of an active delivery process (e.g. injection) or after patch removal at the end of passive drug delivery through long-lived micro-channels.

4.2. Flow Conductivity in Human Skin During Microneedle Infusion

4.2.1. Introduction

Hollow microneedles of various geometries and materials have been fabricated as a less painful and potentially more effective alternative to hypodermic needles for delivering liquid drug formulations into the skin by targeting the dermal capillaries for systemic uptake and the dermal dendritic cells for vaccine delivery. However, to date, arrays of microneedles have been shown to deliver only 1 µl (Sivamani, Stoeber et al. 2005) of fluid into the skin of human subjects without significant pain while single microneedles have been used to deliver 120 µl (Laurent, Bonnet et al. 2007). This is due to the resistance to fluid flow offered by the dense dermal structure.

Previous studies have demonstrated that the low flow conductivity of skin to microneedle-based delivery is due to the skin itself as a result of compression of the dermal structures and not the microneedles alone (Sivamani, Stoeber et al. 2005; Martanto, Moore et al. 2006b). The dermis is a dense matrix consisting of a continuous phase (e.g. water, electrolytes) within a network of coarse fixed elements such collagen fibrils and elastin, as well as fibrous molecules such as GAGs, and PG core proteins that are imobilized by collagen mesh. All these materials together offer dermal resistance to fluid flow (Levick 1987; Swartz and Fleury 2007). However, the extent of this dermal

resistance to microneedle-based fluid delivery, the parameters effecting it, and its effect on pain have not been studied in human subjects.

Further, the skin has a vast network of nerves, which can potentially be stimulated by fluid injection. Several cutaneous branches of spinal and cranial nerves pass through the subcutaneous space into the dermis, where the axons spread to form three horizontal plexuses (Kiernan and Barr 2008). The papillary plexus lies in the papillary layer, just below the epidermis (at the dermal-epidermal junction) and consists of Merkel receptors and Meissner's corpuscles which are usually sensitive to touch and pressure (Kandel, Schwartz et al. 2000); the dermal plexus lies within the dense reticular dermis, and the subcutneous plexus lies in the hypodermis (Kiernan and Barr 2008). Several free nerve endings which are sensitive to pain lie in the subcutaneous tissues and the dermis and a few extend to the cells of the epidermis. The free nerve endings in the dermis run parallel to the skin's surface whereas the nerve endings near the epidermis typically lie perpendicular to the skin's surface (Palastanga, Field et al. 2006). The subcutaneous and dermal layers also contain several additional nerve corpuscles and receptors with larger receptive fields. Pain associated with hypodermic needle injection is typically stimulated by deeper nerve receptors instead of superficial receptors (Gajraj, Pennant et al. 1994).

In order to use hollow microneedles for clinical applications it is essential to understand the parameters affecting the skin's flow conductivity. It is also important to understand the effect of these parameters on patient pain perception. Th objective of this study was to determine the effect of the following parameters: microneedle insertion depth, needle retraction, infusion flow rate, and the presence of hyaluronidase (an agent responsible for breaking down the dense dermal matrix) on flow conductivity of skin to

microneedle-based fluid delivery as well on associated pain. The resulting data were used to determine optimum delivery characteristics for practical clinical applications.

4.2.2. Flow Conductivity

The flow conductivity of skin was determined by measuring the pressure associated with fluid delivery into skin through microneedles since pressure is inversely related to flow conductivity of tissue (Levick 1987; Jackson, Hussain et al. 2006).

4.2.2.1. Effect of Depth

To determine the pressures associated with microneedle-based fluid delivery in skin and to validate the hypothesis that the dermis offers resistance to fluid flow through microneedles *in-vivo*, saline was delivered to skin through microneedles inserted at 90^{o} into the dermis at 500 μm (T1)[1], 750 μm (T2), and 1 mm (T3) and into the subcutaneous space at 4 mm (T4). A hypodermic needle (T5) was also inserted into the dermis almost parallel to the skin's surface using the Mantoux technique (Laurent, Bonnet et al. 2007). Figure 4.6 depicts the pressure versus volume profile at a constant delivery flow rate of 0.3 mL/min. As seen in Figure 4.6, intradermal microneedle delivery (T1-T3) led to an increase in pressure as more saline volume was delivered into the skin. Pressures reached as high as 3000 mmHg upon delivery of the entire 1 mL dose. There were no significant differences (one-way ANOVA; $p > 0.05$) in pressures at any of the volumes between the three intradermal depths indicating that regardless of the insertion depth, the dermal resistance is the same at a given flow rate.

[1] T1 – T9 nomenclature described in section 3.5.2.

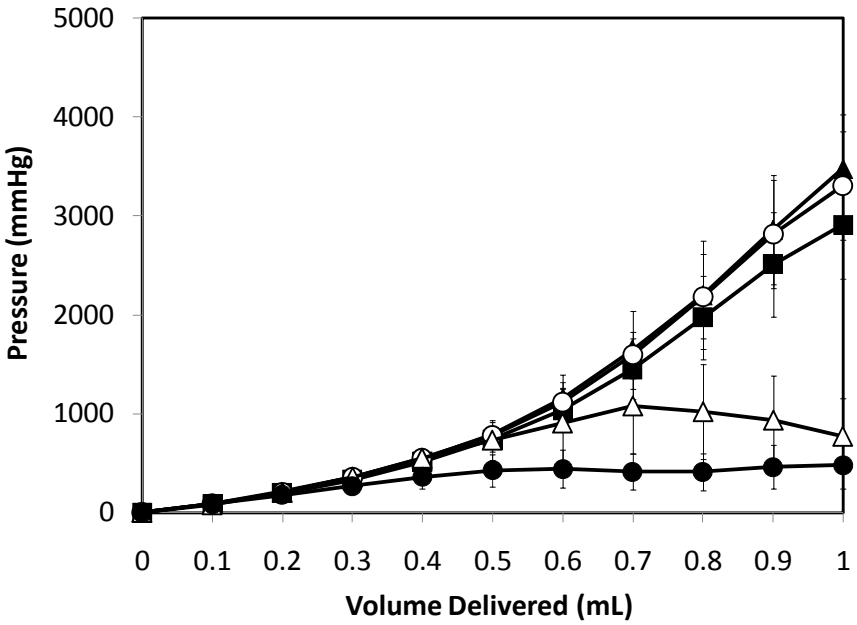

Figure 4.6: Effect of needle insertion depth on skin resistance to flow. Microneedles were inserted into the dermis at (▲) T1 = 500 µm, (■) T2 = 750 µm, and (○) T3 = 1 mm. A microneedle was inserted into the subcutaneous space at (△) T4 = 4 mm. A hypodermic needle (●) T5, was also inserted intradermally. All infusions were performed at the medium flow rate of 0.3 mL/min. Data are expressed as mean values ± SD, n = 10.

Insertion of microneedles into the hypodermis at 4 mm (T4) led to an initial increase in pressure up to ~ 600 µl after which the pressures appeared to somewhat stabilize (Student's t-test; $p > 0.05$) and then decline (Student's t-test; $p > 0.05$ for comparison between 0.9 and 1 mL) leading to a significant difference in pressures between sites T1-T3 and T4 during the last 300 µl (one-way ANOVA, Tukey's post-hoc comparison; $p < 0.05$). This stabilization in infusion pressure during subcutaneous delivery is due to the loose tissue network of the subcutaneous space and due to the large volume of interstitial fluid available in the hypodermis. This observation of stabilization of pressures during subcutaneous delivery confirmed the hypothesis that the dermis offers resistance to fluid flow through microneedles. However, as seen in Figure 4.6, it was

also noted that delivery into the dermis via a hypodermic needle (Mantoux method) did not lead to high pressures as seen in T1-T3, but rather a slight increase in pressure to ~ 300 mmHg until delivery of 300 µl, beyond which the pressures remained constant (one-way ANOVA; $p > 0.05$). The pressure for T5 was significantly less than that of T1-T3 throughout the infusion procedure except the first 300 µl (one-way ANOVA; $p > 0.05$ for volumes ≤ 300 µl). This observation appears to contradict the hypothesis that the dermis offers high resistance to fluid flow. However, it must be noted that hypodermic needle (T5) insertion and flow occurred at an orientation almost parallel to the skin whereas microneedle insertion and flow occurred perpendicular to the skin surface. The dermal fibers are generally aligned parallel to the skin's surface and fluid flow in the same orientation as the fibers offers significantly less resistance than flow perpendicular to the dermal fibers (Swartz and Fleury 2007). Therefore, hypodermic needle-based fluid flow which was almost in the same orientation as the dermal fibers experienced significantly less resistance to flow. On the other hand, hollow microneedle-based infusion occurred perpendicular to the fiber orientation and hence these fibers offered higher resistance to flow. Additionally, the vertical microneedle insertion led to compression and compaction of the dense coiled fibers in the dermis. This compaction led to a decrease in hydration (due to pushing away of interstitial fluid between the dermal components) and tissue porosity which caused an increase in pressure and flow resistance (Levick 1987; Bert and Reed 1998; Martanto, Moore et al. 2006a). On the other hand, the hypodermic needle did not lead to this tissue compression. Figure 4.6 also showed that the pressures appeared to increase gradually first and then increased more quickly after approximately 500 µl. We hypothesize that this is due to the following flow pattern: when fluid flows out of the

needle bevel, it first accesses the fiber layers near the micron-sized needle opening and flows along these tightly packed layers, leading to increasing pressures. Since the tissue beneath the needle tip is compacted due to compression from the needle, the fluid then accesses the fiber layers located above the bevel opening towards the less dense papillary dermis leading to stretching of the skin and an increase in fluid pressures. Flow into these layers located at the level of the needle tip and above is likely able to stretch the skin enough due to its viscoelastic nature to accommodate 500 µl of fluid while leading to increased pressures and the formation of a skin wheal (as will be seen later in this chapter). At this point, the coiled collagen fibers are likely stretched significantly and in order to allow more fluid to flow into the skin, the fluid now has to access the deeper, compressed, dense, reticular dermis layers below the needle tip, which leads to a more rapid increase in pressure.

Overall, the results from this graph demonstrated that the skin's structure offers increased resistance to flow for microneedles inserted vertically into the skin's surface due to flow against dermal fibers and compaction of the dermal structures.

4.2.2.2. Effect of Retraction

Previous *in-vitro* studies have shown that microneedle insertion into the dermis followed by retraction increases flow conductivity of skin, with almost complete needle retraction leading to a significant increase in flow due to de-compression of the dermal tissue components that were compacted during perpendicular needle insertion (Martanto, Moore et al. 2006a; Martanto, Moore et al. 2006b). However, since these studies were performed *in-vitro* where skin elasticity and tension conditions were far from that of

living human tissue and since only micro-liter quantities of fluid were delivered, the true extent of microneedle retraction effect on flow conductivity was not characterized.

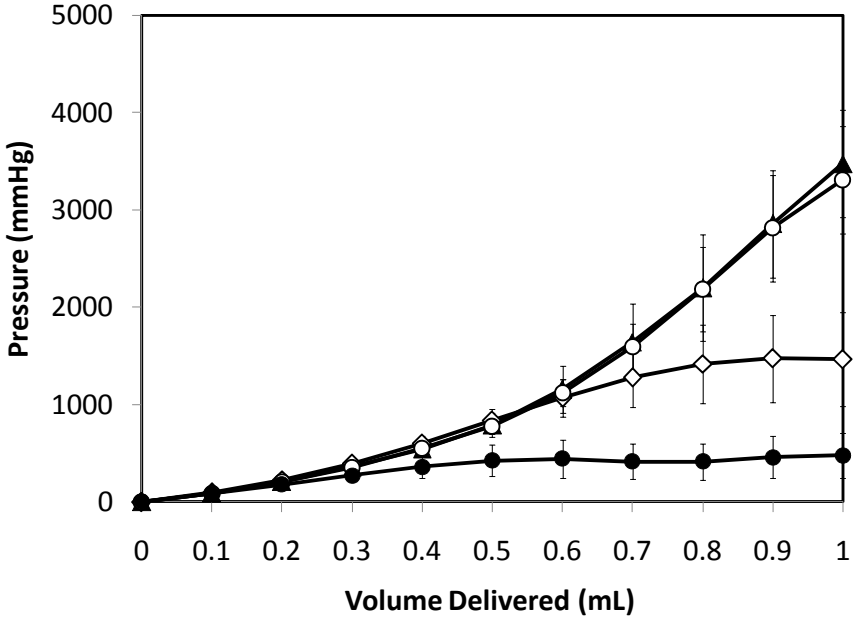

Figure 4.7: Effect of needle retraction on skin resistance to flow. Microneedles were inserted into the dermis at (▲) T1 = 500 µm, (○) T3 = 1 mm, and at 1 mm followed by retraction back to 500 µm, (◇). A hypodermic needle (●) T5, was also inserted intradermally. All infusions were performed at the medium flow rate of 0.3 mL/min. Data are expressed as mean values ± SD, n = 10.

In this study, saline was infused at a rate of 0.3 mL/min through a single microneedle that was inserted 1 mm into the dermis for approximately 5 seconds and then retracted to 500 µm. Figure 4.7, shows that the infusion pressure for the retracted needle (T6) increased up to a volume of 600 µl beyond which the pressure increased very gradually and started to stabilize (one-way ANOVA; $p > 0.05$). Delivery of 1 mL with retraction required pressures less than half of that required to deliver to 500 µm (T1) or 1 mm (T3) in the absence of retraction. A two-way ANOVA revealed that the pressures for T1, T3, and T6 were comparable up to 600 µl beyond which the T6 values were significantly lower than that of T1 and T3 indicating retraction began to play a significant

role at this point. We hypothesize that this behaviour of flow conductivity is likely due to initial flow of fluid into the pathway created by retraction (<< 10 µl), followed by flow into the less dense papillary dermis and then the more dense reticular dermis leading to an increase in pressure and formation of a skin wheal (as seen later in this chapter). As more fluid was infused and the pressure continued to increase, the retraction pathway likely expanded leading to tissue damage and ultimate reduction of pressures due to flow into the damaged dermis and possibly into the deeper dermis. This hypothesis of tissue damage and flow to the deeper dermis is further confirmed by the results of the infusion pain scores as seen later in this chapter. An additional reason for the lower later pressures seen by retraction as compared to T1 to T3 could be the one described by previous *in-vitro* studies (Martanto, Moore et al. 2006a; Martanto, Moore et al. 2006b), that microneedle insertion followed by retraction reduced compression of the dermis at the needle tip and hence did not lead to as high pressures as without retraction. It should, however, be noted that although retraction reduced infusion pressures (compared to T3) due to likely reduction in tissue compaction, the pressure was still higher than that of hypodermic needles. This is presumably due to the delivery of fluid perpendicular to the fibers via vertically inserted microneedles as described previously. Additionally, while tissue compression might have been reduced due to retraction, it may not have been completely eliminated. Overall, while all three microneedle conditions (T1, T3, T6) allowed delivery of 1 mL of fluid into the skin, the later low pressures seen by T6 indicate that retraction increases flow conductivity of skin which is consistent with the previous *in-vitro* data.

4.2.2.3. Effect of Infusion Flowrate

To determine the effect of infusion rate on flow conductivity, saline was delivered into the dermis at a depth of 750 μm at three different flow rates of 0.1 mL/min (T8 = low), 0.3 mL/min (T2 = medium), and 1 mL/min (T7 = fast). As seen in Figure 4.8, the slow flow rate saw an increase in pressures until 700 μl was infused after which the pressures started to stabilize (one-way ANOVA; $p > 0.05$). This is presumably due to the fact that at this point as more saline was infused, the saline depot created near the needle tip would slowly clear from the insertion site creating space for more saline to enter with minimal additional resistance. The stabilization of pressure beyond this point indicates that the rate of saline clearance from the needle tip region was the same as the infusion flow rate of 0.1 mL/min (steady-state) and more saline could continue to be delivered at this flow rate.

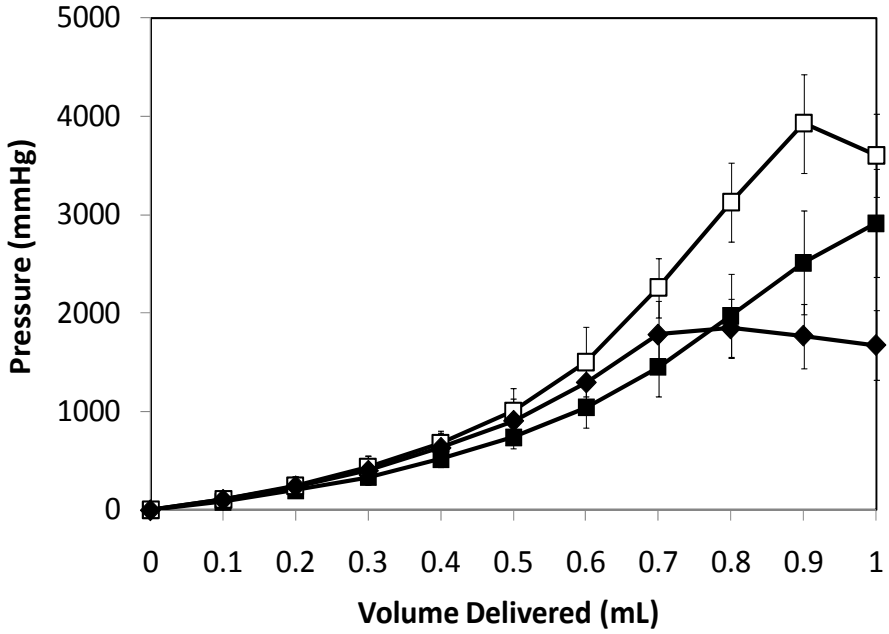

Figure 4.8: Effect of infusion flowrate on skin resistance to flow. Microneedles were inserted into the dermis at 750 μm and saline was infused at rates of (◆) T8 = 0.1 mL/min, (■) T2 = 0.3 mL/min, and (□) T7 = 1 mL/min. Data are expressed as mean values ± SD, n = 10.

Infusion at the medium flow rate (T2) led to an initial gradual increase in pressure up to approximately 500 µl beyond which the pressure continued to increase in a slightly more rapid manner as described previously. On the other hand, infusion at the faster flow rate saw higher pressures than T2 and T8 (beyond 400 µl, one-way ANOVA, Tukey's post-hoc comparison; $p < 0.05$) that appeared to increase more rapidly than the low and medium flow rates. However, as the pressures continued to rise, upon reaching almost 4000 mmHg (at 900 µl), the pressure appeared to decrease, however, the difference was not significant (Student's t-test; $p > 0.05$). We hypothesize that this might be due to tissue damage in the deeper dermis caused by the high fluid pressure within the skin. Most subjects reported a sharp piercing pain at this high pressure (discussed later in this chapter) which further validates our hypothesis that tissue damage may have occurred. Overall, an increase in flow rate led to an increase in skin flow resistance for undamaged skin while a decrease in flow rate led to stabilization of skin flow resistance at higher volumes.

4.2.2.4. Effect of Hyaluronidase

To further test the hypothesis that the dermis offers resistance to fluid flow, hyaluronidase, an enzyme which is known to reduce skin's flow resistance by breaking down glycosaminoglycans within collagen fibrils (Levick 1987) was delivered via microneedles at 0.3 mL/min and compared to saline delivery at the same conditions. The pressure associated with hyaluronidase delivery increased up to 600 µl beyond which the pressures started to stabilize (one-way ANOVA; $p > 0.05$), while the saline delivery pressures continued to rise. This reduction in pressure shows that the dermal structural components consisting of proteoglycans and glycosaminoglycans are a contributing

factor to skin's resistance to flow as their subsequent degradation by the infusion of hyaluronidase led to an increase in flow conductivity.

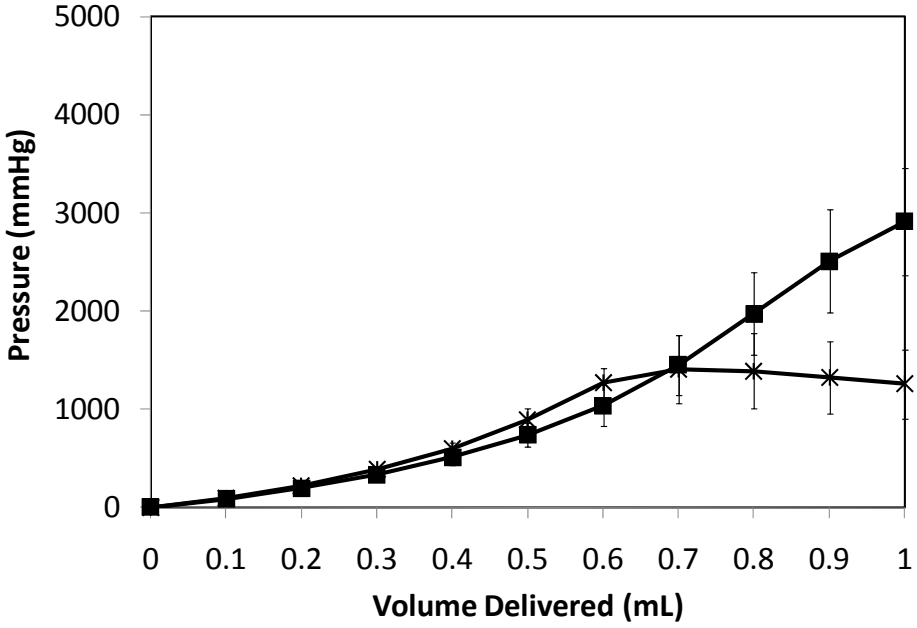

Figure 4.9: Effect of hyaluronidase on skin resistance to flow. Microneedles were inserted into the dermis at 750 µm and (■) saline, T2 and (✳) hyaluronidase, T9 were infused at a rate of 0.3 mL/min. Data are expressed as mean values ± SD, n = 10.

4.2.3. Microneedle Insertion Pain

Analysis of pain scores was performed for microneedle insertion and fluid infusion. First, to determine the pain associated with microneedle insertion, retraction, and hypodermic needle insertion, subjects were asked to rate the pain they felt using the VAS scale. Figure 4.10 shows that all microneedle-based intradermal insertions, including needle insertion followed by retraction, were less painful than the hypodermic intradermal needle control insertion (one-way ANOVA, Tukey's post-hoc comparison; $p < 0.05$). These hollow microneedle results are consistent with previous solid microneedle pain study results (Kaushik, Hord et al. 2001; Gill, Denson et al. 2008; Haq, Smith et al.

2009). While previous studies compared results to hypodermic needles inserted vertically into the subcutaneous space where it is expected that needle insertion will cause pain due to the stimulation of nerve bundles in the subcutaneous region; the results in this study show that microneedles are also less painful than hypodermic needles inserted intradermally using the Mantoux method. This is likely due to the fact that the hypodermic needle was inserted into the skin at an acute (almost parallel) angle to a length of almost 3 mm, thereby leading to piercing of a larger tissue area and consequently increasing the chances of encountering dermal nerve endings. Additionally, due to lack of a depth control mechanism for the Mantoux technique, the intradermal insertion of hypodermic needles could still reach the deeper dermis and further stimulate the free nerve endings located in the deeper nerve plexus. Moreover, the microneedles used in this study were thinner than the 26-gauge intradermal hypodermic needle and hence had a lower chance of stimulating dermal nerve endings (Arendt-Nielsen, Egekvist et al. 2006). The 4 mm subcutaneous microneedle insertion was as painful as the hypodermic needle insertion (Student's t-test; $p > 0.05$). This is presumably due to stimulation of nerve fibers in the deeper dermis as well as the subcutaneous space.

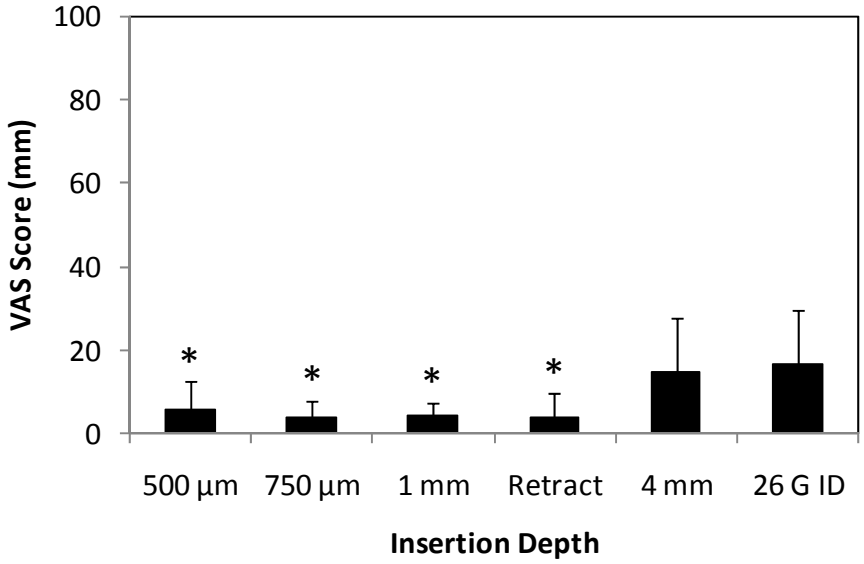

Figure 4.10: Absolute microneedle insertion pain scores on a 100 mm VAS scale for the five microneedle depths and the 26-gauge intradermal needle. Data are expressed as mean ± SD and n = 10 for all cases, except 750 µm where pain scores from T2, T7-T9 were averaged and n = 40 in this case. * $p < 0.05$.

4.2.4. Fluid Infusion Pain

Analysis of pain associated with fluid infusion was performed to determine which study parameters led to more painful delivery and thereby determine parameters to minimize pain. The pain scores were also used to interpret the flow conductivity data as changes in pain sensation during infusion may help understand what is happening in the skin. In order to do this, subjects were asked to rate the pain they felt during infusion at 200 µl intervals. The pain scores were normalized relative to the hypodermic needle insertion scores and plotted as a function of volume.

4.2.4.1. Effect of Depth

The effect of needle depth of infusion pain was studied at a constant flow rate of 0.3 mL/min (Figure 4.11). The pain for the shallowest insertion depth site, T1 at 500 µm was not affected by an increase in volume delivered (or infusion pressure). The pain for

T1 remained almost constant throughout the 1 mL delivery (one-way ANOVA; $p > 0.05$). Upon delivery of the final 200 µl, the pain slightly increased, however, it was not significant from the previous 800 µl. This is presumably due to the fact the fluid remained in the upper dermal layers and in spite of the high infusion pressure, did not flow deep enough to contact the deeper dermal free nerve endings. The slight (but non-significant) increase during the last 200 µl indicates that further fluid delivery may lead to further increase in pain at volumes greater than 1 mL. Comparison of the T1 infusion pain scores at all volumes with the T1 insertion scores revealed no significant difference (one-way ANOVA; $p > 0.05$).

The pain scores for T2 (750 µm) and T3 (1 mm) infusion increased gradually over the infusion procedure, however, the increase was not significant until the last 200 µl (one-way ANOVA, Tukey's post-hoc comparison; $p < 0.05$). This increase in pain after delivery of 800 µl could be due to fluid flowing into the deeper dermis under high pressure experienced by T2 and T3 at these volumes, subsequently stimulating the dermal pain receptors in the dermal plexus. While T1 also experiences similar pressures, it is likely that the 250 µm difference in depth between T1 and T2 was enough to prevent fluid from flowing deep enough to cause pain. This pain could also be due to large spreading of fluid within the dermis itself thereby increasing the chances of encountering nerves. The increased pain during the last 200 µl (for T2 and T3) was described by subjects as slight burning which confirms that mechanical receptors in the dermis were stimulated as they are responsible for eliciting burning sensation (Rook, Burns et al. 2004). Comparison of the T2 and T3 infusion pain scores with their respective insertion scores revealed no significant difference until the last pain measurement (one-way

ANOVA; $p > 0.05$ till 800 µl). Further, there was no significant difference between the pain scores for T1, T2, and T3 during the entire infusion process (two-way ANOVA; $p > 0.05$) indicating that increasing or decreasing microneedle depth within the dermis did not significantly affect infusion pain.

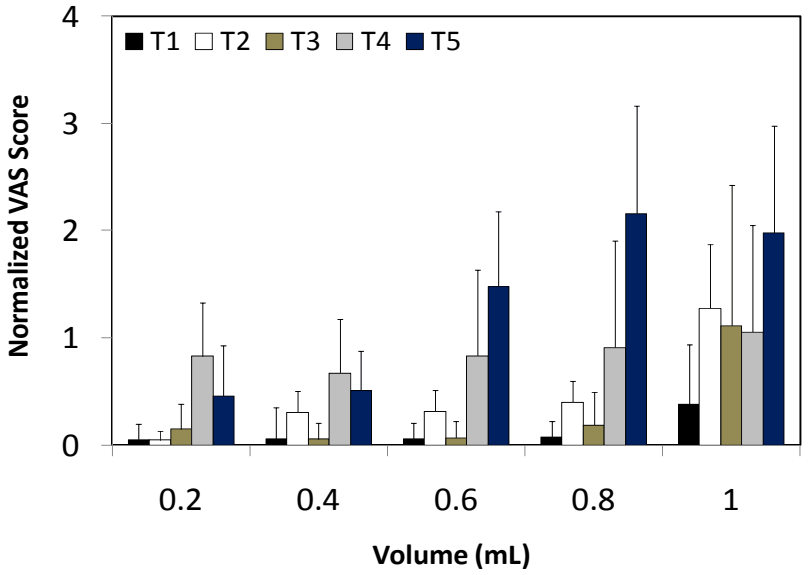

Figure 4.11: Normalized (relative to hypodermic needle insertion) pain scores over the 1 mL infusion process to determine the effect of microneedle depth on infusion pain. T1 = 500 µm, T2 = 750 µm, T3 = 1 mm, T4 = 4 mm (subcutaneous), and T5 = hypodermic needle (intradermal). All infusions took place at the medium flow rate of 0.3 mL/min and delivered saline. Data are expressed as mean ± SD and n = 10 for all sites.

Subcutaneous delivery through the 4 mm microneedle (T4) led to pain scores that were as high as the 4 mm insertion pain throughout the 1 mL infusion (one-way ANOVA; $p > 0.05$). This is possibly due to the needle being in contact with the subcutaneous nerves during the entire infusion process and also due to flow of fluid in to the hypodermis where nerve fibers and corpuscles with large receptive fields are present. Further, even though subjects were asked to not consider the insertion pain in the infusion scores, it is possible that some of this high infusion pain is attributed to residual pain

from the needle insertion procedure itself. Overall, there was no effect of volume on the pain associated with infusion through microneedle site T4 (one-way ANOVA; $p > 0.05$).

Intradermal delivery through the hypodermic needle (T5) led to pain scores lower than the needle insertion itself for the first 400 µl (one-way ANOVA, Tukey's post-hoc comparison; $p < 0.05$). During infusion of the remaining 600 µl, the pain scores continued to increase with volume and were as painful as the hypodermic needle insertion itself (one-way ANOVA, $p > 0.05$). This is probably due to spreading of saline within the dermis leading to an increased probability of contacting nerves and also due to flow into the deeper dermis, and possibly even the hypodermis to some extent, thereby causing stimulation of the nerves in these regions and subsequent increase in pain over time. Further, the hypodermic needle infusion pain scores were relatively higher than that of intradermal microneedle infusions (T1-T3) during the first 400 µl (but not always significantly different). The hypodermic injection pain scores were significantly higher for the next 400 µl (two-way ANOVA, Tukey's post-hoc comparison; $p < 0.05$), and then the pain scores were comparable for the last 200 µl (two-way ANOVA; $p > 0.05$).

4.2.4.2. Effect of Retraction

Although retraction led to a significant increase in flow conductivity, retraction also led to a significant increase in pain upon delivery of 600 µl and beyond (one-way ANOVA, $p < 0.05$). This 600 µl volume is also the point beyond which the delivery pressures started to stabilize (as seen in Figure 4.7). This is probably because during the initial part of the infusion, fluid was delivered into the small tear created by the needle retraction ($<<$ 10 µl) followed by flow to the papillary dermis above the needle tip and the reticular dermis near the needle tip leading to stretching of the skin and an increase in

pressure. As the infusion pressure continued to the rise, the fluid continued to flow into the tear created by the needle retraction causing expansion of this region and possibly leading to tissue damage, thereby causing pain. Further, since the pain score for T6 at 600 µl is comparable with that at 1 ml for the 1 mm infusion, it is also likely that some of the fluid might have flown deeper into the dermis which may also be the cause of pain. Further, the retraction infusion pain scores were comparable with the pain scores associated with needle insertion and retraction procedure for the first 400 µl (one-way ANOVA; $p > 0.05$) after which the infusion pain scores were significantly higher for the remainder of the infusion (Tukey's post-hoc comparsion; $p < 0.05$). The retraction delivery pain scores were significantly higher than the T1 and T3 scores for the 600 µl and 800 µl measurements.

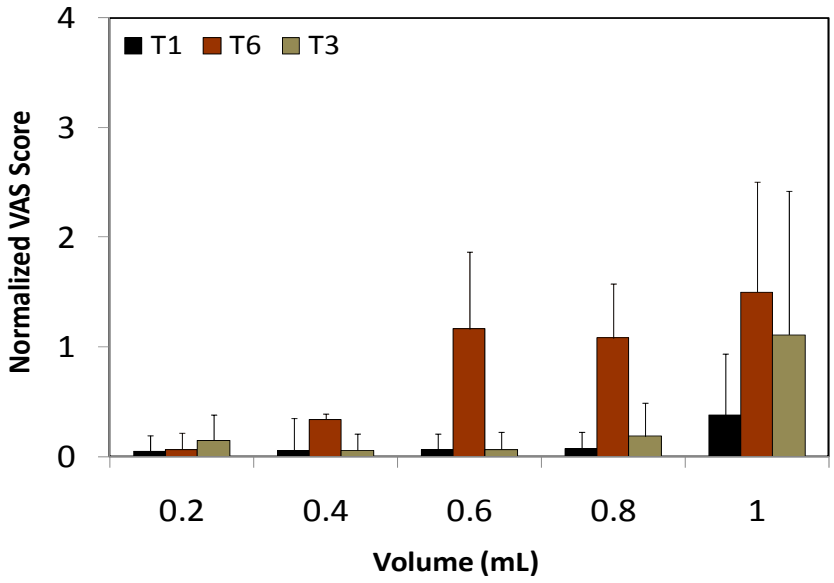

Figure 4.12: Normalized (relative to hypodermic needle insertion) pain scores over the 1 mL infusion process to determine the effect of retraction on pain. T1 = 500 µm, T2 = 750 µm, T6 = 1 mm insertion followed by retraction to 500 µm. All infusions took place at the medium flow rate of 0.3 mL/min and delivered saline. Data are expressed as mean ± SD and n = 10 for all sites.

4.2.4.3. Effect of Infusion Flowrate

The lowest flow rate, T8 = 0.1 mL/min led to minimal pain scores (Figure 4.13) which increased slightly during the infusion process, however, the difference was not significant (one-way ANOVA; $p > 0.05$). These pain scores were also similar to the corresponding T8 insertion pain scores which were significantly less than that of hypodermic needles. This low pain throughout the 1 mL saline infusion is presumably due to the clearance of saline from the delivery site leading to low pressures which did not lead to saline flow to the deeper dermis. As described previously, the medium flow rate (T2) saw an increase in pain during the last 200 µl, presumably due to flow of fluid into the deeper dermis, thereby contacting free nerve endings in the dermal nerve plexus or due to spreading of fluid within the dermis increasing the possibility of encountering nerves. The high flow rate of 1 mL/min (T7) also saw an increase in pain scores with increasing volume; however, the pain was not significant until the last 200 µl. During the last 200 µl, the pain was also significantly higher than the needle insertion pain (one-way ANOVA, Tukey's post-hoc comparison; $p < 0.05$). As seen in (Figure 4.8) previously, the flow conductivity also appeared to slightly decrease towards the end of infusion. This is likely due to tissue damage caused by the high fluid pressure and also due to the subsequent flow of saline into the deeper dermis. Further, (70%) of subjects reported a sharp piercing sensation during infusion of the last 200 µl during T7 delivery indicating that there was likely damage to the skin structure leading to this pain. Comparisons of pain scores among the three different flow rates revealed no significant differences until the last 200 µl at which point the pain associated with low flow rate delivery was significantly less than that of the high flow rate (two-way ANOVA, Tukey's post-hoc

comparison; $p < 0.05$). Therefore increasing infusion flow rate did not have a significant effect on increasing pain for delivery up to 800 µl.

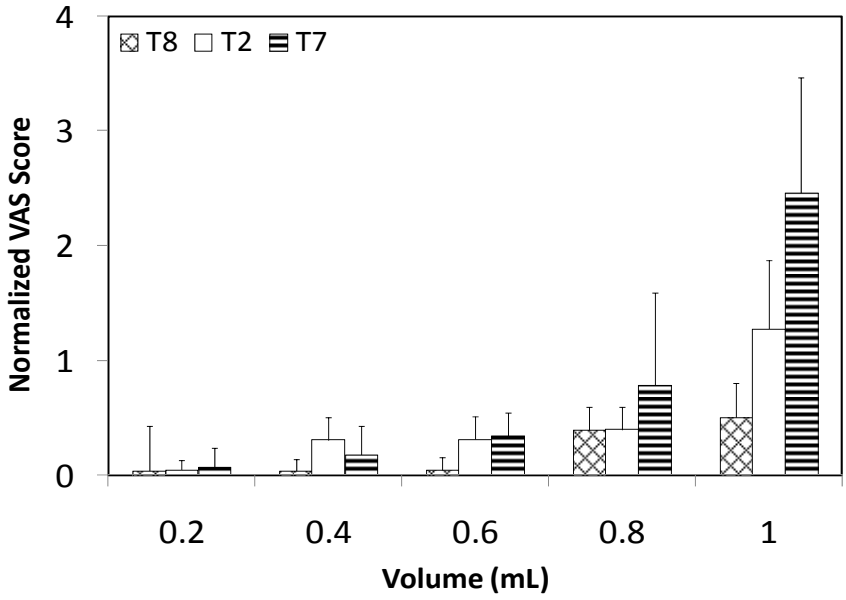

Figure 4.13: Normalized (relative to hypodermic needle insertion) pain scores over the 1 mL infusion process to determine the effect of infusion flow rate on pain. T8 = 0.1 mL/min (low flow rate), T2 = 0.3 mL/min (medium flow rate), T7 = 1 mL/min (fast flow rate). All infusions took place at the depth of 750 µm and delivered saline. Data are expressed as mean ± SD and n = 10 for all sites.

4.2.4.4. Effect of Hyaluronidase

As seen from Figure 4.14, the VAS pain scores for hyaluronidase, T9, remained constant throughout the delivery procedure (one-way ANOVA; $p > 0.05$). This is because the hyaluronidase broke down the dense dermal tissue structure which could allow the fluid to access a larger volume of skin and thereby reduced the need to form micro-cracks in the tissue which could be painful. Comparisons of pain scores for the saline (T2) and hyaluronidase (T9) infusion procedures indicated similar pain scores, except for the final measurement point where the saline delivery was more painful than hyaluronidase (two-way ANOVA, Tukey's post-hoc comparison; $p < 0.05$). The T9

infusion and needle insertion pain scores were comparable at all volumes (one-way ANOVA; $p > 0.05$).

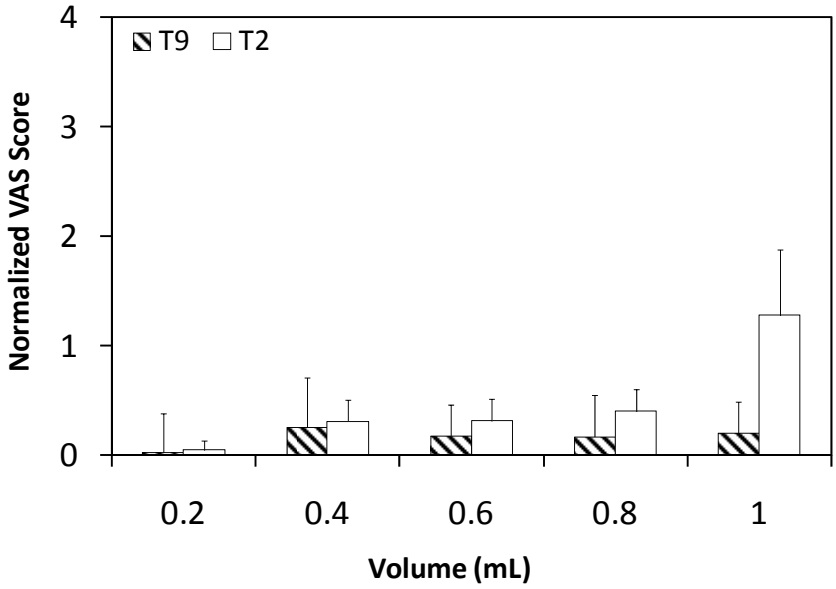

Figure 4.14: Normalized (relative to hypodermic needle insertion) pain scores over the 1 mL infusion process to determine the effect of hyaluronidase on pain. T8 = hyaluronidase, T2 = saline. All infusions took place at the depth of 750 µm and a flow rate of 0.3 mL/min. Data are expressed as mean ± SD and n = 10 for all sites.

4.2.5. Pain and Pressure Relation

As seen from the analysis of pain scores, the pain values typically increased with volume towards the end of the infusion process. However, as seen in Figure 4.15, which shows a scatter plot representation of the normalized VAS pain scores versus pressure; pain scores did not always increase with pressure. As seen from this figure and from the infusion pain analysis described above, only sites T2 (750 µm depth), T3 (1 mm depth), and T7 (high flow rate, 1 mL/min) saw a significant increase in pain scores with increasing pressure.

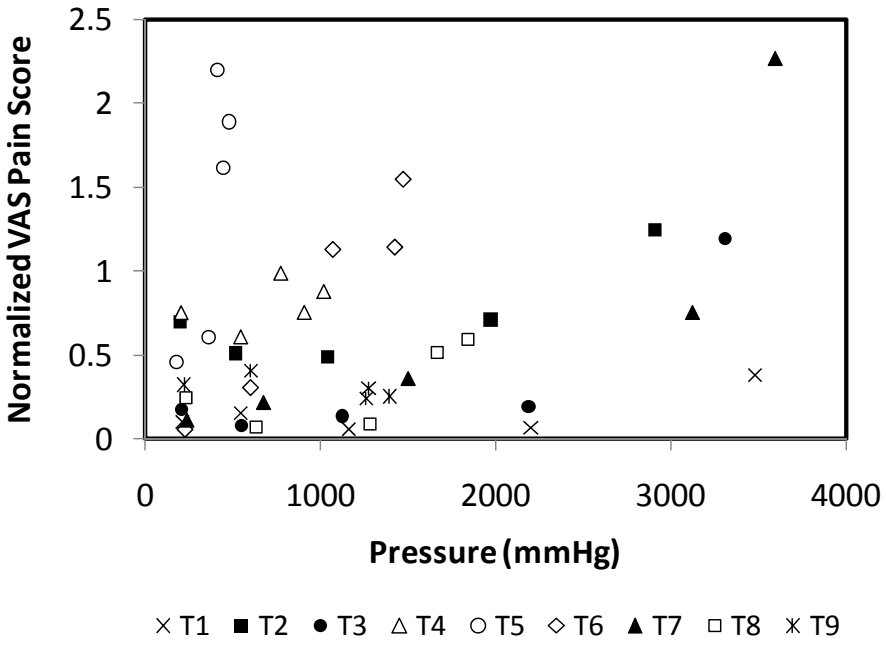

Figure 4.15: Scatter plot representation of the normalized VAS scores for all experimental conditions as a function of pressure. T1 (×) = 500 µm, 0.3 mL/min; T2 = (■) 750 µm depth, 0.3 mL/min; T3 (●) = 1 mm depth, 0.3 mL/min; T4 (△) = 4 mm depth, 0.3 mL/min; T5 (○) = 26-gauge intradermal hypodermic needle, 0.3 mL/min; T6 (◇) = 1 mm insertion, 500 µm retraction, 0.3 mL/min; T7 (▲) = 750 µm depth, 1 mL/min; T8 (□) = 750 µm depth, 0.1 mL/min; T9 (✳) = hyaluronidase, 750 µm depth, 0.3 mL/min. Data are expressed as mean for n = 10.

To determine the pressure levels that caused pain to increase significantly, the normalized VAS scores were plotted for these 3 sites over the pressure ranges measured (Figure 4.16). Pain scores for sites T2 and T3 significantly increased above 3000 mmHg and those for T7 increased significantly above 3500 mmHg (two-way ANOVA, Tukey's post-hoc comparison; $p < 0.05$). This could be attributed to either extreme stretching of the skin under high pressures, thereby leading to pain or due to flow of saline into the deeper dermis under high pressure thereby stimulating nerves or also due to subsequent tissue damage within the skin.

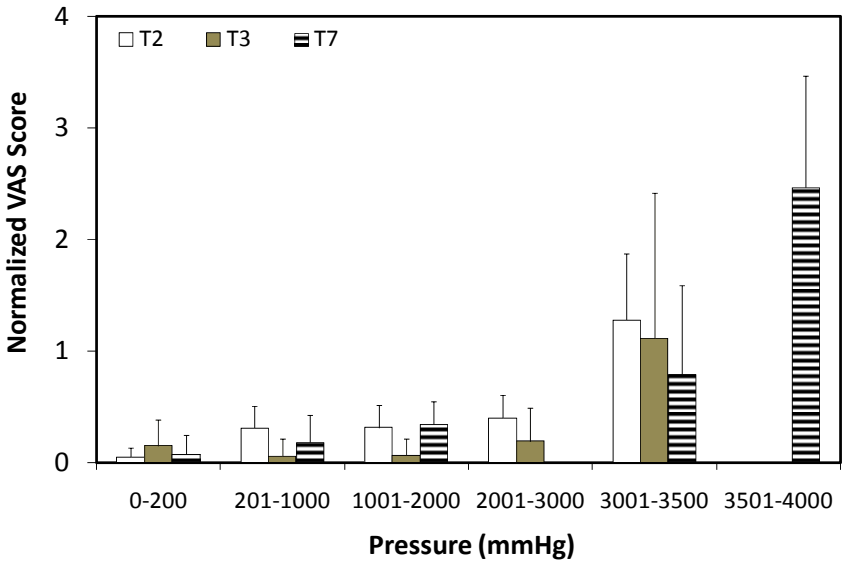

Figure 4.16: Normalized pain scores (relative to hypodermic needle insertion) as a function of pressure for sites T2 (saline, 750 µm, 0.3 mL/min), T3 (saline, 1 mm, 0.3 mL/min), and T7 (saline, 750 µm, 1 mL/min).

4.2.6. Overall Perception of Pain

Upon completion of infusion for each treatment site, subjects were asked to rate their perception of pain for the overall infusion procedure ranging from no pain to worst possible pain. Figure 4.17, shows the results from this survey. More than 75% of the subjects rated all microneedle treatment sites, including the 4 mm subcutaneous insertion as being no more than mildly painful whereas only 36% rated hypodermic needles this way. Further, approximately 25% of the subjects rated the shallow (T1 = 500 µm), slow (T8 = 0.1 mL/min), and hyaluronidase (T9) delivery procedures to be not painful at all. Moreover, almost 10% of subjects considered the subcutaneous 4 mm delivery (T4) and the hypodermic needle intradermal delivery (T5) to be severely painful. No intradermal microneedle procedures were considered to be severely painful or as the worst possible pain.

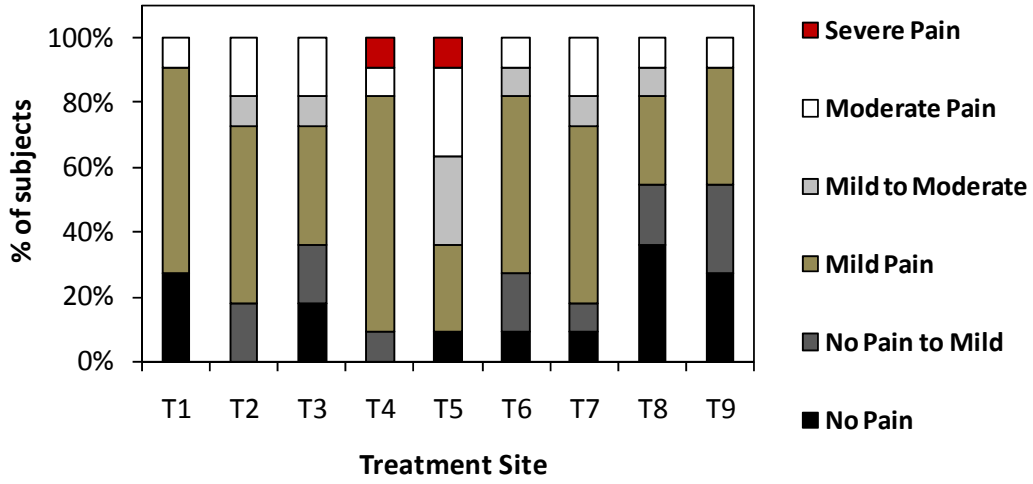

Figure 4.17: Overall perception of pain for the 9 treatment sites. Subjects were asked to rate the overall pain (insertion and infusion) for each treatment site as no pain, no pain to mild pain, mild pain, mild to moderate pain, moderate pain, moderate to severe pain, severe pain, and worst possible pain. n = 10 for each treatment site.

4.2.7. Skin Observation

Lastly, all skin sites were visually examined and imaged by photography and ultrasound echography before and after treatment as seen in Figure 4.18. Visual observation immediately after infusion revealed that all sites with the exception of subcutaneous injection via T4 were characterized by skin the formation of a characteristic skin wheal or bleb (raised skin surface due to stretching of the skin) indicating that all or part of the fluid delivered was within the dermis. Formation of such a bleb is a well known characteristic of intradermal injections and is expected during microneedle delivery (Springhouse 2005). Raised local blanching was also seen at the injection site. The bleb completely subsided within 2 h for all treatment sites. While most microneedle site blebs had similar characteristics and measured approximately 1.5 cm in diameter, the hyaluronidase bleb appeared slightly less raised and more dispersed laterally (~1.8 cm diameter). This could be due to the fact the hyaluronidase is a spreading agent and hence

flowed more readily within the skin due to breakdown of the dermal matrix. Further, the 4 mm subcutaneous microneedle injection did not produce any bleb either since no saline was deposited within the dermis. All 9 treatment sites experienced slight erythema which was mostly resolved within 2 h and completely resolved in 24 h. The hypodermic needle site also experienced punctate redness at the needle insertion site which resolved within 24-48 h.

Figure 4.18 also shows ultrasound echographs to supplement the skin photographs. The ultrasound image depicts the different layers of the skin as different echogenic layers. The thin bright white line at the topmost part of the image depicts the epidermis; the green layer (with red and yellow areas) below it is the dermis. The black area below the dermis is the hypodermis. Comparison of before and after echographs for all intradermal microneedle sites (T1-T3, T6-T9) show a thicker dermis and curved skin structure after infusion. The thicker dermis is due to the swelling of skin as a result of fluid injection within the dermis and the curved structure represents the curvature of the bleb. The subcutaneous delivery site does not show these characteristics further confirming that fluid was delivered to the hypodermis, as expected. Further, most intradermal images also show a thin dark region between the epidermis and dermis after infusion (illustrated by red arrows in Figure 4.18). We hypothesize that this dark space may represent saline that is present in the dermal/epidermal junction and the papillary dermis. Further, dark spaces are also seen within the dermis after infusion for all intradermal delivery sites. It is likely that these regions also represent the saline delivered to the dermis. The dark spaces for the T1 to T3 echographs (yellow arrows) show a trend of moving deeper in the dermis for the three images respectively providing

evidence that this region could represent the saline. The insertion/retraction site, T6 also shows a dark space beginning at approximately 500 μm and continuing throughout the thickness of the dermis which could possibly be along the saline flow channel/tissue damage region. The T7 site shows several small dark spaces between the green color representing the dermis beginning at 750 μm. The slow flow rate site, T8 indicated swelling as seen by the thicker green dermal layer, however, does not show any dark deeper regions. This is presumably because the pressures for T8 were not high enough to push fluid deeper into the dermis. The hyaluronidase site, T9 has a low-echogenic (less density of brightness, i.e: less yellow and red) dermis as compared to the before image and also compared to after images of saline infusion sites. Several dark spaces are seen among the green region (orange arrow). These dark regions could represent spaces filled with either interstitial fluid or excess hyaluronidase after the breakdown of the dense dermal matrix.

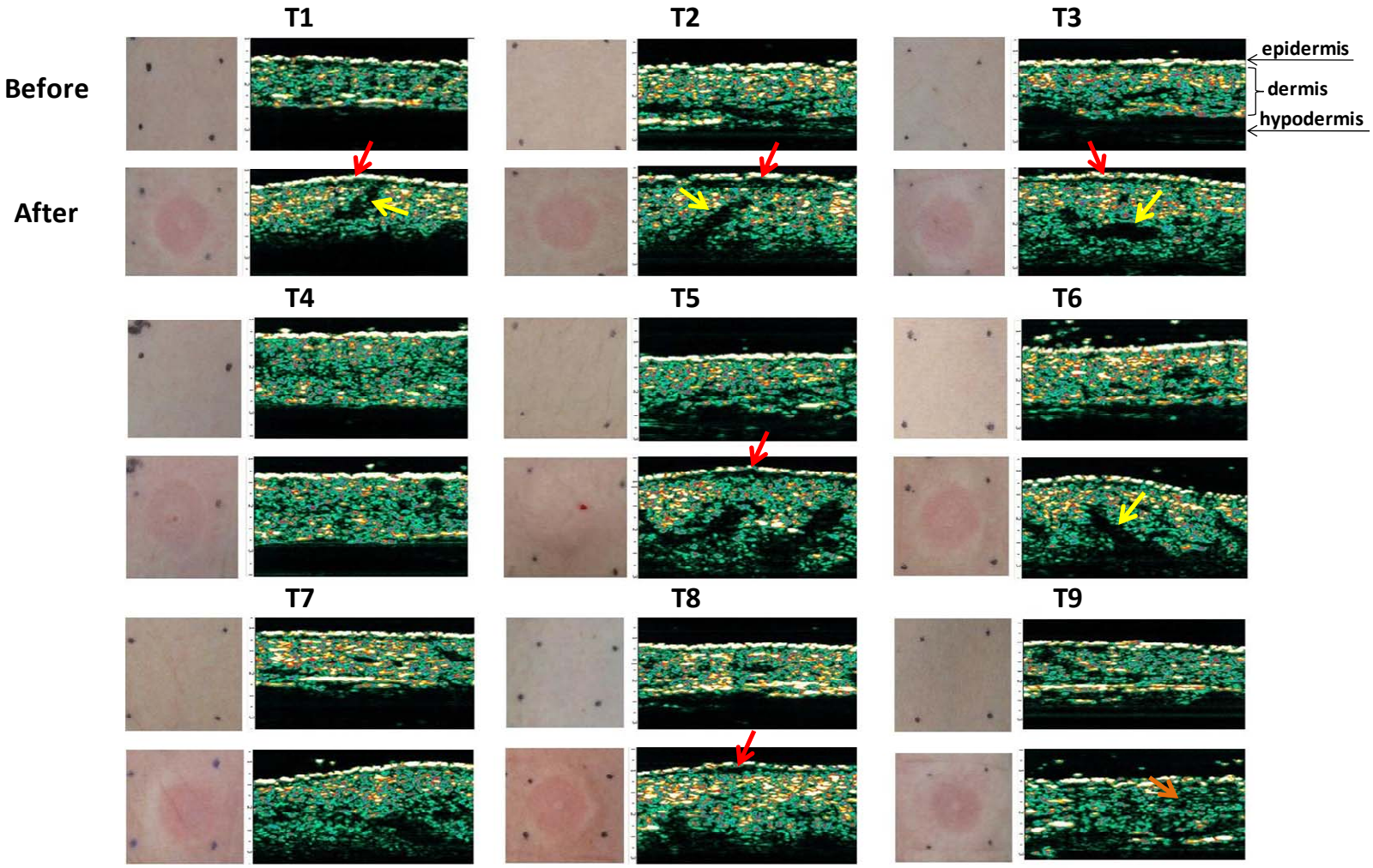

Figure 4.18: Before and after photographs (immediately after) and echographs (~ 5 min after) of skin sites. The bright white line on the top of the echograph represents the epidermis; the green layer below it depicts the dermis; the black region below the dermis is the hypodermis. Red arrows indicates dark space between epidermis and dermis which may possibly depict saline. Yellow arrows indicate possible saline depots/pathways. The orange arrow indicates low echogenic regions after hyaluronidase delivery.

4.2.8. Conclusions

Therefore, in conclusion, this experiment studied the effect of microneedle and infusion parameters on flow conductivity of skin and associated pain for the first time. Microneedle-based delivery within the dermis led to an increase in infusion pressures due to the high resistance offered by the skin. Microneedle retraction and low infusion flow rates helped reduce the skin resistance to allow fluid to be delivered at low pressures. Further, the addition of hyaluronidase led to breakdown of the dermal components, thereby increasing flow conductivity. The pain analysis from this study helped interpret the flow data to understand the possible flow of fluid within the skin and also helped determine the parameters causing pain. Pain scores indicated that microneedles can be used to deliver liquid drugs up to 800 µl in volume regardless of insertion depth (without retraction) and flow rate without significant increase in pain from that of the needle insertion itself. This is practical for clinical purposes, since most intradermal applications are indicated to deliver of no more than 500 µl of bolus drug due to the low volume capacity of the dermis as compared to the hypodermis (Washington, Washington et al. 2001; Lynn and Evans-Smith 2003). In the unusual event that intradermal delivery of larger volumes is required, shallow insertion depth, low infusion flow rates, and the addition of hyaluronidase can help reduce pain.

4.3. Insulin Delivery to Type 1 Diabetes Subjects using Hollow Microneedles[2]

4.3.1. Introduction

Insulin was first administered in 1922 by intramuscular injection. However, it was rapidly determined that subcutaneous insulin delivery had similar efficacy to intramuscular injections but was significantly less traumatic (Cefalu 2004). Subcutaneous administration was subsequently established as the new delivery standard. Insulin is currently delivered through the subcutaneous route by means of hypodermic needles, insulin pens, and catheters connected to insulin pumps. However, these treatment methods are inconvenient and painful and often lead to poor patient compliance, especially among children and adolescents with type 1 diabetes. These patients have a tendency to omit their insulin injections because of fear, pain, anxiety, and inconvenience associated with subcutaneous needles and catheters (Hanas and Ludvigsson 1997; Zambanini, Newson et al. 1999; Mollema, Snoek et al. 2001; Hanas 2004), leading to poor diabetes management.

It has been 87 years since insulin was first given to individuals with diabetes, yet subcutaneous administration continues to remain the prevalent means of insulin delivery. In order to improve patient compliance, there is a need for new and improved delivery systems. Intradermal insulin delivery is an attractive administration route because it is less invasive than subcutaneous delivery. Additionally, the presence of a rich capillary bed in the dermis may allow for rapid uptake of drugs delivered intradermally. Previous studies have shown that intradermal delivery can accelerate the pharmacokinetics of

[2] This work was published in part as Gupta, J., Felner, EI, and Prausnitz, M.R. "Minimally invasive insulin delivery in subjects with Type 1 diabetes using hollow microneedles", Diabetes Technology and Therapeutics 2009;11(6):329-337.

proteins (Guy 2007). The pharmacokinetics and pharmacodynamics of intradermal insulin, however, have not been studied. Additionally, current intradermal systems involve use of the Mantoux technique where a hypodermic needle is carefully inserted at an angle into the skin so as to reach the dermis. This method is unreliable as it is difficult to correctly place the needle within the dermis and requires medical personnel to administer the injection (Mikszta and Laurent 2008). Hence, patients cannot self-administer using this method.

Inhaled insulin is another alternative to subcutaneous insulin delivery, and is noninvasive and can eliminate the pain and apprehension associated with injections. However, introduction of the first Food and Drug Administration approved inhalable insulin, Exubera (Pfizer, New York, NY), failed to achieve patient and physician acceptance for various reasons such as low bioavailability, high cost, cumbersome device design, side effects, and unknown health risks (Bailey and Barnett 2007; Barnett 2008). Moreover, it requires continued delivery of basal insulin through traditional subcutaneous methods. Several other novel and minimally invasive delivery methods such as oral, buccal, transdermal, and nasal systems are being investigated to determine effectiveness and increased patient compliance; however, these technologies are mostly still in preclinical development. Hollow microneedles have the potential to serve as a minimally invasive intradermal insulin delivery system to increase patient compliance. These microneedles can reduce the pain, apprehension, and inconvenience associated with insulin delivery because they are long enough to breach the skin's barrier and allow for transport of large molecules such as insulin, yet short enough to avoid stimulating nerve endings.

This chapter presents the first proof-of-principle study showing delivery of insulin through a microneedle device in human subjects with type 1 diabetes. To first determine the ideal microneedle insertion depth and then evaluate the effect of insulin delivery through a microneedle, the study was carried out in three phases. In the first phase, the minimum microneedle insertion depth was determined based on the pharmacodynamic response to insulin delivery at different microneedle insertion depths within the skin. In the second phase, the minimum depth was used to determine the efficacy of hollow microneedle insulin delivery in reducing postprandial glucose levels. In the third phase, the pharmacokinetics, pharmacodynamics, and pain associated with microneedle-based insulin delivery were compared to that of conventional insulin catheter-based delivery.

4.3.2. Phase 1: Effect of Microneedle Insertion Depth

To determine the minimum transdermal insertion depth of microneedles for effective insulin delivery, we initially administered 10 units of 100-U Humalog insulin to Subject 1 using a conventional 9 mm catheter. As expected, plasma free insulin levels rose, reaching a peak at t_{max} = 1 h (Figure 4.19a), and plasma glucose levels decreased correspondingly (Figure 4.19b). At the next two study visits, the subject received a bolus of 10 and 15 units of 50-U humalog at microneedle insertion depths of 5 mm and 3.5 mm, respectively. Although at both of these depths, t_{max} occurred at 30 min after bolus delivery, both plasma insulin concentration values were lower than that of the catheter. The plasma glucose levels decreased correspondingly, however, at slower rates than in the case of the standard catheter. We then used the microneedle to deliver 15 units of 50-U insulin intradermally at a shallow depth of 1 mm. This led to a significant increase in

insulin levels with a peak at t_{max} = 30 min. Plasma glucose levels declined very rapidly, and the test was discontinued at 1 h because of hypoglycaemia.

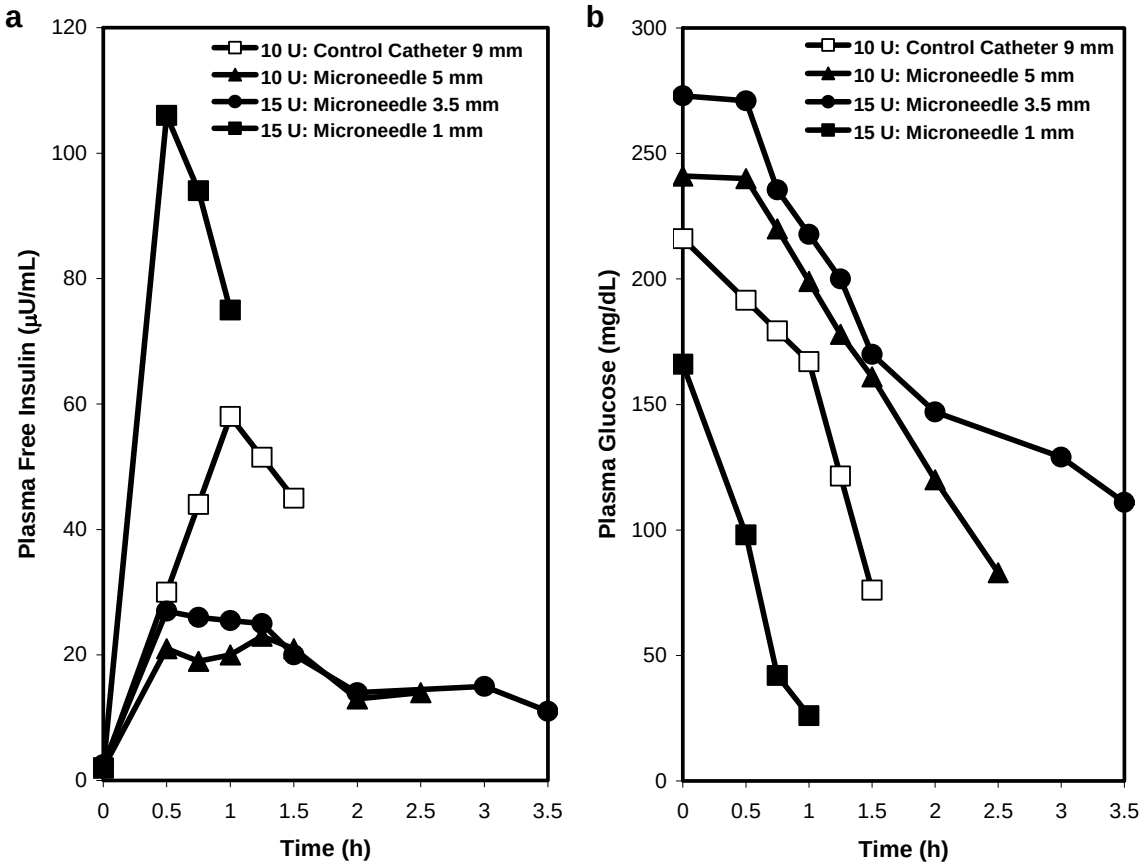

Figure 4.19: Microneedle-based insulin delivery at 1, 3.5, and 5 mm insertion depths in comparison to 9-mm catheter control (Phase 1). a) Plasma free insulin level and b) corresponding plasma glucose level response. Microneedle-based insulin delivery at 1 mm led to high insulin absorption and rapid glucose level reduction.

A comparison of the area under the insulin curves (AUICs) for the first hour after delivery (Figure 4.20a) indicated that the 1-mm microneedle led to higher insulin absorption than the other study and control treatments. Further, comparison of the change in plasma glucose levels over the first hour after insulin delivery (Figure 4.20b) revealed that the shallow 1-mm microneedle delivery was most effective in reducing glucose levels. These comparisons were made only during the first hour since data for all

four delivery conditions were available only for the first hour (as a result of stopping some experiments due to hypoglycaemia).

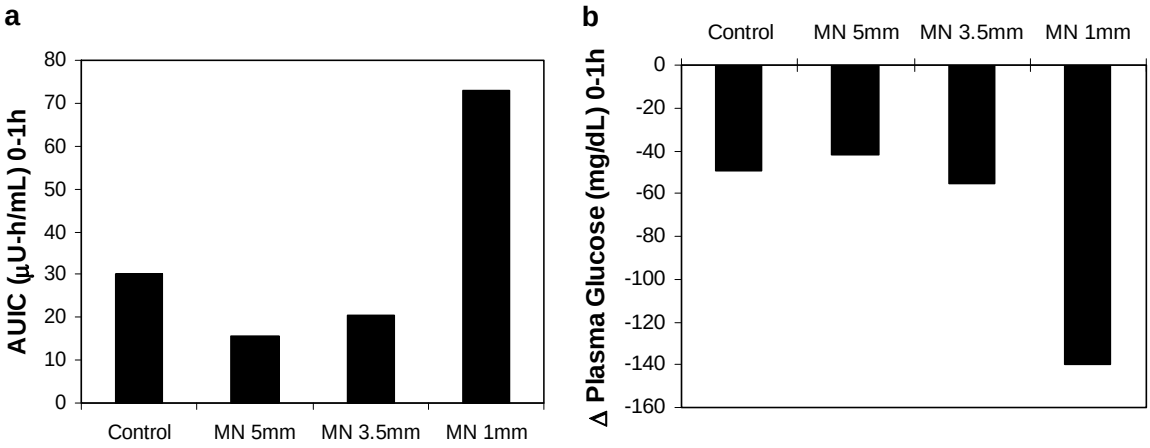

Figure 4.20: Microneedle-based insulin delivery results for Phase 1. a) AUIC for 0-1 h and b) change in plasma glucose levels from 0 to 1 h. Within 1 h of insulin bolus, the 1-mm microneedle (MN) delivery case led to an AUIC more than twice that of the catheter control and produced a higher change in plasma glucose levels.

This phase revealed that the 1 mm microneedle depth had the fastest pharmacokinetics and pharmacodynamics. We hypothesize that this is due to the fact that the microneedle targeted the papillary dermal region, which has a rich capillary network (Lawrence, Bell et al. 2006). It is this heavily vascularized area that likely permits effective insulin uptake and systemic absorption. Although this result could also be attributed to the fact that the experiment at 1 mm involved 50% more insulin than the 9-mm catheter case, the increase in AUIC and change in plasma glucose levels are both more than doubled at 1 mm, which suggests that there may be increased efficacy. Moreover, subcutaneous delivery at 3.5 mm also used a 50% higher insulin dose than the control but had a lower AUIC than both the 1-mm microneedle and the 9-mm control, which also suggests increased efficacy and is consistent with our hypothesis that uptake by dermal capillaries may be the cause of faster pharmacokinetics and dynamics. The

3.5-mm and 5-mm deliveries had lower insulin peaks and slower glucose response compared to the 9-mm catheter, which may be due to the fact that the microneedle was not deep enough in the hypodermis for effective systemic delivery. This explanation is consistent with Subject 1's observation from her daily experience that she typically has poor absorption in the upper hypodermis and generally requires long infusion sets (> 9 mm) for effective delivery.

Overall, this phase of the study led to establishment of the 1-mm microneedle depth as not only the minimum, but also the optimum, transdermal depth for effective insulin delivery among the three microneedle depths considered. Microneedle-based delivery at the 1 mm depth was at least as effective as subcutaneous catheter delivery. Based on these findings, this depth was used in phase 2 on the second subject to determine effect of microneedle insulin delivery on postprandial glucose levels.

4.3.3. Phase 2: Effect of Microneedle-Based Insulin Delivery on Postprandial Glucose Levels (unequal control and microneedle insulin doses)

To determine if microneedle-based insulin delivery is also effective in reducing postprandial glucose levels, insulin delivery was assessed with a bolus infusion immediately before a 75-g carbohydrate meal. Based on the second subject's insulin-to-carbohydrate ratio of 1 unit for every 10 g of carbohydrate ingested, insulin delivery through the subcutaneous catheter was assessed with a bolus of 7.5 units of 100-U Humalog. Plasma free insulin levels rose over the course of the first hour and then steadily declined (Figure 4.21a). Plasma glucose levels initially increased and eventually started to decrease after 1.5 h. Plasma glucose levels approximately returned to the pre-meal glucose value at 3.5 h (Figure 4.21b). The next two visits involved delivery of 15

units of 50-U Humalog at 1 mm through the microneedle device, followed by the consumption of an identical standardized meal within 5 min of bolus infusion. In both microneedle experiments, the t_{max} occurred at 45 min after infusion. Moreover, plasma glucose levels decreased throughout the duration of both experiments. An evaluation of the AUIC over a 1-h and a 2-h period immediately after delivery revealed that the pharmacokinetics of the insulin delivery were faster for the microneedle as compared to the subcutaneous catheter (Figure 4.22a). Similarly, measurement of plasma glucose levels showed that microneedles were more effective than the catheter (Figure 4.22b).

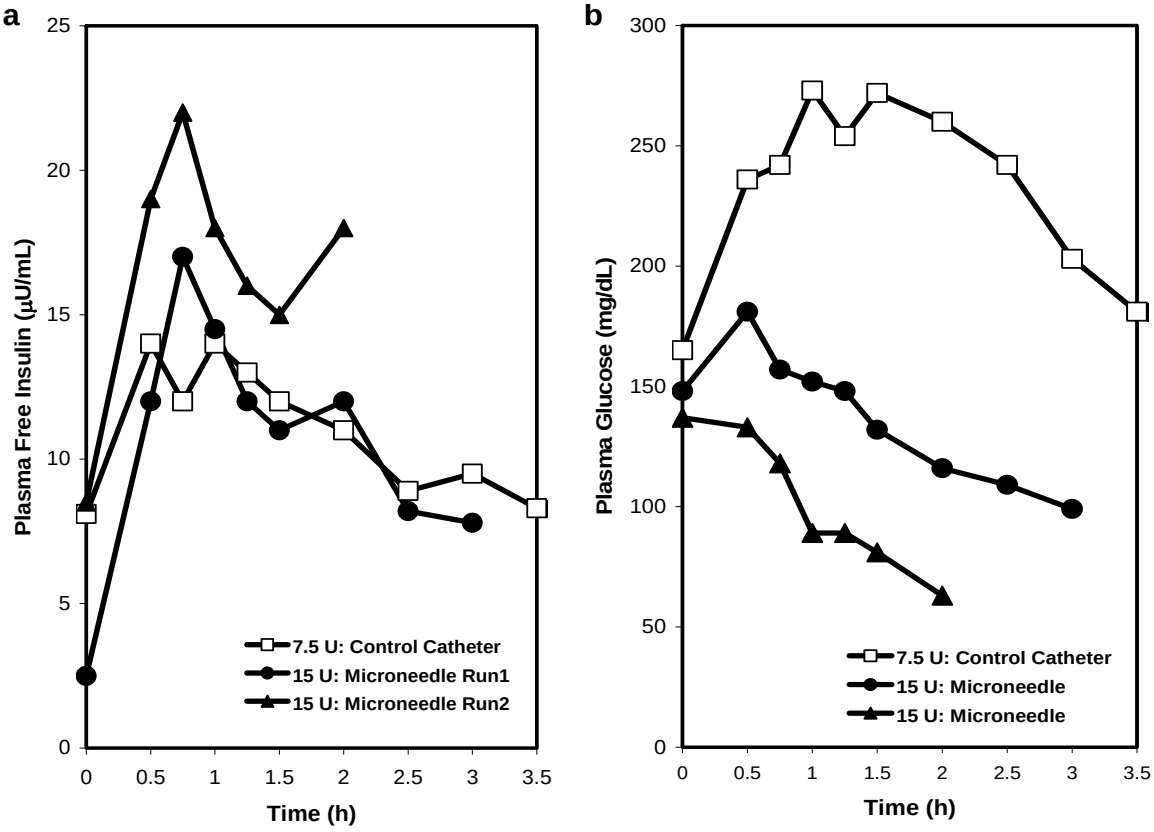

Figure 4.21: Microneedle-based insulin delivery at 1 mm insertion depth in comparison to 9-mm catheter control following consumption of a standardized meal immediately after insulin bolus (Phase 2). a) Postprandial plasma free insulin level profile and b) corresponding plasma glucose level response. Microneedle-based delivery led to rapid decline in postprandial plasma glucose levels.

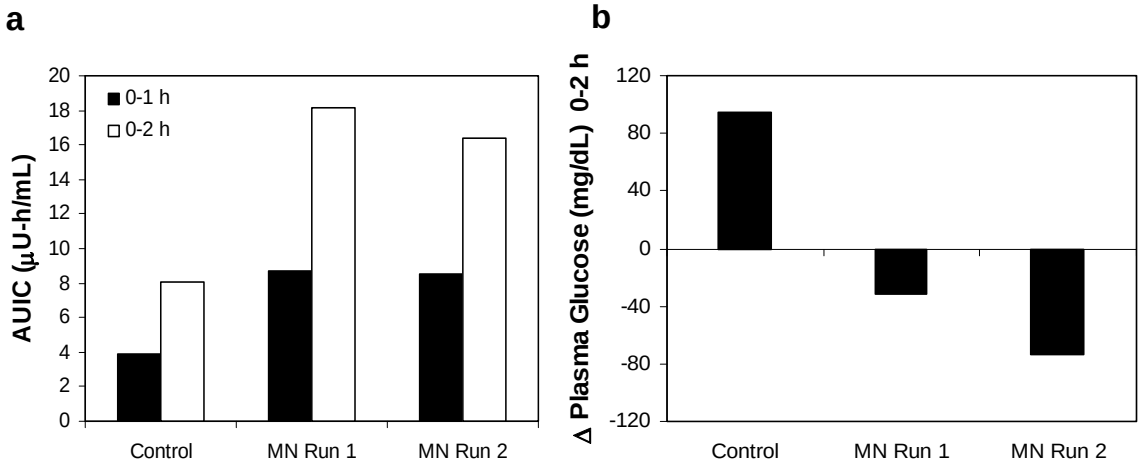

Figure 4.22: Microneedle-based insulin delivery results for Phase 2. a) AUIC for 0-1 h and 0-2 h and b) change in plasma glucose levels from 0 to 2 h. Microneedle (MN)-based insulin delivery led to an AUIC slightly more than double that of the catheter control for both 0-1 h and 0-2 h periods and larger reduction in plasma glucose levels. Similarity of results from the two microneedle runs demonstrates reproducibility.

This phase demonstrated that microneedles can be used to effectively reduce postprandial glucose levels in a reproducible manner as seen by the two trials on the same subject. The first two test phases of the study involved delivery of insulin doses that were 1.5 to two times higher than the subject's usual dose to ensure that insulin delivered via microneedles reached the systemic circulation. However, the rapid decline in postprandial glucose levels and the high AUIC values indicate that the doses administered in this study were higher than required. Guided by the results of these two phases and to make a stronger claim that microneedles are more effective than catheters, phase 3 of this study was carried out in five subjects with the same insulin doses being administered for both microneedle and catheter treatments.

4.3.4. Phase 3: Effect of Microneedle-Based Insulin Delivery on Postprandial Glucose Levels (equal control and microneedle insulin doses)

To further strengthen the claim that microneedles lead to faster pharmacokinetics and improved postprandial glycaemic control, plasma free insulin (Figure 4.23a-b) and change in plasma glucose (Figure 4.23c-d) profiles for equal microneedle and catheter bolus doses were analyzed over a period of 2.5 h.

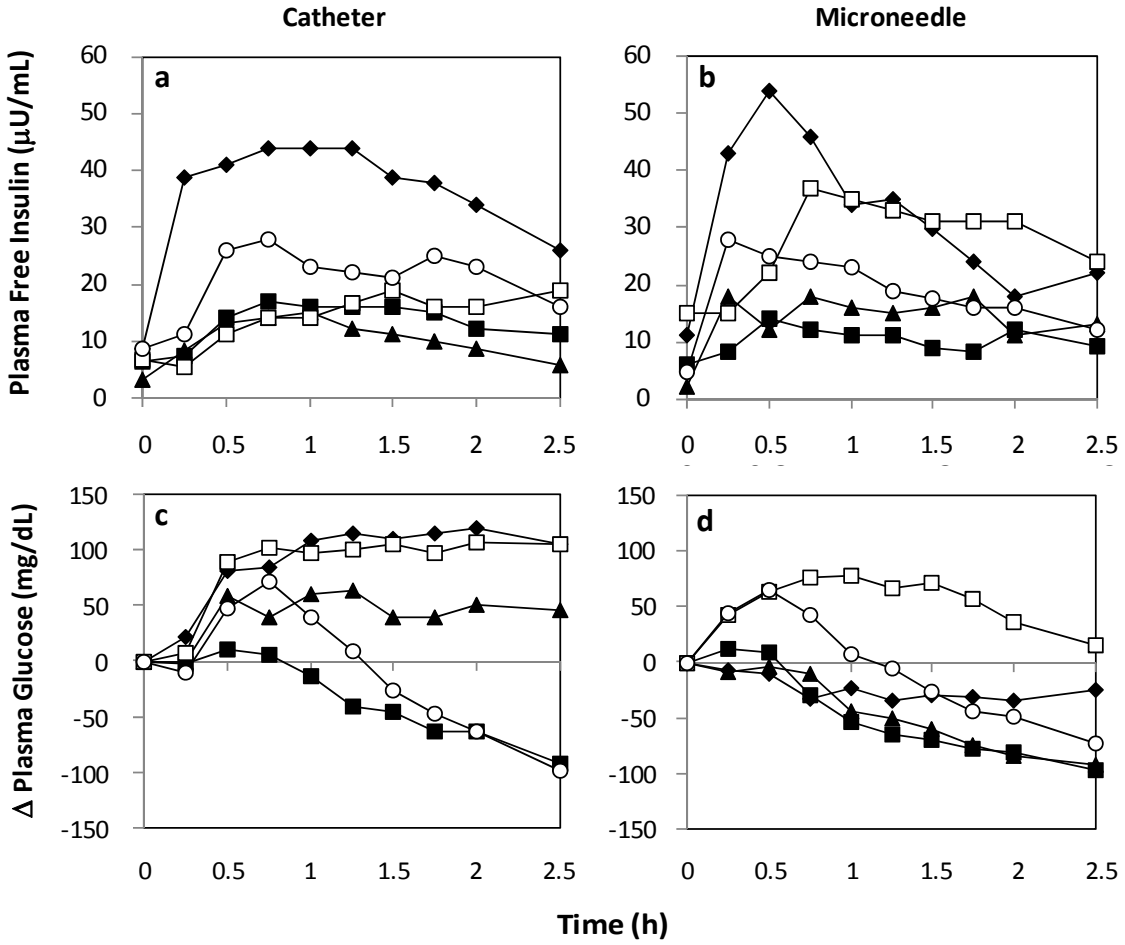

Figure 4.23: Plasma free insulin levels for a) catheter-based and b) microneedle-based insulin delivery for the five study subjects over 2.5 h. Change (△) in plasma glucose levels for c) catheter-based and d) microneedle-based insulin delivery for the five subjects. Although the study was carried out over 3.5 h, the data were analyzed up to 2.5 h as some trials had to be stopped at this time point due to hypoglycaemia. ▲ = subject 1, age: 44 administered 6 units of lispro insulin; ■ = subject 2, age: 39, administered 10 units; ◆ = subject 3, age: 11, administered 15 units; □ = subject 4, age: 19, administered 15 units; ○ = subject 5, age: 18, administered 10 units.

Using the above insulin profiles, the pharmacokinetic parameters of C_{max}, t_{max}, and AUIC (from equation 3.2) were determined. These values together with the insulin profile data from Figure 4.23 and Equations 3.3-3.5) were used to calculate the rate constants for absorption (k_a) and elimination (k_{el}) for the two treatment methods. The results are summarized in the table below.

Table 4.2: Pharmacokinetic parameters for phase 3 insulin delivery

Parameter	***Catheter***	***Microneedle***	***p-value***
C_{max} (μU/mL)	24.6 ± 7.5	32.2 ± 14.0	0.07
$^{*}t_{max}$ (min)	57.0 ± 20.0	27.0 ± 13.0	0.01
AUIC (μU-h/mL)	29.3 ± 18.2	32.6 ± 14.8	0.51
$^{*}k_a$ (min^{-1})	$4.1\times10^{-3}\pm 2.1\times10^{-3}$	$7.7\times10^{-3}\pm 3.2\times10^{-3}$	0.03
k_{el} (min^{-1})	$5.9\times10^{-2}\pm 1.3\times10^{-2}$	$8.1\times10^{-2}\pm 3.3\times10^{-2}$	0.21

* indicates $p < 0.05$ via Student's t-test; data are expressed as mean ± SD; n = 5

As summarized in Table 4.2 above, intradermal microneedle delivery achieved a 31% higher peak insulin concentration than subcutaneous catheter delivery in less than half the time, in spite of administration of the same insulin dose for both treatments. This significant difference in the PK parameter of t_{max} indicates that microneedle-based insulin delivery had faster pharmacokinetics than the catheter. The area under the insulin curve over a 2.5 h time period was not significantly different between the microneedle and catheter deliveries indicating both treatments led to comparable insulin absorption overall. Therefore, although both treatments led to similar relative insulin bioavailability, intradermal microneedle-based delivery led to much faster absorption. This faster absorption via microneedle-based insulin delivery is evident by comparing the absorption

rate constants (k_a) for the two treatments as seen in Table 4.2. The absorption rate constant for intradermal microneedle treatment was significantly higher, being almost two times that of the subcutaneous catheter treatment (Student's t-test; $p < 0.05$). This is due to rapid uptake of insulin by the dermal vasculature, achieved by targeting microneedle-insulin delivery to the papillary dermal region having a rich capillary network. The elimination rate constants for the two treatment methods were not significantly different (Student's t-test; $p > 0.05$).

Considering the pharmacodynamic response, as seen in Figure 4.24, three out of five subcutaneous catheter treatments did not lead to any blood glucose reduction over the entire study period, whereas all intradermal microneedle treatments led to reduction either close to or below initial glucose levels. The average changes in blood glucose levels for the microneedle and control treatments over a 2.5 h period were $\Delta BG_{microneedle}$ = -55 ± 49 mg/dL and $\Delta BG_{catheter}$ = + 13 ± 102 mg/dL. Thus, although subjects were administered the same insulin dose and started at similar baseline glucose levels for their microneedle and control treatments, intradermal microneedles were much more effective than subcutaneous catheters in reducing postprandial glucose levels.

Overall, intradermal microneedle delivery enabled faster onset, higher peak insulin concentration, and faster return/maintenance of normoglycaemia. This suggests that intradermal microneedles may provide better glucose control, which is critical to reducing diabetic complications, and enable more efficient utilization of insulin, thereby potentially allowing for reduced insulin doses.

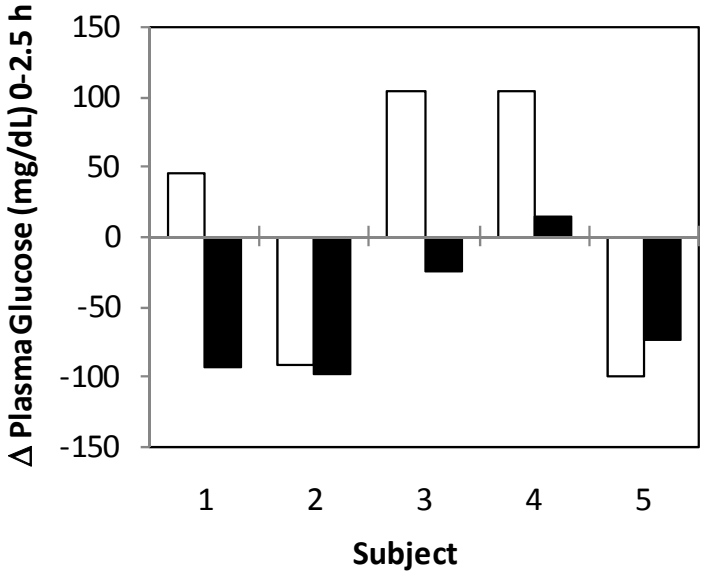

Figure 4.24: Comparison of the net change in plasma glucose levels between the two treatment methods, (□) catheter and (■) microneedle, for each of the five subjects. For the same dose and baseline glucose, microneedles were more effective than catheters in reducing plasma glucose levels either to or below the baseline glucose levels.

4.3.5. Assessment of Pain

In addition to improved pharmacokinetics and pharmacodynamics, we also hypothesized that microneedles can improve patient compliance by being less painful than catheters. We therefore asked subjects to score the pain associated with the catheter and microneedle insertions as well as with the insulin infusion procedures on a visual analog scale ranging from 0 (no pain) to 100 (worst imaginable pain) mm. The microneedle insertion procedure ($VAS_{MN\text{-}insert} = 8 \pm 9$ mm) was significantly less painful than the catheter insertion ($VAS_{cath\text{-}insert} = 40 \pm 13$ mm) (student's t-test; $p < 0.05$). There was no significant difference in the pain scores for the infusion procedures ($VAS_{MN\text{-}infuse} = 28 \pm 15$ mm and $VAS_{cath\text{-}infuse} = 17 \pm 16$ mm), however, the microneedle infusion score can be further reduced by decreasing the infusion flow rate below 1 mL/min as seen in Chapter 2. All subjects considered microneedles to be less painful than the catheter and

preferred microneedle treatment over their catheters. There were no adverse events during the study. These results suggest that insulin delivery using microneedles could increase patient compliance, particularly among children and adolescents, who have the tendency to omit insulin injections due to fear, pain, anxiety, and inconvenience associated with hypodermic needles and subcutaneous catheters (Hanas and Ludvigsson 1997; Zambanini, Newson et al. 1999).

4.3.6. Assessment of Intradermal Delivery and Dermal Irritation

Because skin thickness is approximately 3 mm (Bronaugh, Stewart et al. 1982), microneedle insertion at 900 μm and 1 mm depths is expected to be intradermal. To confirm that the 900 μm (Phase 3) and 1 mm (Phase 2) insertion depths led to intradermal insulin delivery, the skin at the microneedle insertion site was visually observed immediately after bolus infusion until the end of the experiment. Upon observing the skin, a raised wheal extending approximately 4-5 mm (depending on the volume administered) from the point of insertion was seen, consistent with the appearance of an intradermal injection (Figure 4.25a). In comparison, visual observation of the subcutaneous catheter infusion site did not show any skin wheal (Figure 4.25b); however, moderate erythema and punctate redness at the catheter insertion site was observed in this case.

Erythema and edema scores were recorded (using the Dermal Draize scale described in section 3.6.8) throughout the study period for both treatments. The catheter sites experienced well-defined to moderate erythema, while the microneedle sites had very slight erythema as depicted in Figures 4.25 and 4.26.

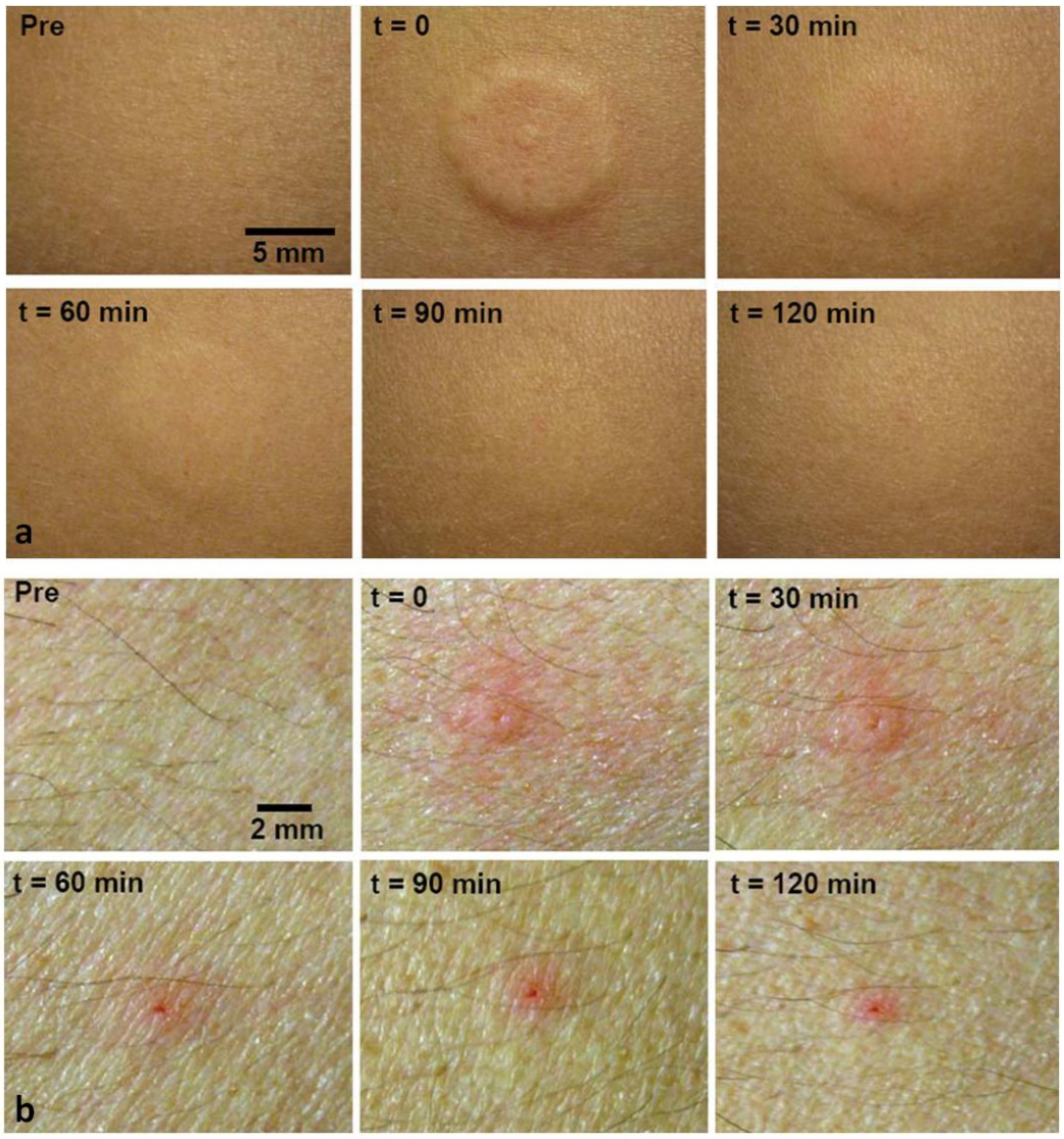

Figure 4.25: Surface view of the abdominal infusion site before, immediately after, and at 30-min intervals after insulin delivery in Subject 2 (Phase 2). a) Insulin infusion site for microneedle-based delivery. A raised skin wheal was seen immediately after delivery. Over time, the wheal subsided, and skin returned to normal. Slight erythema was also observed which resolved over time, b) Insulin infusion site for catheter-based delivery. Moderate erythema was seen at the point of catheter insertion and well-defined erythema in the vicinity of the insertion site. The erythema decreased over time but still remained mild at 2 h. No edema was observed for catheter delivery sites.

Erythema scores gradually decreased for both treatments over time and were completely resolved upon 2.5 h for the microneedle treatments. Catheter treatments still

experienced very slight erythema at the end of the experiment and also had punctate redness at the needle insertion site. With regards to edema, the catheter sites did not experience any edema as all insulin was deposited in the hypodermis. Microneedle sites experienced moderate edema which was evident by visualization of a raised skin wheal. Overtime the skin wheal became less apparent, gradually subsiding over the course of the study and was completely resolved within 2.5 h for all subjects.

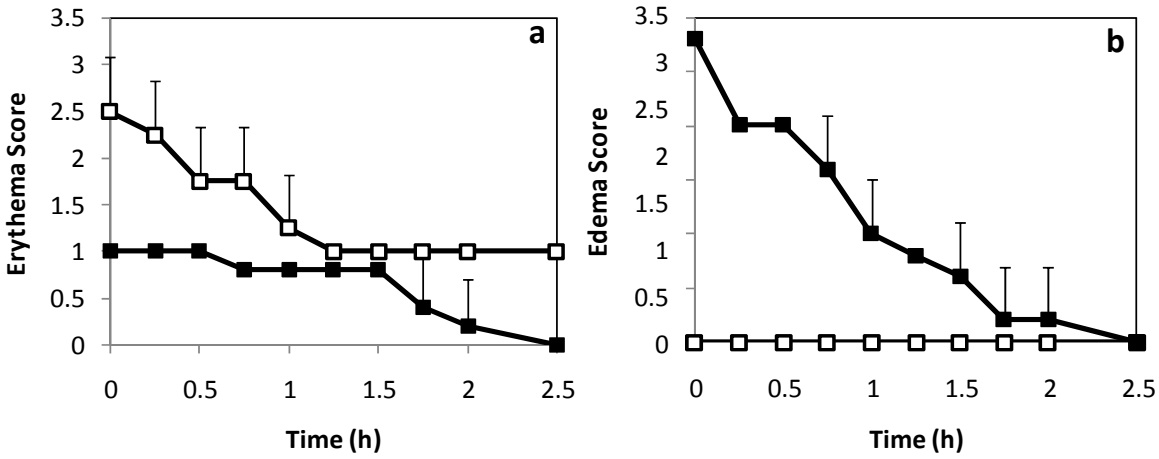

Figure 4.26: a) Erythema and b) edema scores for (□) catheter and (■) microneedle treatment sites using the Dermal Draize scale. Data are expressed as mean ± SD; n = 5.

4.3.7. Conclusions

This study demonstrated for the first time that microneedle-based intradermal delivery can lead to faster insulin pharmacokinetics and tighter glucose control than subcutaneous catheters while causing significantly less pain in children, adolescents, and adults. The potential clinical significance of these results is that intradermal microneedles may enable a more flexible insulin therapy regimen and allow for improved postprandial glucose control with improved patient compliance, improved health outcomes, and reduced healthcare costs.

4.4. Local Anesthesia Using Hollow Microneedles in Human Subjects

4.4.1. Introduction

Local dermal anesthesia is commonly administered to reduce pain prior to procedures involving needlesticks such as venipuncture, intravenous catheterization, botulinum toxin injections and lumbar punctures, as well as prior to cutaneous surgical procedures such as skin biopsies (Houck and Sethna 2005). While several methods of inducing local anesthesia exist, each of them comes with its own limitations.

Hypodermic needle injection is the most common means of administering local anesthesia and allows for rapid onset with good efficacy; however, hypodermic needles can also cause pain, anxiety and distress to the patient and lead to poor patient compliance, especially among children (Holmes 1994; Zempsky 2008) and also require administration by experienced medical personnel. Topical anesthetic creams and gels provide a painless and simple means of administering anesthesia, however, they have to undergo passive diffusion across the skin's outermost barrier layer (stratum corneum) which leads to slow onset times ranging from 30 min to 1.5 h depending on the properties of the topical anesthetic agent (Houck and Sethna 2005; Zempsky 2008). This delayed onset is the main barrier to widespread use of topical anesthetics for venous access procedures. Some topical anesthetics also have the tendency to cause vasoconstriction and skin irritation (Houck and Sethna 2005) and many patients still experience pain in spite of using these anesthetics (Kleiber, Sorenson et al. 2002).

More recently, several needle-free active drug delivery devices such as iontophoresis, sonoporation, jet-injection, laser ablation and thermal energy-based systems have been developed to enhance the rate of anesthetic delivery across the stratum

corneum barrier. However, these procedures still require 2-15 min for preparation/loading, administration and onset, which is not practical in a busy clinical setting and these procedures can also lead to variable anesthesia (Houck and Sethna 2005; Young 2007; Zempsky 2008). Moreover, these devices can be cumbersome (Zempsky, Sullivan et al. 2004; Benson and Namjoshi 2008) and generally require a power source which adds cost and complexity to the device (Prausnitz, Gill et al. 2008). Due to these reasons, several such commercialized devices have had poor market acceptance (Vyteris Annual Report, 2008) and have been discontinued over the past few years (Anesiva Annual Report, 2008).

An ideal local anesthesia system for use in ambulatory clinical environments should be effective, have rapid onset, cause minimal pain, be fast and easy to load and administer with minimal user training, be portable without bulky equipment and be cost effective (Houck and Sethna 2005).

Microneedles have the potential to meet these criteria and provide a significant advance over current available methods. This study demonstrates for the first time a) microneedle based drug delivery for a local therapeutic effect, b) efficacy of lidocaine delivery using microneedles to cause local anesthesia in comparison to hypodermic needles, and c) the pain associated with hollow microneedle injection of a drug. The objective of this study was to test the hypothesis that minimally invasive microneedles cause less pain during injection of lidocaine but induce local anesthesia in human subjects with the same onset and efficacy as intradermal lidocaine injection using hypodermic needles.

4.4.2. Study Population

Fifteen healthy subjects were consented to participate in the study. Of the enrolled subjects, data from 13 (87%) subjects were included in the forearm phase of this study. The other two subjects experienced incomplete lidocaine delivery as determined by leakage of fluid from the microneedle prototype device (1 subject) and hypodermic needle (1 subject) during the injection procedure. Data from 11 (73%) subjects were analyzed for the dorsum of the hand phase of the study due to leakage from the microneedle prototype device.

4.4.3. Assessment of Pain

To test the hypothesis that microneedle-based injection is less painful than hypodermic needle-based injection, VAS pain scores were measured for the two delivery methods (Figure 4.27). Results indicated that microneedles were significantly less painful (Student's t-test; $p < 0.05$) than hypodermic needles for both forearm and dorsum of the hand lidocaine injection procedures. The pain scores for the forearm procedures were $VAS_{MN\text{-}forearm} = 8.2 \pm 10.4$ mm for the microneedle and $VAS_{H\text{-}forearm} = 24.6 \pm 21.2$ mm for the hypodermic needle while the pain scores for the dorsum of the hand delivery were $VAS_{MN\text{-}dorsum} = 4.8 \pm 7.9$ mm and $VAS_{H\text{-}dorsum} = 22.0 \pm 17.2$ mm. Therefore, on average, the hypodermic needle was 3 times more painful than the microneedle for the forearm injections, and was greater than 4 times more painful than the microneedle for the dorsum injections. Further, upon being asked if they considered the lidocaine injection procedures to be painful, 92% of the forearm protocol subjects indicated that they did not consider the microneedle procedure to be painful as compared to only 25% for the hypodermic needle. For the dorsum of the hand injection, 82% of the subjects

said they did not consider the microneedle procedure to be painful, while only 27% thought the hypodermic needle was painless.

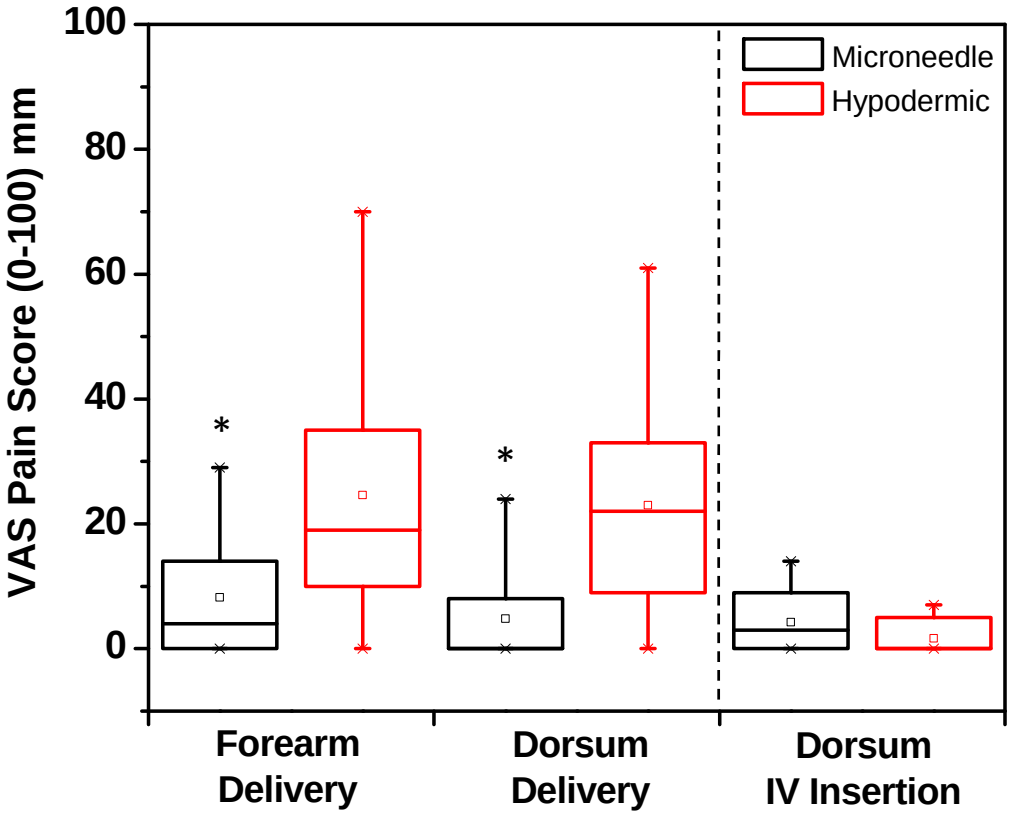

Figure 4.27: Box plot representation of the visual analog pain scores associated with lidocaine injection for the forearm and dorsum of the hand and for the IV catheter administration procedure following lidocaine anesthesia on the dorsum of the hand. The rectangular box represents the interquartile range (25% to 75%) of the VAS pain scores for each treatment procedure for the different study protocols (forearm delivery, dorsum delivery, and IV insertion on dorsum of the hand). The vertical lines extend from the upper and lower boundary of the box to the maximum and minimum data points. The hollow square inside the box represents the mean pain score for each treatment procedure. The horizontal line inside each box represents the median for the corresponding treatment procedure. (* $p < 0.05$).

4.4.4. Area of Numbness

To determine if microneedle injection was as effective as hypodermic needles in inducing anesthesia over a clinically relevant area, the area of numbness was measured via a pin- prick test for the forearm protocol at t = 0, 7.5, and 15 min after delivery.

Figure 4.28 depicts the values for the numb areas extending radially from the injection point.

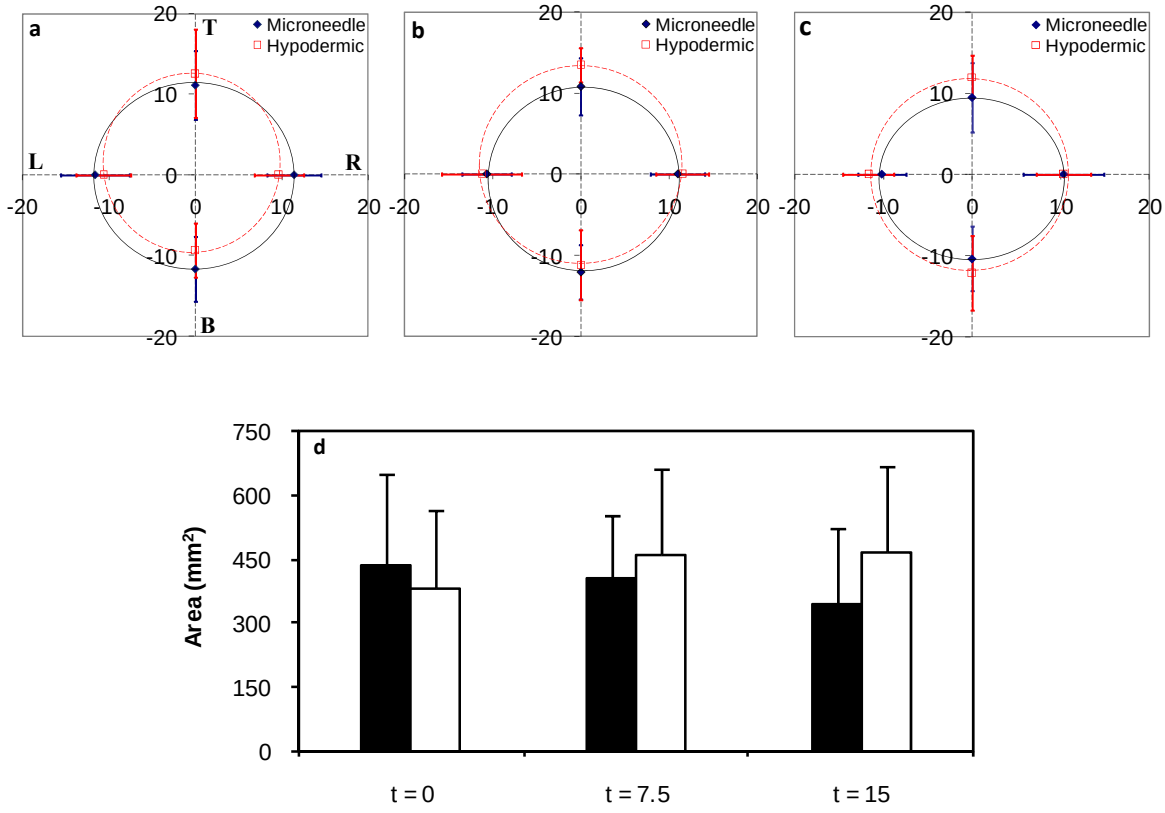

Figure 4.28: Map of the area of numbness from the injection site (0,0) extending along the four axes (T, B, L, R) as described in Figure 3.7 for a) t = 0 min, b) t = 7.5 min, and c) t = 15 min. The axes are in millimeters. The distances from the injection site to the point of first sensation felt upon pin-prick testing were measured as radii along each axis for each time point, d) total area of numbness for the three measurement periods. The radii for each treatment method at each time point were averaged to produce an average radius for each period. The average radius was used to calculate the average numb area using the equation for a circle (πr^2, where r is the average radius). Microneedles were as effective as hypodermic needles in immediately inducing and maintaining anesthesia for at least 15 min. ■ = microneedle; □ = hypodermic needle.

As seen in Figures 4.28 a-c, uniform anesthesia was achieved in all directions, creating a circular area of numbness for both delivery methods. There were no significant differences in the anesthetized regions along any of the four axes of

measurements between the two treatment methods (repeated measures three-way ANOVA: $p > 0.05$) for all time points. The average radii in all directions for the microneedle sites were $r_{0min\text{-}MN} = 11.5 \pm 2.7$ mm, $r_{7.5min\text{-}MN} = 11.2 \pm 2.3$ mm, and $r_{15min\text{-}MN} = 10.1 \pm 2.8$ mm for times t = 0, 7.5, and 15 min respectively. The corresponding average radii for the hypodermic needle were $r_{0min\text{-}H} = 10.6 \pm 3.1$ mm, $r_{7.5min\text{-}H} = 11.0 \pm 2.5$ mm, and $r_{15min\text{-}H} = 11.9 \pm 2.6$ mm.

The areas of numbness calculated as a circle with the average radius at each time point are shown in Figure 4.28d. The average areas over the 15 min measurement period were 4.0 ± 1.8 cm^2 and 4.3 ± 1.9 cm^2 for the microneedle and hypodermic needle treated forearm sites respectively. There were no significant differences (repeated measures two-way ANOVA: $p > 0.05$) among the anesthetized areas for both treatment methods at any time point over the 15 min time period. Thus, microneedles were as effective as hypodermic needles in inducing anesthesia over a clinically relevant area.

4.4.5. Depth of Numbness

To test the depth of anesthesia induced by lidocaine injected using a 500-μm microneedle compared to a hypodermic needle, a 26-gauge, 9.5 mm long hypodermic needle was inserted into the forearm skin at the site of lidocaine injection until subjects indicated they felt a sensation. This depth was measured at t = 0, 7.5, and 15 min after injection and is shown in Figure 4.29. The depth of numbness for the microneedle sites were $d_{0min\text{-}MN} = 9.1 \pm 1.6$ mm, $d_{7.5min\text{-}MN} = 9.1 \pm 1.2$ mm, and $d_{15min\text{-}MN} = 8.7 \pm 1.8$ mm at t = 0, 7.5, and 15 min respectively. The corresponding depth of numbness for the hypodermic needle sites were $d_{0min\text{-}H} = 9.4 \pm 1.5$ mm, $d_{7.5min\text{-}H} = 9.5 \pm 1.1$ mm, and $d_{15min\text{-}H} = 9.5 \pm 0.8$ mm. There was no significant difference in the depth of anesthesia for the

two delivery methods across all time points (repeated measures two-way ANOVA: $p > 0.05$). Therefore, microneedles were as effective as hypodermic needles in inducing anesthesia to a depth of at least 9 mm.

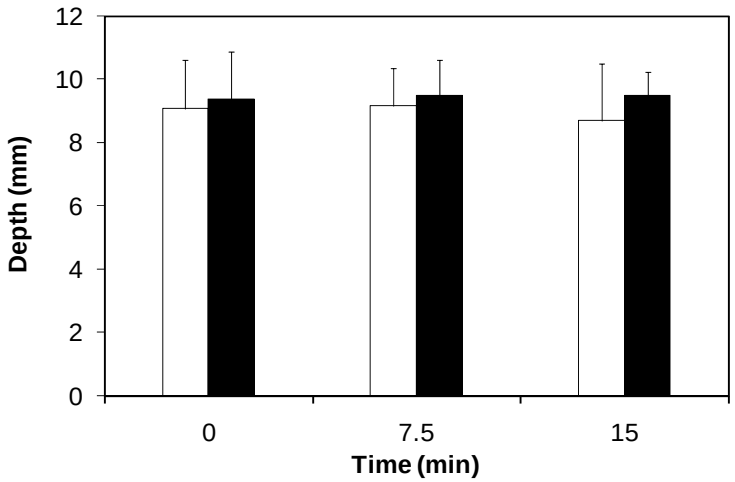

Figure 4.29: Depth of numbness for each treatment procedure at the three different time points after lidocaine delivery on the forearm. Microneedles were as effective as hypodermic needles in immediately inducing deep anesthesia for at least 15 min. ■ = microneedle; □ = hypodermic needle.

4.4.6. Efficacy of Delivery Method Based on Venous Cannulation

To further test the efficacy of microneedle-based lidocaine delivery for use in clinical applications, lidocaine was delivered close to a vein on the dorsum of the hand. This was followed immediately by insertion of an IV catheter into the vein and measurement of pain. Figure 4.27 (seen previously) shows the VAS pain scores for the IV insertion procedure. The average VAS pain score for the IV cannulation procedure for the microneedle treatment was $VAS_{MN\text{-}IV} = 4.2 \pm 4.8$ mm and the score was $VAS_{H\text{-}IV} = 1.6 \pm 2.7$ mm for the hypodermic needle. Statistical analysis indicated that there was no significant difference between the pain scores for the two treatment methods (Student's t-test: $p > 0.05$). Therefore, microneedles were as effective as hypodermic needles in administering rapid dermal anesthesia for venous cannulation. Eighty-two

percent (9 out of 11) of the subjects considered the IV insertion post microneedle treatment to be painless and 91% (10 out of 11) considered cannulation following hypodermic needle treatment to be painless.

4.4.7. Onset of Anesthesia

As seen from Figures 4.28 and 4.29, the area and depth of numbness from the forearm protocol were the same at t = 0 min for both the microneedle and hypodermic needle injections. Further, there was no significant difference in the IV catheter administration pain scores for the two treatment methods immediately after lidocaine injection. These results indicate that microneedle-based lidocaine injection had the same rapid onset of anesthesia as hypodermic needles.

4.4.8. Preference of Treatment Method

To establish if microneedles would be clinically accepted by patients, at the end of each protocol (forearm and dorsum of the hand), subjects were asked which treatment method they would prefer (first procedure versus second procedure) to receive in a clinical setting. Seventy-seven percent (10 out of 13) of the subjects from the forearm injection protocol said they would prefer microneedles over hypodermic needles. For the dorsum protocol, treatment preference was assessed for the overall procedure (i.e. lidocaine injection and IV catheter insertion) with 82% (9 out of 11) of the subjects indicating that they would prefer the microneedle delivery system. Thus, even though the subjects were blinded to the treatments, a large majority of the subjects preferred microneedle-based lidocaine injection over hypodermic needles.

4.4.9. Local Skin Reaction and Adverse Events

To study the effect of microneedles on skin irritation, the treatment sites were visually examined for local skin reactions. Immediately after injection, a distinct raised skin wheal confirming intradermal delivery was observed at the treatment site (Figure 4.30). In subjects with light skin, very mild erythema and slight skin blanching was also observed. Both the skin wheal and erythema were either reduced or gone within 1 h of treatment. Within 24 h of treatment, subjects self-reported that there were no signs of erythema or edema. Upon treatment with hypodermic needles, a similar raised skin wheal was also observed which either reduced or disappeared in 1 h. In contrast, hypodermic needle insertions led to the presence of a drop of blood at the injection site immediately after treatment which was never seen after microneedle injection. Punctate redness at the hypodermic needle insertion point also often appeared 1 h after treatment. Subjects reported no wheal after 24 h, however, in some cases subjects still observed punctate redness at the hypodermic needle injection site 24 h after treatment. There were no adverse events observed or reported during or after the study. Overall, skin responses to microneedle and hypodermic needle injection were similar, although hypodermic needle caused bleeding and appeared to cause more lasting local trauma to the skin.

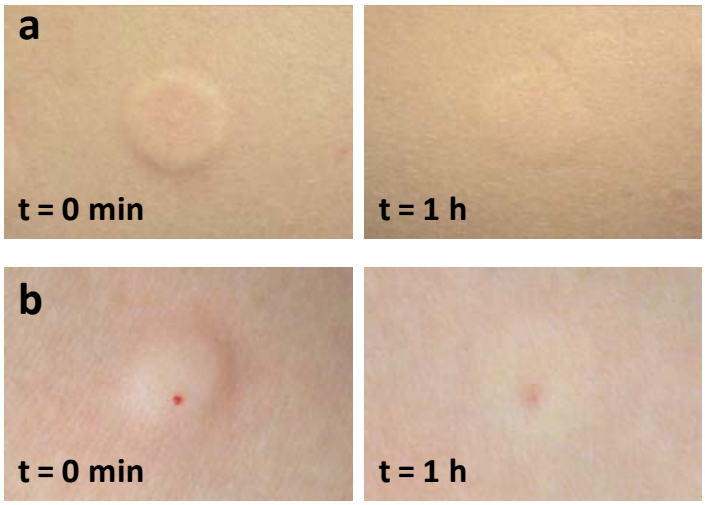

Figure 4.30: Representative images of the forearm injection sites immediately after lidocaine delivery and 1 h after delivery. a) microneedle: a distinct symmetric skin wheal and slight erythema is seen immediately after delivery. There is no evidence of blood. One hour post injection, there is a faint wheal still present. hypodermic needle: a distinct raised skin wheal with slight blanching of the skin and a drop of blood at the needle insertion point is seen immediately after delivery at t = 0. Very slight erythema is also observed. One hour after delivery, there is slight blanching and punctate redness at the injection site. All sites returned to normal 24 h after the injection procedures with the exception of some hypodermic needles sites which still had punctate redness.

4.4.10. Discussion

This study tested the hypothesis that minimally invasive microneedles cause less pain during injection of lidocaine but induce local anesthesia in human subjects with the same onset and efficacy as intradermal lidocaine injection using hypodermic needles. In terms of injection pain, microneedles were less painful than hypodermic needles for both the forearm and dorsum protocols as indicated by the VAS pain scores. Previous studies have shown that the minimum difference in VAS scores for the results to be considered clinically significant is between 9 and 13 mm (Todd, Funk et al. 1996; Kelly 1998). Therefore, our results with differences of 16.4 mm and 17.2 mm between the average

pain scores for the two treatment methods for the forearm and hand dorsum delivery procedures were also significant from a clinical standpoint.

Further, both microneedle and hypodermic needle-based lidocaine delivery induced anesthesia immediately after injection, indicating rapid onset time as seen from the results of area and depth of numbness at t = 0 and from the IV catheter insertion pain scores. The 200 μl hypodermic needle injection on the forearm took approximately 5 s to complete while the microneedle injection took approximately 40 s due to the 300 μl/min flow rate set on the infusion pump. The 100 μl hypodermic injection on the back of the hand took almost 3 s to complete while the microneedle infusion took 20 s. While the microneedle injection required well under 1 min to perform, it was still significantly slower than hypodermic needle injection. However, it must be noted that the infusion rate in this study was set to 300 μl/min. This flow rate can be increased more than 3 times to 1 ml/min, thereby, bringing down delivery times almost on par with hypodermic needle injection without leading to significant increase in pain for volumes as low as 200 μl as seen in section 4.2. From a clinical standpoint, when compared to other minimally invasive transdermal device alternatives such as iontophoresis, sonophoresis, and jet-injectors which have application and onset times varying between 2-15 min, this time on the order of seconds is considerably shorter and is still shorter when compared to topical creams and gels which can have onset times > 1 h (Zempsky 2008) making microneedles attractive for use in busy clinical environments.

This study also showed that the area of numbness produced by microneedle injection was similar to hypodermic needles on the order of 4 – 4.3 cm^2. Although statistical analysis reveals no significant difference in the area of numbness between the

microneedle and hypodermic needle injections over time, the visual maps of the areas in Figure 4.28 depict a decrease in microneedle numb areas over time while the hypodermic needle numb areas are increasing. This may be due to the fact that in order for the lidocaine to have its complete effect, it must be injected in the upper dermis, just below the epiderms. Failure to do so will lead to a delay in the complete effect until the deeper injected anesthetic diffuses to the target areas in the dermal-epidermal region (Holmes 1994). Since lidocaine injection via hypodermic needles was performed using the Mantoux method, whereby the needle depth cannot be controlled, it is likely that some of the lidocaine injected through hypodermic needles was delivered into the deeper dermis, leading to an increase in numb area over time as lidocaine made its way towards the upper skin layers. By using a single microneedle in this study, we were able to induce clinically relevant anesthesia areas for applications in venipuncture, venous cannulation, lumbar puncture, port access and dermatologic procedures. However, we hypothesize that by using multiple microneedles assembled as arrays, even larger areas could be generated.

The results of this study indicated no significant difference between the depth of anesthesia induced by using microneedles and hypodermic needles. While the maximum depth of numbness for both devices was measured to be ~ 9.5 mm in this study, it is possible that the depth of induced anesthesia could be deeper had the measurement needle been inserted deeper (> 9.5 mm) into skin. Nonetheless, this depth of anesthesia is almost two times larger than that induced by EMLA (5 mm) (Bjerring and Arendt-Nielsen 1990) and on par with the depths induced by iontophoresis which range from 6

mm to 10 mm (Zempsky 2008). Thus, by inserting a microneedle 500 mm deep into skin, we were able to generate numbness to a depth almost 20 times the needle length.

With regards to cost, microneedles can be manufactured at low cost expected to be just a few cents each in mass production (Prausnitz, Mikszta et al. 2006). Therefore, microneedles are likely to be cost competitive with other disposable/consumable systems such hypodermic needles and topical anesthetics which are significantly cheaper than some jet-injection systems which are priced on the order of $500 as well as energy based methods that require an investment in a controlling device, which can be as high as $5000 (Young 2007). Thus, microneedles appear to be a cost effective solution for reducing time to anesthesia onset in a minimally invasive and significantly less painful manner.

In this experiment, some of the microneedle injections were not completed (1 in forearm phase and 4 in dorsum phase) due to fluid leakage from the device. The four leakage events on the dorsum of the hand occurred due to the relatively large ball shaped surface of the device which was difficult to optimally place near the raised veins on the dorsum of the hand. It should be noted that the device used in this study was an initial lab prototype and that the final clinical device would be designed to eliminate leakage events.

The potential medical significance of this work is that microneedles can provide a less painful yet efficacious alternative to current local anesthesia delivery systems. The ability of microneedles to induce significantly less painful and rapid anesthesia prior to venous cannulation as shown in this study can have a large impact in reducing pain associated with venipuncture and IV cannulation. This impact can be even more significant amongst children who consider these two procedures to be the two most

common sources of pain in the hospital and the second most common cause of worst pain during hospitalization (second only to the patient's underlying disease) (Wong and C.M. 1988; Cummings, Reid et al. 1996). Further, the small size of these needles makes the needle visually less apparent to patients and might be a suitable alternative to hypodermic needles for patients with needle phobia. Additionally, the rapid anesthesia onset makes microneedles extremely attractive for use in busy clinical settings and the envisioned simple device which requires minimal to no user training together with its low cost properties has the potential to increase uptake of microneedles among medical professionals.

4.4.11. Conclusions

This study demonstrated for the first time that minimally invasive microneedles cause less pain during injection of lidocaine but induce local anesthesia in human subjects with the same onset and efficacy as intradermal lidocaine injection using hypodermic needles. Additionally, a large majority of subjects considered microneedles to be painless and preferred microneedle treatment over hypodermic needles. These characteristics combined with the simple, miniature, and easy to use, low-cost, disposable device features fulfill the qualities of an ideal local anesthesia system making microneedles an attractive clinical standard for administrating local dermal anesthesia.

CHAPTER 5: DISCUSSION

While several microneedle delivery systems have been developed over the last decade, most studies have been performed *in-vitro* and in *in-vivo* animal models. To date, only a limited number of studies have been performed to study the application of microneedles in human subjects. The research in this thesis is translational in nature and among some of the first to understand the applications of microneedle treatment in human subjects.

As described in Chapter 1, an ideal transdermal drug delivery system would be one that i) is safe by maintaining skin permeability only during the desired period of drug delivery, ii) can create sustained or bolus delivery profiles, iii) can deliver therapeutic volumes/doses of drug quickly with minimal discomfort, iv) has rapidly responsive pharmacokinetics and pharmacodynamics, v) causes minimal pain and irritation, and vi) is simple, inexpensive, and well-accepted by patients. This chapter describes the significance of this thesis in determining that microneedles possess these characteristics of an ideal transdermal drug delivery system.

The skin impedance study showed that microneedles can be used to increase permeability of skin over timescales ranging from as little as 2 h to as long as 40 h by modulating the skin's occlusive conditions and microneedle geometry. From an efficacy standpoint, piercing the skin with microneedles can allow for increased skin permeability to facilitate drug delivery from a transdermal patch for a period of almost 2 days. From a safety standpoint, skin permeability can be quickly resealed in the absence of occlusion due to the rapid skin resealing that occurs under these conditions. Therefore, skin

occlusion following microneedle treatment acts like a switch that can turn drug delivery through microneedle-created channels "off" as desired. This result satisfies the first characteristic of an ideal microneedle system described above, i.e., is safe by maintaining skin permeability only during the desired period of drug delivery. Most other transdermal delivery systems such as ultrasound, iontophoresis, electrophoresis, and ablation do not possess this characteristic as they alter the SC lipid structure or remove the SC such that the skin remains permeable for several hours even in the absence of occlusion. For example, Appendix C shows elevated skin permeability after sonication in the absence of occlusion for a period of at least 7 h. This elevated permeability can be a safety concern as unwanted absorption of pathogenic substances across the skin may take place during this time. Hence, proper care must be taken to avoid absorption of exogenous substances after drug delivery has been completed for these types of transdermal systems.

Further, the skin impedance study also demonstrated that microneedles can increase skin permeability to allow for sustained drug delivery for almost 2 days in the presence of occlusion. The naltrexone delivery study carried out with collaborators at the University of Kentucky (Appendix B), confirmed this finding by delivering clinically relevant doses of naltrexone for 72 h in human subjects. These findings show that microneedle-based poke-and-patch delivery satisfies the characteristic of an ideal microneedle system that microneedles can create sustained delivery profiles in human subjects. This study also showed that solid microneedles ($\leq$ 750 in length) caused less pain than hypodermic needles. The study further demonstrated that skin resealing time and insertion pain are not directly coupled, thereby presenting opportunities for design of

microneedle devices that cause prolonged skin permeability (under occlusion), but still cause little or no pain. Results showed that using larger numbers of needles with larger cross-sectional area, rather than long needles, can accomplish this goal (e.g., geometry E), thereby meeting the characteristic that microneedles should cause minimal pain.

Further, two decades ago, Lackermeier et al. (Lackermeier, McAdams et al. 1999) suggested that measurement of skin impedance may have the potential to determine the recovery of skin following treatment with a drug delivery system as well as to predict the penetration of drug through the skin. While a few studies have been performed using skin impedance to study recovery of skin following treatment with transdermal drug delivery systems such as iontophoresis (Kalia, Nonato et al. 1996; Curdy, Kalia et al. 2000; Curdy, Kalia et al. 2002), and *in-vitro* studies have examined and developed relationships between skin impedance and skin permeability (Karande, Jain et al. 2005), this thesis applied skin impedance measurements to determine skin barrier recovery and also to develop a model to predict the quantity of drug within the body following microneedle treatment. The model (equation 4.5) developed in this study used electrical skin impedance measurements to predict *in-vivo* plasma concentrations of naltrexone and yielded results that were well correlated with the experimental naltrexone results from Appendix B. These results provide a promising opportunity for using skin impedance measurements to predict transdermal drug delivery *in-vivo*

The next study in this thesis was carried out to study the flow conductivity of skin during *in-vivo* microneedle infusion. Previous studies using hollow microneedles have demonstrated that the skin offers significant resistance to flow of fluid, however, the effect of microneedle parameters and infusion parameters on flow conductivity has not

been previously quantified *in-vivo*. Therefore, the volume of drug that can be delivered into skin via microneedles, the pressures associated with it, and the corresponding pain were previously unknown. In order for hollow microneedle delivery to be effective, clinically significant volumes of drug need to be delivered into the skin and in order to be competitive with hypodermic needles, in addition to having faster PK and PD profiles, they should also deliver these volumes with significantly less pain than hypodermic needles. The flow conductivity study in this thesis produced the first set of results showing the effect of microneedle insertion, retraction, and infusion parameters on skin resistance to flow and associated pain. By inserting a single microneedle into the dermis, volumes up to 1 mL can be delivered at shallow depths or low flow rates and up to 800 µl can be delivered at higher flow rates with low levels of pain that are significantly less than hypodermic needle insertion pain. These volumes are clinically significant as most intradermal injections are generally indicated to not exceed 500 µl (Lynn and Evans-Smith 2003). Further, even most bolus subcutaneous injections do not exceed 1-2 mL (Chapman 2003) due to pain, distortion and tearing of the tissue (Bookbinder, Hofer et al. 2006). Therefore, microneedles could provide a less painful alternate delivery route for drugs that would be typically administered subcutaneously, although the different route of administration may affect pharmacokinetics and other parameters. These results show that microneedles fulfill the characteristic of being able to deliver therapeutic volumes/doses of drug quickly with minimal discomfort.

Further, fabricating hollow microneedles that are strong enough to deliver large quantities of fluid into the skin without leakage, breakage, or occlusion, especially through arrays has been a challenge (Down and Harvey 2003; Mikszta, Haider et al.

2006). The results obtained in this study provide significant information to aid in the design of hollow microneedle structures that are strong enough to withstand the pressures obtained at higher volumes while being flexible enough to conform to the skin wheal formed during injection to prevent leakage.

The next study in this thesis involved delivery of insulin to Type 1 diabetes subjects, which since 1922, has been achieved via the subcutaneous route. Over the past several decades, many different delivery routes such as oral, buccal, nasal, pulmonary, and transdermal have been studied to improve the pharmacokinetics and pharmacodynamics of insulin. However, most of these methods have had limited success (Cefalu 2004). Exubera, a form of pulmonary insulin was the first insulin delivery system to be approved by the FDA as an alternate to subcutaneous insulin delivery in 2006. However, this product was discontinued the following year due to safety and usability reasons such as low bioavailability, cumbersome device, unknown adverse effects, etc. as described in section 4.3. Several insulin analogues have also been developed to improve insulin pharmacokinetics; however, still faster-acting insulin is desired to enable even better glycaemic control (Brange 1997; Hirsch 2005).

The insulin delivery experiments in this thesis demonstrated for the first-time that intradermal insulin delivery via hollow microneedles can lead to a) faster pharmacokinetics, b) more stable glycaemic control, and c) less administration pain than conventional catheters in children, adolescents, and adults with Type 1 diabetes. These three characteristics provide a significant step forward in the field of diabetes management and microneedles. By targeting the microneedles to the dermis, microneedles allow for rapid uptake of insulin by rich dermal capillary and lymphatic

network leading to better insulin PK and PD profiles. Further, the shallow depth of the microneedles reduces stimulation of the sensory nerve endings located in the skin, allowing for minimal administration pain. The potential medical significance of these results is that microneedles may reduce healthcare complications associated with diabetes due to improved glycaemic control as well as reduce pain and apprehension related with insulin delivery. With pain, anxiety, and fear of needles being the main reason for noncompliance among diabetes patients, microneedles may provide a means to increase patient compliance. Further, designing the microneedle device to be a simple, miniature integrated patch-like device without any tubing, bulky pumps, or catheter may further improve patient compliance by increasing comfort and convenience. Overall, improved patient compliance would ultimately lead to reduced healthcare costs for diabetes patients due to potential lower frequency of hypo- and hyperglycaemic events and related hospitalizations. Further, the improved glycaemic control achieved due to faster PK would further reduce the hypo- and hyperglycaemic events associated with insulin delivery. The results of this study show that microneedles fulfill the characteristics of creating bolus drug delivery profiles, having fast pharmacokinetics and pharmacodynamics, and causing minimal pain and irritation as seen in section 4.3.

The last study performed in this thesis used hollow microneedles to deliver lidocaine for administering local anesthesia. Current methods of administering local anesthesia involve hypodermic needles which cause pain, anxiety, and distress leading to poor patient compliance, especially among children. Topical anesthetics are the most common alternative, however, these substances have very slow onset times ranging from 30 min to 1.5 h which is not practical for ambulatory clinical purposes. Several alternate

transdermal systems have been developed as described in section 4.4, however, they too have relatively slow application/loading and onset times ranging from 2-15 min and have cumbersome devices that require user training. The lidocaine delivery results in this thesis demonstrated that microneedles can be used to induce local anesthesia with rapid onset immediately after completion of delivery with the same efficacy and less pain as hypodermic needles. This result fits the criteria that microneedles can deliver therapeutic volumes/doses of drug quickly with minimal discomfort. Further, > 77% of the subjects preferred microneedle-based lidocaine delivery to hypodermic-needle based delivery implying that microneedles are well accepted by patients. Moreover, > 82% of subjects found microneedles to be not painful. Therefore, the results of this study provide a significant advance over current methods available to administer local anesthesia as they provide features that are attractive to patients (effective anesthesia with significantly less pain) and to physicians (application speed and simplicity). The reduced pain is especially beneficial for children who report pain associated with venipuncture and IV cannulation as the second most common cause of worst pain during hospitalization (Wong and C.M. 1988; Cummings, Reid et al. 1996). With regards to the criteria of microneedles being in-expensive, previous studies have indicated that microneedles can be manufactured relatively cheaply on the order of a few cents (Reed and Lye 2004; Prausnitz, Mikszta et al. 2006).

Thus, while microneedles of various geometries and materials have been developed over the last decade, their safety, efficacy, and usability characteristics in human subjects which are critical in determining the future clinical application of microneedles were studied in this thesis. This thesis provides some of the first

translational research studies to facilitate the transfer of microneedles from the laboratory into the clinical environment.

CHAPTER 6: CONCLUSIONS

In conclusion, this thesis presented the first-in-humans microneedle data to characterize the skin repair responses to microneedle insertion, characterize the effect of microneedle and infusion parameters on flow conductivity of skin, and assess the efficacy of systemic and local therapeutic effects via microneedle-based intradermal drug delivery of insulin and lidocaine.

This first aim showed that skin occlusion significantly slowed down skin barrier recovery following microneedle treatment. Results indicated that in the absence of occlusion, microneedle treated sites recovered barrier properties within 2 h, while occluded sites recovered more slowly, with recovery windows ranging from 3-40 h depending on microneedle geometry. Upon subsequent removal of occlusion, the skin barrier recovered rapidly. Additionally, longer microneedles, increased number of needles, and larger cross-sectional area demonstrated slower recovery kinetics under occlusion indicating that microneedle geometry played a significant role in the barrier recovery process. Results also showed that skin resealing time and insertion pain were not directly correlated, leading to opportunities for designing microneedles that cause prolonged skin permeability (under occlusion), while causing little to no pain, by increasing the number of microneedles and/or the needle cross-sectional area. The impedance-based pharmacokinetic model (without any fitted parameters) showed that impedance spectroscopy following microneedle treatment can be a good predictor of transdermal drug delivery across skin *in-vivo.* Overall, this study showed for the first time that pre-treatment of skin with microneedles before applying an occlusive

transdermal patch can increase skin permeability for more than one day, but nonetheless allow skin to reseal rapidly after patch removal.

The second part of this thesis performed the first studies to characterize the effect of microneedle insertion and infusion parameters on flow conductivity of skin and associated pain during *in-vivo* hollow microneedle delivery. Results showed that microneedle-based delivery within the dermis led to a decrease in flow conductivity regardless of intradermal depth at moderate flow rates. Microneedle retraction, slow delivery flow rates, and the addition of hyaluronidase helped increase flow conductivity, while increasing infusion flow rate increased skin's resistance to flow more rapidly. Intradermal microneedle insertion VAS pain scores at all depths were significantly lower than that of hypodermic needles. Analysis of infusion pain scores demonstrated that intradermal microneedles can be used to deliver up to 800 µl of fluid at moderate to high flow rates with significantly less pain than hypodermic needle insertion. Delivery of 1 mL of fluid can be achieved with less pain than hypodermic needles at either low flow rates, shallow insertion depths, or through the addition of hyaluronidase. These results are practical for clinical applications since most intradermal injections are indicated to not exceed 500 µl.

The final parts of this thesis determined the clinical feasibility of microneedle-based drug delivery by studying the efficacy of hollow microneedles for systemic and local drug effects by delivering insulin to Type 1 diabetes subjects and lidocaine to healthy subjects. Insulin delivery results demonstrated for the first time that intradermal insulin delivery via microneedles leads to improved pharmacokinetics as demonstrated by higher values of C_{max}, t_{max}, and k_a and tighter glycaemic control as seen by effective

reduction in plasma glucose levels, while causing significantly less pain than conventional catheters. The lidocaine study demonstrated for the first time that microneedle-based lidocaine injection can induce local anesthesia in human subjects with the same rapid onset and efficacy as intradermal injections using hypodermic needles, while being significantly less painful. Therefore, these results show that microneedle-based intradermal drug delivery can be used to effectively deliver drugs for systemic and local therapeutic effects in a less painful manner than conventional needles.

As mentioned previously, the research in this thesis is translational in nature and among some of the first to address microneedle treatment in human subjects. The results in this thesis provide answers to questions regarding the safety, efficacy, and usability of microneedles in a clinical setting and will help enable the transfer of microneedles from the laboratory to clinical practice.

CHAPTER 7: RECOMMENDATIONS

Based on the results of this thesis, I recommend the following studies to further advance this research. This thesis developed an impedance-based pharmacokinetic model for predicting the concentration profile of drug in the body following placement of a transdermal patch on microneedle created channels. Results showed that the predicted and experimental naltrexone concentration profiles were in good agreement. This model should be further validated by conducting experiments with other drugs having properties that differ from naltrexone (diffusion coefficient, volume of distribution, and clearance). Successful validation of this model would allow for a high-throughput method of determining plasma concentration of drugs administered via poke-and-patch microneedle systems and would aid in determining the appropriate number of needles or cross-sectional area to achieve target plasma concentrations.

With regards to the flow conductivity study, this thesis postulated the fate of fluid infused into the skin based on pressure, pain, and echographic image data. In order to more accurately determine the fluid path and distribution, studies should be carried out whereby a biocompatible dye is delivered to the dermis followed by skin biopsy and histology. The goal of microneedle delivery is to obtain reliable intradermal injections. While histological pig studies have been performed to show that 100 µl delivered via hollow microneedles remains in the dermis (data not shown), and the ultrasonic imaging results in this thesis appear to show that delivery of 1 mL of saline through 500 µm, 750 µm, and 1 mm long needles remains in the dermis at moderate flow rates, it is possible that infusion at high flow rates may lead to deeper delivery at large volumes. If this

occurs, it is important to determine at what volume the fluid starts to flow deeper beyond the target region. Further, understanding the flow and distribution of drug within the skin based on the different infusion and microneedle geometry parameters would help determine which conditions best target the papillary dermis (for faster absorption). Histological studies would help confirm this result. Alternatively, a contrast agent yielding high echogenicity may also be infused and imaged via ultrasonic imaging, as a non-invasive alternative. However, a suitable contrast agent with low viscosity that can be infused via microneedles to volumes as high as 1 mL needs to be identified. Additionally, future studies should be carried out to determine the resistance offered by skin while using microneedle arrays. This thesis showed that single needles led to high resistances upon delivery of large (> 500 µl) volumes at moderate and high flow rates without retraction. It is likely that multiple needles arranged in arrays will experience even higher resistances due to compression of the skin at multiple sites, thereby blocking the flow pathways nearby each needle. Further, the formation of a skin wheal may further affect the resistance of the needles in the array. Studies by others have shown that delivery of 100 µl of fluid into skin via four hollow microneedles is more painful than intramuscular injection (Van Damme, Oosterhuis-Kafeja et al. 2009). This may possibly be due to higher pressures generated during delivery through arrays which may push the fluid deep enough to stimulate dermal nociceptors. Hence, flow conductivity through microneedle arrays and its effect on pain should be further studied.

The insulin delivery study in this thesis demonstrated that hollow microneedles can lead to significantly improved insulin pharmacokinetics and improved glycaemic control while causing significantly less pain than subcutaneous catheters. These results

have promising implications for the improvements of diabetes management. However, this thesis only studied bolus insulin delivery which is typically administered at mealtimes. In order for microneedles to be well-accepted by diabetes patients, basal insulin delivery whereby low insulin volumes are delivered throughout the day also needs to be evaluated. One of the reasons for the failure of Exubera inhaled insulin was that it only provided bolus insulin delivery. Therefore, since Exubera only provided half the solution, patients had to continue to use their subcutaneous needles or catheters to meet their basal insulin requirements. This thesis has shown that microneedle-based bolus insulin delivery can lead to improved PK and PD. Therefore, successful application of microneedles for insulin delivery will depend on their ability to provide basal pharmacokinetic and pharmacodynamic profiles that are at least as effective as subcutaneous delivery systems. Once successful basal delivery has been achieved, the next challenge in the acceptance of microneedles for diabetes management will be the development of microneedle patches that are able to strongly adhere to the skin surface during normal day-to-day activities. Further, with regards to safety, it would also be of future interest to study if an immune response is elicited via injection of insulin to the dermis.

APPENDIX A: MATLAB CODE FOR PREDICTING PLASMA NALTREXONE CONCENTRATION USING IMPEDANCE DATA

Combining parameters

$$A = \frac{N \rho D \Delta C_{patch}}{V_{dist}} = 3.55\ \Omega\text{-ng/mL sec}$$

$$B = \frac{Cl}{V_{dist}} = 4.3 \times 10^{-5}\ \text{sec}^{-1}$$

dt = 3600 sec

Code to solve equation 4.5

% solves equation 4.5 up to t = 30 h.

```
clear;
clc;

c0=0;
A=3.55;
B=4.3e-5;

t0=0;
tf=108000;
h=3600;

T=t0:h:tf;
T=T';
N=size(T,1);
c=zeros(N,1);
c(1)=c0;

for n=1:N-1,
    c(n+1)=
    (1-h/2*B)/(1+h/2*B)*c(n)+(h/2*A)/(1+h/2*B)*(1/z(n+1)+1/z(n));
end;

figure;
plot(T./3600,c,'r*-');
xlabel('Time (h)');
ylabel('c(t) (ng/mL)');
```

```
title('Plot of c(t) vs. time');
grid;



function y=z(n)

Z=[ 19244;
    18381;
    19283;
    22598;
    24336;
    24610;
    24299;
    25950;
    25827;
    25440;
    25398;
    26968;
    21413;
    25784;
    28148;
    29358;
    31374;
    33054;
    34588;
    37851;
    36199;
    36992;
    39557;
    47444;
    50119;
    49049;
    49492;
    50359;
    52277;
    54210;
    55760];

y=Z(n);
```

APPENDIX B: MICRONEEDLES PERMIT TRANSDERMAL DELIVERY OF A SKIN-IMPERMEANT MEDICATION TO HUMANS[3]

B.1. Abstract

Drugs with poor oral bioavailability usually are administered by hypodermic injection, which causes pain, poor patient compliance, the need for trained personnel, and risk of infectious disease transmission. Transdermal (TD) delivery provides an excellent alternative, but the barrier of skin's outer stratum corneum (SC) prevents delivery of most drugs. Micrometer-scale microneedles (MNs) have been used to pierce animal and human cadaver skin and thereby enable TD delivery of small molecules, proteins, DNA, and vaccines for systemic action. Here, we present a clinical study of MN-enhanced delivery of a medication to humans. Naltrexone (NTX) is a potent mu-opioid receptor antagonist used to treat opiate and alcohol dependence. This hydrophilic and skin-impermeant molecule was delivered from a TD patch to healthy human subjects with and without pretreatment of the skin with MNs. Whereas delivery from a standard NTX TD patch over a 72-h period yielded undetectable drug plasma levels, pretreatment of skin with MNs achieved steady-state plasma concentrations within 2 h of patch application and were maintained for at least 48 h. The MNs and NTX patch were well tolerated with mild systemic and application site side effects. The MN arrays were painless upon administration and not damaged during skin insertion, and no MNs were broken off into the skin. This human proof-of-concept study demonstrates systemic administration of a

[3] This work was carried out in collaboration with researchers at the College of Pharmacy and College of Medicine at the University of Kentucky. This work has been published as: Wermeling DP, Banks SL, Hudson DA, Gill HS, Gupta J, Prausnitz MR, Stinchcomb AL. Microneedles permit transdermal delivery of a skin-impermeant medication to humans. Proc Natl Acad Sci USA 2008;105(6):2058-2063.

hydrophilic medication by MN-enhanced TD delivery. These findings set the stage for future human studies of skin-impermeant medications and biopharmaceuticals for clinical applications.

B.2. Introduction

Transdermal (TD) drug delivery has proven to be of great therapeutic utility (Guy and Hadgraft 2003; Prausnitz, Mitragotri et al. 2004). Patient acceptance of the technology is evident given the commercial success of products intended for chronic pain management, angina and congestive heart failure, and hormone replacement therapies. A TD patch can provide continuous drug administration, minimizing peaks and troughs in plasma levels throughout the day. TD systems can take the place of more risky and invasive injection-based drug delivery, thus improving regimen compliance. Moreover, they are more efficient, use less medication, and are less variable compared with some oral medications that undergo presystemic metabolism.

Even greater utilization of TD delivery for systemic drug administration is inhibited by several key factors. First, the stratum corneum (SC) outer layer of the skin is a very effective barrier at preventing entry of xenobiotics, infectious agents, and other substances into the body. This barrier prevents therapeutic delivery of most drugs other than those with high potency (dose in milligrams or less), low molecular mass (<1,000 Da), and optimal octanol-water partition coefficient (Hampton 2005).

Design of TD product formulations has attempted to overcome some of these limitations and enhance drug permeation (Prausnitz, Mitragotri et al. 2004). Chemical formulation methods may include the use of solvents, surfactants, and other chemical additives to diffuse and partition drug into the skin or to act as a carrier. Chemical

enhancers may also disrupt SC structure (Williams and Barry 2004). Prodrug and codrug medicinal chemistry, whereby physicochemical properties are modified through chemical synthesis with additional nontherapeutic or therapeutic substrates, has also been attempted (Vaddi, Hamad et al. 2005; Kiptoo, Hamad et al. 2006).

Physical approaches apply energy to enhance permeation, causing disruption of the SC, generally on a temporary basis (Cross and Roberts 2004). Successful methods include iontophoresis for polar molecules, electroporation and sonophoresis, the use of ultrasound, and even microdermabrasion or laser ablation.

Microneedles (MNs) represent a unique technological approach to enhance drug permeation across the SC (Prausnitz 2004). MN-based delivery involves micrometer-scale solid or hollow needles that painlessly pierce the SC. For example, an array of stainless steel, solid MNs produces a grid of holes, or micropores, through which medications delivered via a standard patch, may be delivered to the skin for local or systemic drug absorption (McAllister, Wang et al. 2003). Modern microfabrication techniques have been used to make MNs by methods suitable for inexpensive mass production (Reed and Lye 2004). In addition to solid, stainless-steel arrays, a number of other designs have been created, including hollow needles through which a drug solution may be transported, MNs that have been coated with a drug for dissolution upon application, and polymer MNs that dissolve upon application (Gardeniers, Luttge et al. 2003; Ito, Yoshimitsu et al. 2006; Gill and Prausnitz 2007).

MNs have been used to pierce the skin and thereby enable TD delivery of small molecules, proteins, DNA, and vaccines for systemic action, as shown in numerous *in-vitro* and animal studies (Mikszta, Alarcon et al. 2002; Gardeniers, Luttge et al. 2003;

McAllister, Wang et al. 2003; Cormier, Johnson et al. 2004). Although there have been a number of studies in animals, there is very little scientific literature describing the use of MNs on humans. Kaushik *et al.* (Kaushik, Hord et al. 2001) reported that blinded healthy volunteers could not distinguish a MN array from a smooth surface relative to pain sensation. The same subjects could clearly distinguish a MN array from a 26-gauge hypodermic needle. Mikszta *et al.* (Mikszta, Alarcon et al. 2002) compared microarrays to ECG electrode pads for their ability to disrupt human skin, cause pain, or induce inflammation. MNs of 200 μm in length were successful in breaching the SC as measured by transepithelial water loss. Pain perception was negligible and a minor skin irritation lasting to 48-h postapplication was noted in several subjects. Sivamani *et al.* (Sivamani, Stoeber et al. 2005), in a test of localized drug deposition and effect, found greater skin blood flow after injection of 1 μl of methyl nicotinate with MNs as compared with topical methyl nicotinate alone.

To date, there are no published human reports describing MN- enhanced TD delivery of a medication to the systemic circulation to our knowledge. Our article builds on previous preclinical publications and describes a study in which MN arrays were administered to humans in conjunction with TD systemic delivery of a therapeutic molecule. We selected naltrexone (NTX), which is used to block opioid effects in detoxified patients and treat alcohol dependence, as a model drug because it would benefit from TD administration and is difficult to deliver across intact skin (Vaddi, Hamad et al. 2005; Anton, O'Malley et al. 2006; Kiptoo, Hamad et al. 2006). NTX is a small, hydrophilic molecule that when administered orally undergoes significant first-pass metabolism with a highly variable 5–40% systemic bioavailability. A recently

marketed 30-day NTX depot injection provides therapeutic levels for 1 month but with a 10- to 15-fold peak-to-trough variation and in an administration system most patients find objectionable (Turncliff, Dunbar et al. 2005). Relatively constant NTX blood levels, and perhaps lower side effects, could be achieved if a TD product was developed that provided a relatively constant delivery rate (King, Volpicelli et al. 1997).

The following study was conducted to determine, in an initial human proof-of-concept study, whether water-soluble NTX hydrochloride could be successfully administered systemically from a TD patch after pretreatment of the SC with MNs. As reported by Vereby *et al.* (Verebey, Volavka et al. 1976), a 2 ng/ml plasma concentration in humans resulted in an 85.6% narcotic blockade in response to a 25-mg i.v. injection of heroin. A study performed in healthy volunteers who were given a single oral dose of 50 mg NTX showed maximum plasma concentration values ranging from 20 to 25 ng/ml, and after 24 h those levels had dropped to ≈3 ng/ml (Licko 1980; Wall, Brine et al. 1981). Plasma levels of NTX are in the 2–4 ng/ml range for days 7–28 of the monthly depot injection regime (Turncliff, Dunbar et al. 2005) and could be a target concentration range for this study.

Given the preclinical data on MNs and the known pharmacokinetics of NTX administered by other routes, our hypotheses are that (*i*) a modest TD NTX dose of ≈10 mg per day will produce steady-state plasma levels of 2 ng/ml when the skin is pretreated with MNs, (*ii*) control subjects whose skin is not pretreated with MNs will demonstrate no significant systemic absorption of NTX, and (*iii*) the MNs and NTX TD system will be well tolerated by healthy subjects.

B.3. Results

B.3.1. NTX Pharmacokinetics in Humans after TD Administration

The principal question we wanted to address was whether pretreatment of skin with MNs, and subsequent placement of a TD patch, would permit rapid attainment of pharmacologic, clinically relevant and sustained plasma levels of a hydrophilic molecule not normally absorbed across intact skin. To address this question, our data show that MN pretreatment of the skin permitted rapid systemic exposure to NTX. Measurable plasma levels were demonstrable within 15 min after patch placement in three MN-treated subjects and within 30 min for the remaining three subjects. The concentration–time curve (Figure B.1) shows a rapid rise or burst of absorption within the first several hours of application. Maximum concentrations occurred within a range of 1.5 to 18 h.

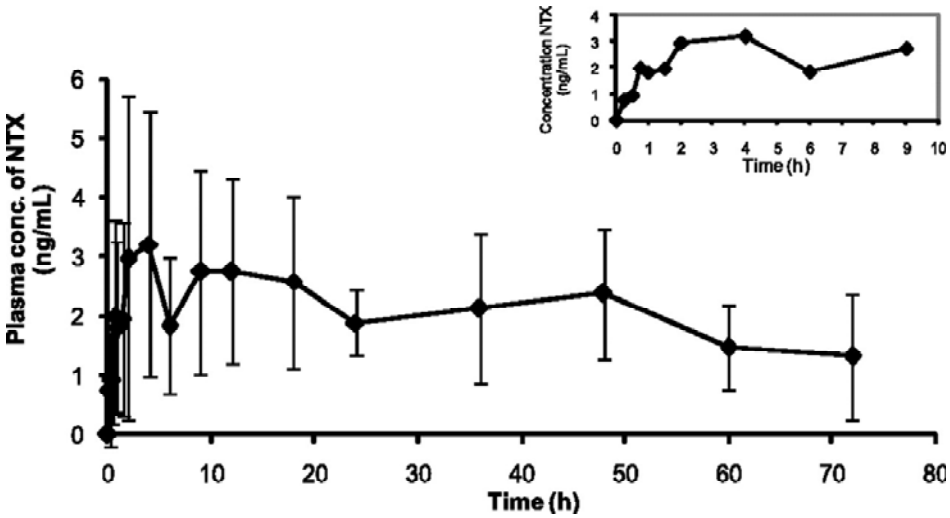

Figure B.1: Mean (SD) NTX plasma concentrations for 72 h of patch application. (*Inset*) Early sampling points.

Additional questions regarding our technique relate to the length of time the micropores remain open. Would the pore function for several days, permitting relatively

constant rates of drug delivery for systemic absorption, or rapidly undergo healing changes that would retard drug absorption? We demonstrate steady-state or a relatively constant plasma concentration of NTX was achieved within hours, to at most 1 day after patch placement, which indicates rapid transit, localized diffusion, equilibrium of NTX through dermal layers, and absorption into capillary beds (Table B.1). Approximately zero-order delivery appeared to be achieved for 48 h with a steady-state plasma concentration of ≈2.5 ng/ml, consistent with levels associated with pharmacologic activity. The maximum concentration obtained was somewhat variable and ranged from 1.6 to 8.1 ng/ml. Subjects with the lower concentration profiles tended to have lower peak-to-trough differences over the 72-h administration period. Similarly, the time to maximum concentration had a wide range, from as little as 1-2 h in two subjects, to as long as 18 h in two other subjects.

Table B.1: NTX and NTXOL exposure after MN-enhanced TD delivery

Parameters	NTX	NTXOL
C_{ss}, ng/ml	2.5 (1.0)	0.6 (0.5)
T_{lag}, h	1.8 (1.1)	1.4 (1.4)
C_{max}, ng/ml	4.5 (2.4)	1.9 (1.3)
T_{max},h	8.8 (7.6)	37.5 (31.3)
AUC_{0-t}, ng·h/ml	142.9 (43.9)	39.7 (25.9)
C_{last}, ng/ml	1.8 (1.0)	0.4 (0.6)

Results are expressed as means ± SD (in parentheses) for six MN-treated subjects. C_{ss} = concentration at steady-state condition; T_{lag} = time to reach steady-state condition; C_{max} = maximum concentration achieved; T_{max} = time to achieve maximum concentration; AUC_{0-t} = area under the concentration-time curve from time 0 to 72 h; C_{last} = concentration at time of patch removal after 72 h of application.

Skin micropores appeared to have remained open for at least 48 h as plasma levels appeared to be relatively constant for the first 48 h of administration. Two subjects had a profile suggesting drug permeation up to 72 h. Average plasma levels appeared to be

consistent for at least 48 h, with a modest average decline of NTX concentration by ≈50% at 72 h. The 72-h time-point average concentration of 1.8 ng/ml was ≈25% of the maximum concentration and 50% of the steady-state concentration. Pharmacologically active plasma concentrations were still evident at the last time point, 72 h after patch placement. The apparent plasma clearance of NTX indicates an approximate half-life of 4.4 h, suggesting that 95% of NTX would be eliminated within 24 h of patch removal. In contrast to the MN-treated subjects, the control subjects had undetectable (<1 ng/ml) NTX plasma levels, indicating minimal transfer of drug across the skin. Average peak levels in MN-treated subjects were 4.5 times larger than the assay detection limit.

Drug delivery systems that avoid presystemic drug clearance have been demonstrated to remarkably change the metabolite profile of certain medications. Similarly, we wanted to understand whether the TD system would significantly alter, and perhaps even reverse the ratio of the parent drug NTX to the metabolite. Naltrexol (NTXOL; primary metabolite of NTX) plasma concentrations were significantly less than the parent drug NTX (Figure B.2). This finding is consistent with avoiding presystemic first-pass metabolism of NTX. In contrast, NTXOL plasma concentrations are significantly higher than the parent drug NTX after oral administration (Licko 1980). The reversal of parent-to-metabolite ratio is a desirable outcome, because the NTXOL metabolite is associated with adverse effects.

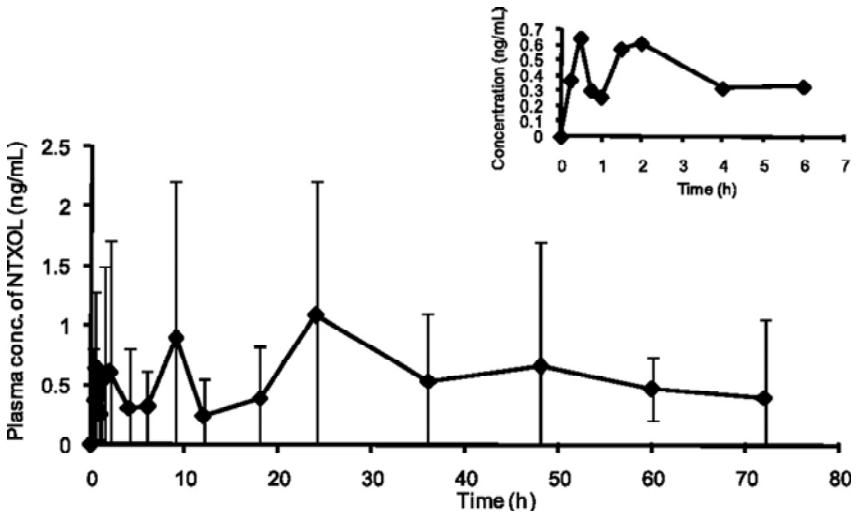

Figure B.2: Mean (SD) NTXOL plasma concentrations for 72 h of patch application. (*Inset*) Early sampling points.

A steady-state concentration of 0.6 ng/ml NTXOL was obtained throughout the 72-h patch placement. The time to reach steady state was comparable to NTX, indicating a slight delay in presentation to the hepatic system for metabolism. Maximum NTXOL concentrations were also modest and were not obtained until an average of 45 h after patch placement. Thus, the MN-facilitated TD delivery of NTX resulted in generation of a much lower quantity of the metabolite (NTXOL) and at a much later time, i.e., 45 h after TD administration using MN versus 1 h after administration of a tablet. The study by King *et al.* (King, Volpicelli et al. 1997) suggests our result could lower the side-effect profile of NTX, and improve compliance and retention in treatment, because withdrawal from oral drug treatment is associated with subjects who generate high levels of NTXOL.

B.3.2. Effect of MNs and NTX Patch on Human Skin

Limited previous studies have been reported on local tolerance of MNs themselves in humans. In our study we wanted to determine the tolerability of the MN arrays combined with a drug formulation and delivery system in humans. Our article

demonstrates the tolerability of the combined technologies in humans. MN arrays and patches were easy to administer. Administration of MNs simply required removing their protective liner and pressing the MN against the skin by hand. Application time for MNs and TD patches took 1–2 min, which is quite short, given the nature of the prototype MN and patch systems. MN arrays were examined for physical damage after their application to each subject. No MN array had bent or broken needles, and no needles were broken off into the subjects' skin.

The MN-treated subjects tolerated the MN and patch application system well. Subjects reported no pain when MNs were applied to their skin. The sensation of placement was described as simply of pressure applied at the site. Two subjects reported mild systemic side effects associated with NTX, such as nausea and lethargy, which are believed to be drug-specific and not directly associated with the MN delivery route. There was no clinically significant change in vital signs or liver function tests as a result of TD NTX administration. Control subjects also tolerated the patch system and reported no systemic-related side effects.

Four of the six MN-treated subjects did have skin changes observed when the patch and occlusive dressing were removed after 72 h of application, such as localized irritation and erythema outside of the patch placement site but within the dressing area for two of the subjects. Upon removal of the patch, two of the four subjects demonstrated contact dermatitis that exactly outlined the dimensions of the MN arrays insertion grid. Inside the raised areas were very small crusts that may represent the insertion points of the MNs and the subsequent micropores. The affected subjects were prescribed diphenhydramine capsules (antihistamine) and topical hydrocortisone cream as treatment.

Subjects were seen in the clinic 4–6 days later and had responded to treatment. Re-examination of the skin demonstrated the contact dermatitis was greatly diminished and within 1–2 weeks had disappeared. However, the crusts continued healing throughout the 2-week observation period, with a faint outline of the MN array insertion points still evident. Only one control subject demonstrated any finding on skin examination. The subject complained of itchiness and irritation, which was under the occlusive dressing and the patch. The findings disappeared upon removal of the patch.

To better understand the possible causes of skin irritation seen in this study, we carried out an additional study in 10 subjects to assess the effect of just MN insertion followed by occlusion of the skin. No NTX or patch formulation was used. Immediately after insertion, erythema was typically seen at the punctate sites where each MN penetrated into the skin (data not shown). The degree of erythema varied from barely visible to moderate, highly localized, submillimeter spots of redness. Within a few hours, erythema disappeared in most cases, such that it was not possible to distinguish between MN-treated skin and adjacent skin. The more dramatic effects of contact dermatitis observed in the two patients administered NTX were not seen in any of the subjects treated with MNs alone. We therefore conclude that MNs themselves cause little to no skin irritation that is highly transient and that the NTX and/or formulation excipients were responsible for the skin irritation observed in some subjects in this study. Further optimization of patch formulation could reduce or eliminate this irritation.

To better understand the lifetime of TD transport pathways created in the skin by MNs, we carried out a supplemental study in which skin electrical resistance was measured as a function of time after piercing the skin with MNs in 10 human subjects.

Skin electrical resistance has been shown to correlate well with skin permeability to various molecules (Karande, Jain et al. 2006). Average skin resistance dropped from 397 ± 183 kΩ before treatment to 11.7 ± 5.5 kΩ after MN insertion and removal. After covering with an occlusive dressing, skin resistance steadily increased but remained significantly less than the resistance of an adjacent control site of untreated skin for 30 h (Student's t-test; $p < 0.05$). These measurements are consistent with the measurements of NTX pharmacokinetics, which both show that brief treatment of skin with MNs creates long-lived permeability. There are quantitative differences between the measurements, however, because the electrical resistance measurement indicated a permeability lifetime of 30 h, whereas the NTX delivery measurement indicated a lifetime up to 72 h. This difference may exist because the electrical measurement assessed the barrier properties of skin's SC, whereas the NTX measurement assessed the kinetics of drug delivery into the bloodstream, which is influenced not only by the SC barrier, but can also be influenced by diffusion, pooling, and possible binding in the skin en route to the bloodstream, which can delay the kinetics of drug clearance.

B.4. Discussion

B.4.1. Delivery of NTX from the TD Patch

This study demonstrates MN pretreatment of the skin and subsequent TD delivery of a drug to humans. Previous research to demonstrate TD transport has been conducted on human cadaver skin and small animals. Studies in humans have focused on the aesthetic nature of avoiding pain upon administration of the MNs or local action in the skin itself. Thus, this work is a significant advancement by combining the MN technology enabling skin permeation with a drug formulation and delivery system for

administration of a drug of clinical significance. This report provides the scientific basis and justification for future studies to test MN technology with skin-impermeant medications of different chemistry, such as peptides and proteins, married with a TD drug delivery system.

This proof-of-concept study supports the hypothesis that *in-vivo* insertion of MNs into the skin before placement of a standard TD patch drug delivery system results in pharmacologically active and clinically relevant plasma levels of a skin-impermeant medication. The MN-facilitated TD delivery was very efficient by providing pharmacologically active steady-state plasma levels of 2.5 ng/ml at a very modest estimated dose of 12.6 mg per day. The absorbed TD daily dose is roughly one-quarter of the daily dose administered as an oral tablet to achieve similar plasma levels. This observed increase in efficiency is ascribed to the avoidance of gastrointestinal and hepatic first-pass metabolism.

Moreover, as a result of avoiding first-pass metabolism, the ratio of plasma NTX to NTXOL at steady state was dramatically different from oral delivery. TD delivery using MNs produced a ratio of 4:1, such that most of the drug remained in the parent NTX form. In contrast, the NTX/NTXOL ratio after oral delivery is 1:5, with NTXOL being formed rapidly after gastrointestinal absorption. Moreover, the NTX depot injection also does not achieve the desired metabolic ratio of NTX/NTXOL. The C_{max} ratio of NTX to NTXOL is 3:4 on the second day after injection (Licko 1980). Altering this ratio through constant rate TD delivery could result in an improved side-effect profile because at least one report (Karande, Jain et al. 2006) suggests the commonly observed side effects (nausea, lethargy, dizziness) seen after acute oral administration are

associated in subjects with more rapid metabolism and greater relative formation of NTXOL.

Variability in pharmacokinetic parameters across subjects was small after TD delivery using MNs. For comparison, bioavailability of the oral NTX tablet has an 8-fold variation, from 5% to 40%, and similar variability in pharmacokinetic parameters. Rate and extent of NTX exposure was similar across the subjects, with standard deviations being approximately half of the mean, which is a characteristic desirable for drugs and delivery systems. This result is encouraging, given the relatively early proof-of-concept prototype design used in this pilot study.

Of great interest is the observation that most subjects appeared to have an initial burst of NTX into the systemic circulation. The result suggests that there is a loading-dose phenomenon, in which rapid absorption to therapeutic levels takes place initially and then is moderated over the course of the next few days. Subsequent to the burst, steady-state concentrations were achieved in a matter of hours, which is unusually fast for a TD delivery system. For example, conventional clonidine and fentanyl TD delivery systems do not achieve steady-state concentrations for 1–2 days (Catapres TTS and Duragesic Transdermal System product labels; www.fda.gov). The rapid and consistent achievement of steady-state drug concentrations observed in our study provides a pharmacokinetic profile that is ideal for many medication classes.

The observation of a burst of systemically available medication could potentially be explained by the combination of two effects. The first effects concern the relatively hydrophilic nature of NTX. Without the use of MN, or other enhancement techniques, drugs that can cross the skin are very hydrophobic and therefore form a large depot in the

hydrophobic environment of the SC (Guy and Hadgraft 2003). The filling of this depot delays drug delivery into the circulation. The use of MNs created hydrophilic micropores across the SC, which bypassed the SC depot and permitted the use of a hydrophilic drug (i.e., NTX) that would not form a depot. This expedited NTX delivery to the circulation.

The second effect is that micropores close over time. Our electrical resistance measurements indicated that skin conductivity steadily decreased with time after MN insertion. NTX plasma levels also were reduced over time, suggesting a slow return of skin barrier properties caused by initiation of the healing process after microinjury to the epidermis. Elastic rebound of the skin back to its original conformation, release of cytokines upon skin piercing, closure of the pore by interstitial fluid proteins, reepitheliazation initially through cell migration and subsequent regeneration, and forming a crust over the pore all may contribute to this resealing process (Clark 1996; Martanto, Moore et al. 2006a).

B.4.2. Tolerability of MNs and NTX Patch

In general, the subjects tolerated the MN insertion and application of the NTX gel patch. Most subjects had mild erythema underneath the occlusive dressing that was added to further secure the prototype patches for several days and protect them from water. Several subjects also had skin changes under the patch system, in contact with the gel and at the MN insertion sites. These effects were not seen when applying MNs without an NTX patch. Observation of contact dermatitis could be related to the medication, NTX, because opiate structures are known to cause histamine release after local or systemic administration. Another possible explanation for local skin irritation is

the use of benzyl alcohol as an antimicrobial preservative. Another form of asepsis for the drug product could eliminate this potential irritant.

An outline of the MN insertion site grids, along with punctate crusts over the insertion sites, was observable to varying degrees in most subjects. The observation did not appear to cause distress or discomfort in any subject. Disappearance of the outline and crusts over the next 1–2 weeks likely represented a continued healing process of the skin.

B.4.3. Implications for MN-Assisted TD Patch Delivery

This proof-of-concept study in humans demonstrated successful TD delivery of NTX, a small hydrophilic molecule. It is likely that other small hydrophilic molecules would be amenable to delivery using methods similar to those in this article. A significant new test would be to demonstrate human delivery of pharmaceuticals with significantly larger molecular weight, such as peptides and proteins, as shown in animals (Mikszta, Alarcon et al. 2002; Gardeniers, Luttge et al. 2003; McAllister, Wang et al. 2003; Cormier, Johnson et al. 2004). Additional challenges may be faced with larger molecules relative to formulation, the function of the skin barrier that may inhibit delivery such as binding of protein drugs to skin constituents, and exposure to proteases. Moreover, preclinical data suggest that TD vaccination via MN-pretreated skin is feasible.

This pilot study has a number of limitations that must be taken into context relative to the results. The systems used are relatively early-stage prototypes as far as TD delivery systems are usually designed. The patch and gel used standard components assembled to approximate pharmaceutical products. However, these data easily translate

into preparation of 200-needle MN patches and NTX gel patches to deliver the desired dose in a more practical integrated delivery system. Application of MNs with this device was an imprecise manual administration process. Additional engineering is required to standardize the force necessary to insert MNs to the appropriate depth. Results could be impacted by other factors such as choice of subjects and condition of their skin, anatomical site of MN insertion and patch application, and other well known variables to consider for TD drug administration.

In conclusion, this study reports the systemic delivery of a skin-impermeant medication via MN-facilitated TD delivery in humans. This study supports the significant body of preclinical research in animal and human cadaver skin, and in limited *in-vivo* studies, that MN-enhanced TD delivery is feasible, well tolerated, and pain-free. Methods to enhance standardization of MN insertion and patch formulation are necessary for this application. The results open the possibility of further studies to examine the effect of known variables of TD delivery. Moreover, this study opens the possibility of further research of NTX using a zero-order delivery system in the treatment of various substance abuse disorders.

B.5. Materials and Methods

B.5.1. Fabrication and Assembly of Solid MNs.

Using methods described in detail previously, solid MN adhesive patches were fabricated for insertion into the skin (Kaushik, Hord et al. 2001). Briefly, fixed MN geometries were cut into 75-μm-thick stainless-steel sheets (Trinity Brand Industries; McMaster-Carr) using an infrared laser (Resonetics Maestro) and were then manually bent perpendicular to the plane of their metal substrate. For better insertion and adhesion

of patches to the skin, MN arrays were assembled into adhesive patches as described. The adhesive served to hold the MNs firmly against the skin by compensating for the mechanical mismatch between the flexible skin tissue and the rigid MN substrate. The MN patches were assembled in a laminar flow hood for cleanliness and then ethylene oxide-sterilized (AN 74j; Andersen Sterilizers) before use.

MN arrays were fabricated to produce patches containing 50 MNs arranged in 5 × 10 arrays of MNs (Figure B.3A). Each MN measured 620 μm in length, 160 μm in width at the base, and <1 μm in radius of curvature at the tip. To validate that these MNs pierced into the skin to increase skin permeability, individual arrays were inserted into the forearms of 10 human subjects. After removing the MN patches, the skin was stained with a dye that selectively stains sites of skin barrier perforation. As shown in Figure B.3B, all 50 MNs on the patch inserted into the skin and pierced the skin's SC barrier, as indicated by the 5 × 10 array of dyed spots corresponding exactly to the geometry of the MN array. These 10 subjects were also asked immediately after MN insertion and removal to score the pain on a 0–100 visual analog pain scale. The average pain score was 6 ± 5 for the MN patch and 24 ± 16 for a 5-mm-deep hypodermic needle insertion that served as a positive control. Comparing the ratio of these scores indicates that the subjects felt that insertion of the 50-MN array caused just one-fourth of the pain caused by the hypodermic needle.

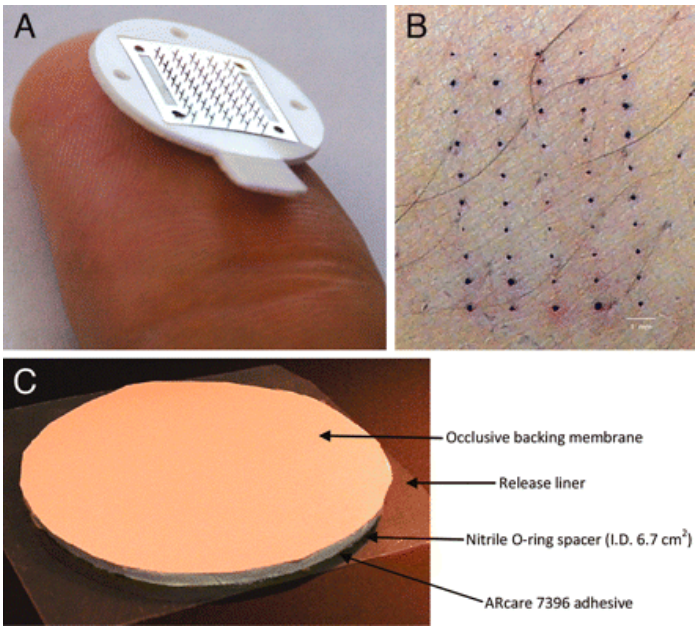

Figure B.3: MN patch for TD delivery. (*A*) Image of a 50-MN patch resting on the tip of a human thumb. (*B*) Image of human skin after insertion of a 50-MN patch and staining with gentian violet, a dye that selective stained sites of skin perforation. (*C*) NTX TD patch and covering.

B.5.2. Dose Estimation for Design of TD Patch

A method was needed to estimate dosing rate and patch size (area) for the initial human study. An initial estimate was derived by simply using the relationship of $K_0 = Cl \times C_{ss}$, where K_0 = the dosing rate in mg per day, Cl is the total body clearance of the medication in liters/min, and C_{ss} is the target plasma concentration at steady state. Assuming a target of 2 ng/ml concentration, and a total body clearance for NTX of 3.5 liters/min, a total daily dose of ≈10 mg was estimated.

In preliminary *in-vitro* studies of NTX HCl on human skin treated with MNs, we were able to achieve a steady-state flux of 14.7 ± 4.9 μg/cm^2 per h at a patch formula NTX concentration of 160 mg/ml. To make an *in-vivo* correlation for patch size we used the equation: $A = Cl \times C_{ss} / J_{s,}$ where A is the area of the applied patch and J_s is the NTX

flux constant. Thus, the patch surface area, at a NTX formulation concentration of 160 mg/ml, and providing 2 ng/ml plasma levels at steady state, was estimated at ≈28 cm^2. The daily dose estimate from four commercially accessible 6.7-cm^2 patches (26.8 cm^2 total) was estimated at 9.5 mg, very close to the previous estimation method.

B.5.3. Preparation of NTX TD Patches

A 16% NTX hydrochloride (HCl) gel was formulated, prepared, and tested according to current good manufacturing practices as outlined by the Food and Drug Administration. The gel formulation composition (% wt/wt) was NTX HCl [16% U.S. Pharmacopeia (USP)], sterile water for injection (20.25% USP), propylene glycol (60.75% USP), 2% Aerosol (hydroxyethyl cellulose), and 1% benzyl alcohol. The 16% NTX formulation was a clear, colorless gel and had a pH of 4.96 ± 0.03 and a viscosity of $1.69 \pm 0.44 \times 10^4$ cP.

The TD occlusive protective covering patches of NTX HCl (6.7 cm^2) were fabricated by using commercially accessible components by sandwiching a rubber-ringed barrier to create a reservoir between a drug-impermeable backing membrane (Scotchpak 1109 SPAK 1.34 MIL heat-sealable polyester film; 3M) and an Arcare 7396 adhesive (Adhesives Research) around the edge of the rubber spacer (Figure B.3C). The impermeable backing laminate was adhered to the rubber retaining ringed barrier with 3M double-sided tape. Finally, Arcare 7396 was placed on the bottom of the rubber-ringed barrier to maintain intimate contact with the skin and prevent evaporation of the gel formulations. The protective patch was placed on a release liner composed of Scotchpak 9742. The circular NTX patch area slightly exceeded the surface area of MN-

treated skin to ensure adequate coverage of the micropores and reduce formulation pooling in square TD patches.

B.5.4. Clinical Study Procedures

This study was approved by the University of Kentucky Institutional Review Board and carried out in compliance with the ethical and scientific principles governing clinical research as set out in the World Medical Association Declaration of Helsinki. Nine male and female healthy volunteers were medically examined and interviewed to determine appropriateness for study. Inclusion/exclusion criteria to confirm general wellness were compared with data collected through a physical examination, blood sample (chemistry, cell counts, hepatitis), urine sample (urinalysis, pregnancy test if applicable, and drug of abuse screen), and drug and medical history. Subjects could not have a history of opiate use/abuse as indicated by verbal report and a negative urine drug screen or hepatitis. A standardized examination of the patch placement skin site was conducted to confirm normal skin. Subjects with inflammatory diseases of the skin, who had recent sunburn, or other conditions that may cause changes in skin physiology, or who used skin exfoliant dermatologic products or antibacterials were excluded. Subjects were not taking any medications at the time of study with the exception of stable use of oral contraceptives. Subjects were nonsmokers, did not use tobacco products, and agreed to not consume alcoholic beverages during the study.

The six MN-treated and three control subjects were admitted to the inpatient facility of the General Clinical Research Center of the University of Kentucky Hospital. Subject's good health was confirmed by interview and brief examination, and urine drug of abuse screens were repeated. Demographic characteristics of the six MN-treated

subjects were average (SD) age of 25.3 (3.2) years, weight of 74 (13.7) kg, and height of 175.9 (7.8) cm, and they were split evenly between males and females. The three control subjects were 23.3 (2.1) years of age, 65.8 (11) kg, 173.9 (7.6) cm, and female.

The morning of NTX gel-patch administration, the subjects had an indwelling i.v. catheter placed in an antecubital or forearm vein contralateral to the arm that received patch placement. Before patch administration, a single blood sample was obtained as baseline, along with vital signs, and a repeat of the standardized skin examination of the test site to document baseline conditions. Six healthy subjects were treated with two 50 MN arrays (100 MN insertions per single patch application site) on the hairless (nonshaved) upper arm before each patch application (four patch sites and 400 MN insertions total per patient). The same procedure, except omission of MN insertion, was used for control subjects. MN insertion simply means placing the MN array over the skin and gently pressing down for a few seconds. The NTX-gel and patch covering were placed over the same area of the skin. An occlusive dressing was placed over the skin site and NTX patches to hold them in place for the study duration.

After patch administration serial blood samples and vital signs were obtained at 15, 30, 45, and 60 min and at 1.5, 2, 4, 6, 9, 12, 18, 24, 36, 48, 60, and 72 h after administration. Subjects were queried, using a standardized instrument, regarding any pain associated with administration and untoward symptoms from the product. An examination of the skin was conducted when the patch was removed and at 4–6 days after administration to detect any irritation, inflammation, discharge, etc., using the standardized skin examination format. A blood chemistry test was repeated to evaluate any gross effects on liver function.

B.5.5. NTX and NTXOL Plasma Assay

The assay was similar to that published by Valiveti *et al.* (Valiveti, Nalluri et al. 2004) The extraction efficiency was 86.0 ± 6.8% for NTX and 78.0 ± 19.6% for NTXOL. The limits of quantification for NTX and NTXOL were 1.0 and 0.5 ng/ml, respectively, with $r^2 > 0.95$ for both NTX and NTXOL.

B.5.6. Assessment of Skin Irritation and Resealing Kinetics

An additional study was conducted to measure skin irritation and resealing kinetics. Ten human volunteers (seven males, 23–51 years of age) were recruited from the Georgia Institute of Technology community. The protocol was approved by the Institutional Review Board at Georgia Institute of Technology and informed consent was obtained from the subjects.

A MN patch (Figure B.3A) was inserted into the volar forearm of the subjects and then immediately removed. Treatment sites were occluded by using an occlusive tape (3M Blenderm surgical tape; 3M Healthcare). The occluded sites were further covered with a waterproof dressing (Nexcare absolute waterproof premium adhesive pad; 3M Healthcare) and Saran wrap (SC Johnson), which was secured with waterproof tape (Nexcare absolute waterproof first aid tape; 3M Healthcare).

Skin electrical resistance was measured hourly with an impedance meter (EIM-105 Prep-Check electrode impedance meter; General Devices) modified with a 200-kΩ resistor (Ack Electronics) in parallel. Ag/AgCl dry electrodes (Thought Technology T-3404; Stens) were used as the measurement electrodes for the MN treatment sites. A large electrode with a highly conductive gel (Superior Silver Electrode with PermaGel; Tyco Healthcare Uni-Patch) was used as the reference electrode to keep the impedance

contribution of the reference site at a negligibly low value. Resistance measurements were made by connecting lead wires to the reference and measurement electrodes, respectively. Immediately after MN insertion and periodically during the study, skin irritation was assessed by visually examining the MN-treated sites for erythema, edema, and other adverse skin reactions and comparing them with adjacent untreated skin sites.

B.5.7. Data Analysis

The pharmacokinetic analysis of NTX and NTXOL plasma-concentration versus time profiles after MN treatment and gel patch application was carried out by fitting the data to a noncompartmental model with extravascular input (WinNonlin Professional, version 4.0; Pharsight). The data generated after TD application were analyzed by a noncompartmental method using WinNonlin. The steady-state plasma concentration of NTX after the application of patches was calculated by using the equation $C_{ss} = AUC_{0\text{-}t}/time$. C_{last} was the final plasma concentration measured from the 72-h sampling time point. The flux constant for human skin was calculated as $J_s = C_{ss} \times Cl/A$. The average daily dose delivered was calculated as $K_0 = C_{ss} \times Cl$. Statistical analysis of the subject and pharmacokinetic data obtained after the TD application of the patches was performed by one-way ANOVA using SigmaStat. Clinical data were analyzed with SAS.

APPENDIX C: RECOVERY OF SKIN BARRIER PROPERTIES AFTER SONICATION IN HUMAN SUBJECTS[4]

C.1. Abstract

The SonoPrep ultrasonic skin permeation system is used clinically to increase skin permeability for rapid, noninvasive delivery of local anesthetics. This study tested the hypothesis that sonication can generate a long-lived increase of skin permeability for continuous transdermal drug delivery and diagnostic metabolite extraction. To accomplish this, the volar forearm skin of ten healthy adult subjects was sonicated. As a surrogate measure of skin permeability, skin electrical impedance was measured at occluded and nonoccluded sites every hour over a period of 48 h. Sonication dramatically increased skin permeability, as demonstrated by a large drop in skin impedance. Under occlusion, sonicated skin remained highly permeable during the entire 42-h period of occlusion, which was followed by an immediate decrease in permeability upon removal of occlusion. Without occlusion, sonicated skin retained elevated permeability throughout the 48-h experiment, but regained its barrier function more quickly. Therefore, sonication can increase skin permeability for prolonged periods of time, especially under the effect of occlusion, and has potential to facilitate continuous transdermal drug delivery and diagnostic metabolite extraction.

[4] This work is in press as Gupta, J and Prausnitz, MR, "Recovery of skin barrier properties after sonication in human subjects", in Ultrasound in Medicine and Biology.

C.2. Introduction

Transdermal drug delivery is severely limited by the low permeability of stratum corneum (Prausnitz, Mitragotri et al. 2004). Although transdermal delivery has grown into a multibillion dollar industry over the past 25 years, this industry is based on fewer than 20 drugs that can currently be delivered across the skin (Prausnitz, Mitragotri et al. 2004). Sonication using low-frequency ultrasound has been shown to create openings in the stratum corneum (Wu, Chappelow et al. 1998) and to increase skin permeability for transdermal delivery of several classes of drugs including insulin, lidocaine, tetanus toxoid antigen and low molecular weight heparin, as well as extraction of interstitial fluid metabolites for glucose sensing (Kost, Mitragotri et al. 2000; Katz, Shapiro et al. 2004; Mitragotri and Kost 2004). To further assess the clinical utility of this approach, this study tested the hypothesis that sonication can generate a long-lived increase of skin permeability for continuous transdermal drug delivery and diagnostic metabolite extraction. This is the first human study to assess permeability of sonicated skin for more than one day and the first to compare skin recovery with and without occlusion. Sonication was carried out in this study using the SonoPrep ultrasonic skin permeation system, which is the only low-frequency ultrasound device that is FDA approved for transdermal drug delivery (Farinha, Kellogg et al. 2006). This device transmits ultrasonic energy to the skin through an aqueous medium, which generates cavitation bubbles at the skin surface that create transport pathways across the stratum corneum. SonoPrep has been approved by the FDA as a pretreatment to premeabilize the skin for rapid delivery of local anesthetics. In this study, skin permeability was monitored after sonication by measuring electrical skin impedance. Skin impedance is a well-accepted measure of the

skin's barrier properties and has been shown to correlate with skin permeability for a variety of compounds over a broad range of impedance values (Karande, Jain et al. 2005).

C.3. Materials and Methods

Ten healthy adult human subjects (3 female, 7 male, age 24 to 52 y) with no history of dermatological disease provided informed consent to participate in the study, which was approved by the Georgia Tech Institutional Review Board. Two sites were identified on the right volar forearm of each subject, one of which was occluded (skin made impermeable to air and moisture by covering with surgical tape and dressings) during the study and the other was nonoccluded (uncovered skin). After measuring pretreatment skin impedances, the identified sites were sonicated by briefly applying low-frequency (55 kHz) ultrasound (intensity = 15 W/cm^2) until the skin was permeabilized, as determined by the inbuilt mechanism in the device (SonoPrep; Sontra Corporation, Franklin, MA). The occluded sites were unoccluded during the sonication procedure followed by immediate occlusion after treatment. Hourly impedance measurements were taken at each site over a period of 48 h. Occluded sites remained covered during the impedance measurement process. After the 42nd hour reading, the occlusive dressings were removed and all sites remained nonoccluded for the final 6 h. Subjects were divided into two groups of five individuals each. The first group provided data for time points 1-11 and 23-35 h, and the second group provided data for time points 12-22 and 36-48 h. Both groups also provided data for time points –1, –0.5 and 0 h (immediately after treatment). Throughout each data collection period, subjects remained seated in the isolated study room maintained at 20-22°C and 40% relative humidity. Impedance

measurements (EIM-105 Prep-Check, 30 Hz, modified with a 200 kΩ resistor in parallel; General Devices, Ridgefield, NJ) were made using Ag/AgCl dry electrodes (Thought Technology T-3404, Stens Corporation, San Rafael, CA) placed at each treatment site with a Ag/AgCl gelled reference electrode (Superior Silver electrode with PermaGel, Tyco Healthcare Uni-Patch, Wabasha, MN) placed approximately 5 mm away.

C.4. Results and Discussion

Skin on the volar forearm of 10 human subjects was exposed to low-frequency ultrasound using a SonoPrep sonication device (Figure C.1a). Visual inspection of the skin immediately before (Figure C.1b) and after (Figure C.1c) sonication showed no differences other than formation of a slight circular indentation because of pressing the sonication hand piece against the skin. This indentation disappeared within 1 h and no erythema or edema was observed at any time on the skin surface for both occluded and nonoccluded skin (Figure C.1d). There were no adverse events and the treatment was well tolerated by all subjects. As a surrogate measure of skin permeability, the electrical impedance of skin was measured before, immediately after and hourly for 48 h after sonication. During this time, the skin was either nonoccluded or was occluded for 42 h and then nonoccluded for the remaining 6 h. Immediately after sonication, skin impedance dropped dramatically from pre-treatment values (>200 kΩ-cm^2) to less than 10 kΩ-cm^2 (Figure C.2). This impedance drop signifies a large increase in skin permeability. Although no drugs were delivered in this study, previous studies suggest that skin with such a low impedance corresponds to skin permeability increased by orders of magnitude that should be sufficient for delivery of hydrophilic molecules and even macromolecules, including proteins (Tezel, Sens et al. 2003).

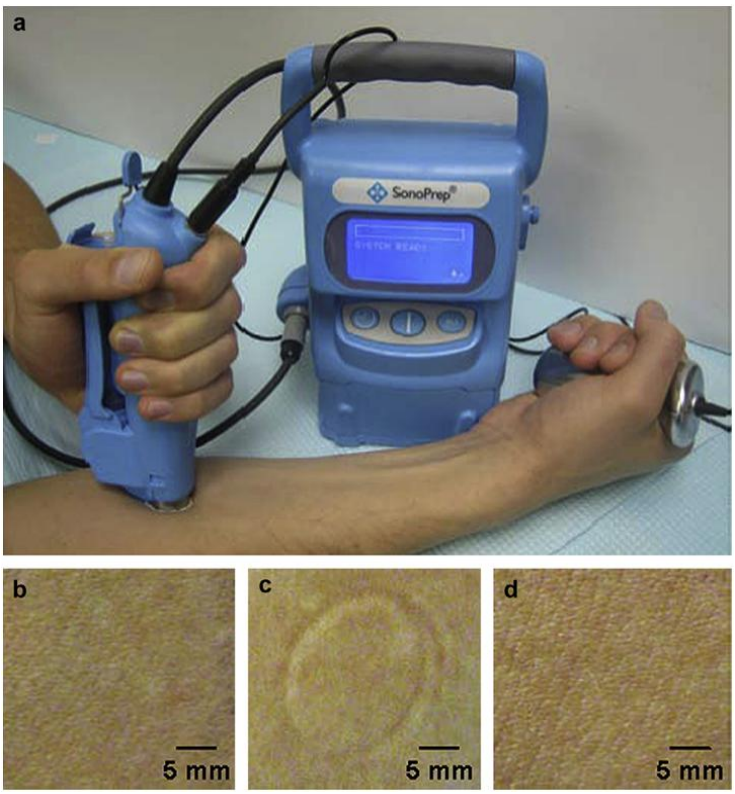

Figure C.1: Sonication of the skin. (a) Sonication was carried out by applying a hand piece containing ultrasound coupling medium to the subject's volar forearm skin. A reference sensor clasped in the subject's hand helped determine the duration of sonication by interacting with the main control console. Photographs of a representative sonicated skin site are shown (b) immediately before sonication, (c) immediately after sonication and (d) 24 h after sonication. No erythema, edema or adverse events were associated with sonication at any time. Only a transient skin indentation caused by application of the hand piece was observed immediately after sonication (c).

The primary goal of this study was to assess the longevity of increased skin permeability after sonication. Over the 48-h experiment, skin impedance values steadily increased for both the occluded and nonoccluded sites, although the increase was slower for the occluded case (Figure C.2). Statistical analysis at each time point using a paired t-test with 95% confidence interval revealed that impedance of the occluded sites remained indistinguishable from the initial post sonication impedance value for up to 42 h. These kinetics are similar to those reported in a previous 24-h study examining the suitability of

sonication as a skin pretreatment for electrophysiology measurements (Farinha, Kellogg et al. 2006) and another 24-h study measuring extraction of interstitial glucose after sonication (Kost, Mitragotri et al. 2000). This long-lived effect suggests that transdermal delivery from an occlusive patch applied to sonicated skin could persist at high levels for at least 42 h. Upon removal of occlusion after the 42nd hour, the impedance jumped and was significantly different from the initial post sonication impedance. This suggests that upon removal of an occlusive transdermal patch from sonicated skin, the skin barrier can rapidly begin to recover. We hypothesize that this slow skin barrier recovery under occlusion is caused by the reduced transepidermal water loss under occlusive skin conditions. Previous studies have shown that stratum corneum barrier repair is mediated by the formation of a water gradient in the skin caused by increased transepidermal water loss through the compromised skin barrier (Grubauer, Elias et al. 1989). In this way, occluded skin is more slowly repaired and removal of occlusion creates a water gradient, allowing normal repair to occur. In contrast, the nonoccluded sites regained their impedance more rapidly and were significantly different from the initial post sonication impedance within 7 h. However, even after the 7-h period, the impedance was still much lower than that of intact skin and thus, the sites could potentially be permeable to, for example, smaller molecules. Experimental and theoretical studies of transport across sonicated cadaver skin indicate that as skin impedance increases, permeability decreases more steeply for larger molecules (Tang, Mitragotri et al. 2001; Tezel, Sens et al. 2003).

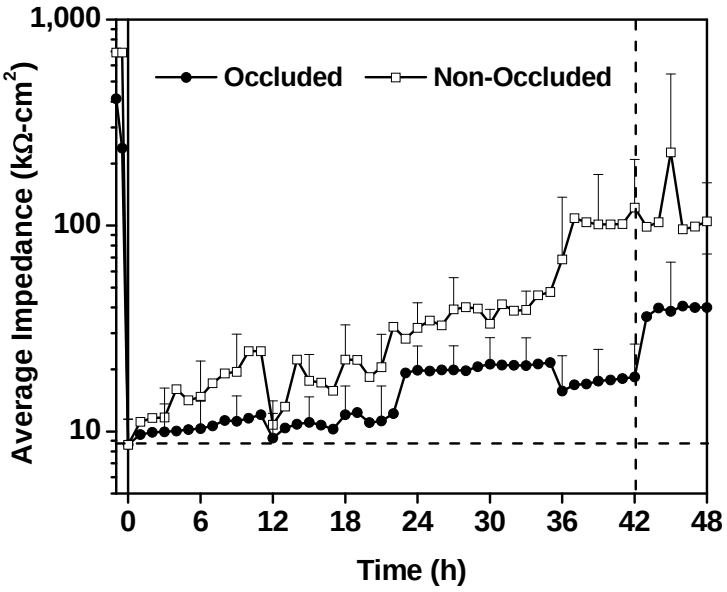

Figure C.2: Average skin impedance for occluded (●) and nonoccluded (□) skin before and after ultrasound treatment, which was carried out at t = 0. Nonoccluded skin remained nonoccluded throughout the experiment. Occluded skin remained occluded until t = 42 h, after which skin was nonoccluded for the final 6 h. Immediately after sonication, skin impedance dropped dramatically from pretreatment values (>200 kΩ-cm^2) to less than 10 kΩ-cm^2, indicating an increase in skin permeability. Skin impedance recovered slowly over time, but the occluded sites recovered more slowly than nonoccluded sites. Upon removal of occlusion at t = 42 h, skin impedance rapidly jumped higher. Data are presented as the average of n = 10 samples (t < 0) or n = 5 samples (t ≥ 0) with standard deviation error bars.

Thus, even though macromolecule delivery may be reduced beyond 7-h post sonication, nonoccluded skin could still be used for delivery of small molecules. This presents opportunities for long-term delivery, but also presents safety concerns after short-term delivery, because of residual permeability after a transdermal delivery procedure is completed. These results can guide the use of sonication for both short-term and long-term transdermal delivery applications. SonoPrep is currently approved as a pretreatment before short-term delivery of local anesthetics over a time course of a few minutes under typically nonoccluded conditions, although the anesthetic formulation itself may provide partial occlusion. Our data showing a large initial drop in skin

impedance, corresponding to a large increase in skin permeability, are consistent with this demonstrated application. However, the persistence of increased skin permeability for hours after delivery of the local anesthetic is complete suggests that patients and clinical personnel should take care to prevent unintentional absorption of exogenous materials during that time. For long-term delivery from an occlusive transdermal patch, our data suggest that drug delivery can persist at relatively steady levels for at least 42 h. Animal studies have demonstrated delivery of a variety of drugs, including that of insulin (Mitragotri and Kost 2004; Park EJ, Werner J et al. 2007), heparin (Mitragotri and Kost 2004) and tetanus toxoid antigen (Tezel, Paliwal et al. 2005). Thus, a sonication pretreatment could be followed by sustained-release delivery of drugs and vaccines from a patch. Similarly, noninvasive glucose monitoring has been demonstrated in diabetic subjects via interstitial glucose extraction from sonicated skin (Kost, Mitragotri et al. 2000). Our data suggest that continuous monitoring for at least one day may be possible after a single ultrasound pretreatment. In conclusion, skin impedance measurements in this study showed that skin permeability can be dramatically increased by sonication and that elevated skin permeability can persist for at least 42 h under occlusion. Skin permeability recovered more rapidly without occlusion.

This suggests that sonication can be used as a pretreatment to generate a long-lived increase of skin permeability for continuous transdermal drug delivery and diagnostic metabolite extraction.

REFERENCES

Alarcon, J. B., A. W. Hartley, et al. (2007). "Preclinical evaluation of microneedle technology for intradermal delivery of influenza vaccines." Clin Vaccine Immunol **14**(4): 375-381.

Allen, L. V., N. G. Popovich, et al. (2005). Ansel's Pharmaceutical Dosage Forms and Drug Delivery Systems. Philadelphia, Lippincott Williams & Wilkins.

Anton, R. F., S. S. O'Malley, et al. (2006). "Combined pharmacotherapies and behavioral interventions for alcohol dependence: The COMBINE Study." J Am Med Assoc. **195**(17): 2003-2017.

Arendt-Nielsen, L., H. Egekvist, et al. (2006). "Pain following controlled cutaneous insertion of needles with different diameters." Somatosens Mot Res. **23**(1-2): 37-43.

Arora, A., M. R. Prausnitz, et al. (2008). "Micro-scale devices for transdermal drug delivery." Int J Pharm. **364**(2): 227-236.

Bailey, C. J. and A. H. Barnett (2007). "Why is Exubera being withdrawn?" British Medical Journal **335**: 1156.

Bal, S. M., J. Caussin, et al. (2008). "*In-vivo* assessment of safety of microneedle arrays in human skin." Eur J Pharm Sci **35**(3): 193-202.

Banga, A. K. (1998). Electrically-Assisted Transdermal and Topical Drug Delivery. Bristol, Taylor and Francis.

Banga, A. K. (2009). "Microporation applications for enhancing drug delivery." Expert Opin Drug Deliv. **6**(4): 343-354.

Banks, S. L., H. S. Gill, et al. (2005). Lifetime of increased skin permeability after treatment with microneedles in hairless guinea pigs *in-vivo* using transepidermal water loss. AAPS Annual Meeting and Exposition. Nashville, TN.

Barnett, A. H. (2008). "The future of inhaled insulin and incretinmimetics in the management of diabetes." Prim Care Diabetes. **2**(1): 59-61.

Barry, B. W. (2001). "Novel mechanisms and devices to enable successful transdermal drug delivery." Eur J Pharm Sci. **14**(2): 101-114.

Benson, H. A. E. and S. Namjoshi (2008). "Proteins and peptides: strategies for delivery to and across the skin." J Pharm Sci. **97**(9): 3591-3610.

Beran, J., A. Ambrozaitis, et al. (2009). "Intradermal influenza vaccination of healthy adults using a new microinjection system: A 3-year randomised controlled safety and immunogenicity trial." BMC Med. **7**(13).

Bert, J. and R. K. Reed (1998). "Hyaluronan, hydration, and flow conductivity of rat dermis." Biorheology **35**(3): 211-219.

Bjerring, P. and L. Arendt-Nielsen (1990). "Depth and duration of skin analgesia to needle insertion after topical application of EMLA cream." Br J Anaesth **64**(2): 173-177.

Bonnette, K. L., D. D. Rodabaugh, et al. (2002). Dermal irritation and sensitization. Handbook of Toxicology. M. J. Derelanko and M. A. Hollinger. Boca Raton, CRC Press**:** 127-202.

Bookbinder, L. H., A. Hofer, et al. (2006). "A recombinant human enzyme for enhanced interstitial transport of therapeutics." J Control Release. **114**(2): 230-241.

Brange, J. (1997). "The new era of biotech insulin analogues." Diabetologia **40**(Suppl 2): S48–S53.

Brazzle, J., S. Mohanty, et al. (1999). Micromachined multiple output port needle. Proceedings of the First Joint BMES/EMBS Conference Atlanta, GA.

Bremseth, D. L. and F. Pass (2001). "Delivery of insulin by jet injection: recent observations." Diabetes Technol Ther. **3**(2): 225-232.

Bronaugh, R. L., R. F. Stewart, et al. (1982). "Methods for *in-vitro* percutaneous absorption studies. II. Animal models for human skin." Toxicol Appl Pharmacol. **62**(3): 481-488.

Burnette, R. R. and J. D. DeNuzzio (1997). Impedance spectroscopy: applications to human skin. Mechanisms of Transdermal Drug Delivery. R. O. Potts and R. H. Guy. New York, Marcel Dekker 215-230.

Cefalu, W. T. (2004). "Concept, strategies, and feasibility of noninvasive insulin delivery." Diabetes Care **27**(1): 239-246.

Chabri, F., K. Bouris, et al. (2004). "Microfabricated silicon microneedles for nonviral cutaneous gene delivery." Br J Dermatol. **150**(5): 869-877.

Chapman, D. G. (2003). Parenteral products. Pharmaceutical Practice. A. J. Winfield and R. M. E. Richards. New York, Churchill Livingstone**:** 247-263.

Clark, R. A. F. (1996). The Molecular and Cellular Biology of Wound Repair. New York, Plenum.

Cormier, M., B. Johnson, et al. (2004). "Transdermal delivery of desmopressin using a coated microneedle array patch system." J Control Release **97**(3): 503-511.

Cross, S. E. and M. S. Roberts (2004). "Physical enhancement of transdermal drug application: is delivery technology keeping up with pharmaceutical development?" Curr Drug Deliv. **1**(1): 81-92.

Cummings, E. A., G. J. Reid, et al. (1996). "Prevalence and source of pain in pediatric inpatients." Pain **68**(1): 25-31.

Curdy, C., Y. N. Kalia, et al. (2000). "Recovery of human skin impedance *in-vivo* after iontophoresis: effect of metal ions." AAPS Pharm Sci **2**(3): Article 23.

Curdy, C., Y. N. Kalia, et al. (2002). "Post-iontophoresis recovery of human skin impedance *in-vivo*." Eur J Pharm Biopharm. **53**(1): 15-21.

Curdy, C., A. Naik, et al. (2004). "Non-invasive assessment of the effect of formulation excipients on stratum corneum barrier function *in-vivo*." Int J Pharm **271**(1-2): 251-256.

Davidian, M. and D. M. Giltinan (1995). Nonlinear Models for Repeated Measurement Data. Boca Raton, CRC Press.

Davis, S. P., M. R. Prausnitz, et al. (2003). Fabrication and characterization of laser micromachined hollow microneedles. TRANSDUCERS, Solid-State Sensors, Actuators and Microsystems, 12th International Conference. **2:** 1435-1438.

Deacon, B. and J. Abramowitz (2006). "Fear of needles and vasovagal reactions among phlebotomy patients." J Anxiety Disord **20**(7): 946-960.

Dean, C. H., J. B. Alarcon, et al. (2005). "Cutaneous delivery of a live, attenuated chimeric flavivirus vaccine against Japanese encephalitis (ChimeriVax)-JE) in non-human primates." Hum Vaccin. **1**(3): 106-111.

Down, J. and N. G. Harvey (2003). Minimally invasive systems for transdermal drug delivery. Transdermal Drug Delivery. R. H. Guy and J. Hadgraft. New York, Marcel Dekker**:** 327-359.

Edelberg, R. (1971). Electrical properties of the skin. Biophysical Properties of The Skin. H. R. Elden. New York, Wiley**:** 513-550.

Eichenfield, L. F., A. Funk, et al. (2002). "A clinical study to evaluate the efficacy of ELA-Max (4% liposomal lidocaine) as compared with eutectic mixture of local anesthetics cream for pain reduction of venipuncture in children." Pediatrics **109**(6): 1093-1099.

Elias, P. M. and K. R. Feingold (2006). Permeability barrier homeostasis. Skin Barrier. P. M. Elias and K. R. Feingold. New York, Taylor & Francis**:** 337-361.

Elias, P. M., J. Tsai, et al. (2002). "The potential of metabolic interventions to enhance transdermal drug delivery." J Investig Dermatol Symp Proc. **7**(1): 79-85.

Farinha, A., S. Kellogg, et al. (2006). "Skin impedance reduction for electrophysiology measurements using ultrasonic skin permeation: initial report and comparison to current methods." Biomed Instrum Technol **40**(1): 72-77.

Finnin, B. C. and T. M. Morgan (1999). "Transdermal penetration enhancers: applications, limitations, and potential." J Pharm Sci **88**(10): 955-958.

Fisher, R. J. and R. A. Peattie (2007). Controlling tissue microenvironments, biomimetics, transport phenomena, and reacting systems. Tissue Engineering II: Basics of Tissue Engineering and Tissue Applications. K. Lee and D. Kaplan. Berlin, Springer**:** 1-74.

Fluhr, J., P. Elsner, et al. (2005). Bioengineering of The Skin: Water and The Stratum Corneum. Boca Raton, CRC Press.

Fluhr, J. W. and P. M. Elias (2002). "Stratum corneum pH: formation and function of the 'Acid Mantle'." Exog Dermatol **1**(4): 163-175.

Gajraj, N. M., J. H. Pennant, et al. (1994). "Eutectic mixture of local analgesics (EMLA) cream." Anesth Analg. **78**(3): 574-583.

Gardeniers, H. J. G. E., R. Luttge, et al. (2003). "Silicon micromachined hollow microneedles for transdermal liquid transport." JMEMS **12**(6): 855-862.

Gerstel, M. S. and V. A. Place (1976). Drug Delivery Device. US 3,964,4882. United States.

Gill, H. S. (2007). Coated microneedles and microdermabrasion for transdermal drug delivery. Department of Bioengineering. Atlanta, Georgia Institute of Technology. **PhD Thesis**.

Gill, H. S., D. D. Denson, et al. (2008). "Effect of microneedle design on pain in human subjects." Clin J Pain **24**(7): 585-594.

Gill, H. S. and M. R. Prausnitz (2007). "Coated microneedles for transdermal delivery." J Control Release **117**(2): 227-237.

Grebenyuk, L. (1994). "Mechanical properties of human skin. Communication I." Human Physiology **20**(2): 157-162.

Grubauer, G., P. M. Elias, et al. (1989). "Transepidermal water loss: the signal for recovery of barrier structure and function." J Lipid Res **30**: 323-333.

Guy, R. H. (2007). "Transdermal science and technology - an update." Drug Delivery System **22**(4): 442-449.

Guy, R. H. and J. Hadgraft (2003). Transdermal Drug Delivery. New York, Marcel Dekker.

Hamilton, J. G. (1995). "Needle phobia: a neglected diagnosis." J Fam Pract. **41**(2): 169-175.

Hampton, T. (2005). "Breaking barriers in transdermal drug delivery." J Am Med Assoc. **293**(17): 2083.

Hanas, R. (2004). "Reducing injection pain in children and adolescents with diabetes: a review of indwelling catheters." Pediatric Diabetes **5**(2): 102-111.

Hanas, R. and J. Ludvigsson (1997). "Experience of pain from insulin injections and needle-phobia in young patients with IDDM." Pract Diabetes Int. **14**(4): 95-99.

Haq, M. I., E. Smith, et al. (2009). "Clinical administration of microneedles: skin puncture, pain and sensation." Biomed Microdevices **11**(1): 35-47.

Henry, S., D. V. McAllister, et al. (1998). "Microfabricated microneedles: a novel approach to transdermal drug delivery." J Pharm Sci. **87**(8): 922-925.

Hirsch, I. B. (2005). "Insulin analogues." N. Engl. J. Med. **352**(2): 174-183.

Holland, D., R. Booy, et al. (2008). "Intradermal influenza vaccine administered using a new microinjection system produces superior immunogenicity in elderly adults: a randomized controlled trial." J Infect Dis. **198**(5): 650-658.

Holmes, H. S. (1994). "Choosing a local anesthetic." Dermatol Clin. **12**(4): 817-823.

Houck, C. S. and N. F. Sethna (2005). "Transdermal analgesia with local anesthetics in children: review, update and future directions." Expert Rev. Neurother. **5**(5): 625-634.

Irion, G. (2002). Comprehensive Wound Management. Thorofare, Slack Inc.

Ito, Y., E. Hagiwara, et al. (2006). "Feasibility of microneedles for percutaneous absorption of insulin." Eur J Pharm Sci. **29**(1): 82-88.

Ito, Y., A. Murakami, et al. (2008). "Evaluation of self-dissolving needles containing low molecular weight heparin (LMWH) in rats." Int J Pharm. **349**(1-2): 124-129.

Ito, Y., Y. Ohashi, et al. (2008). "Antihyperglycemic effect of insulin from self-dissolving micropiles in dogs." Chem. Pharm. Bull. **56**(3): 243-246.

Ito, Y., J. Yoshimitsu, et al. (2006). "Self-dissolving microneedles for the percutaneous absorption of EPO in mice." J Drug Target. **14**(5): 255-261.

Iyer, S. S., W. H. Barr, et al. (2007). "A 'biorelevant' system to investigate *in-vitro* drug released from a naltrexone implant." Int J Pharm. **340**(1-2): 104-118.

Jackson, T. L., A. Hussain, et al. (2006). "Human scleral hydraulic conductivity: age-related changes, topographical variation, and potential scleral outflow facility." Invest Ophthalmol Vis Sci. **47**(11): 4942–4946.

Jiang, J., H. S. Gill, et al. (2007). "Coated microneedles for drug delivery to the eye." Invest Ophthalmol Vis Sci. **48**(9): 4038-4043.

Jiang, J., J. Moore, et al. (2009). "Intrascleral drug delivery to the eye using hollow microneedles." Pharm Res. **26**(2): 395-403.

Kalia, Y. N., L. B. Nonato, et al. (1996). "The effect of iontophoresis on skin barrier integrity: non-invasive evaluation by impedance spectroscopy and transepidermal water loss." Pharm Res. **13**(6): 957-960.

Kandel, E. R., J. H. Schwartz, et al. (2000). Principles of Neural Science. New York, McGraw Hill.

Karande, P., A. Jain, et al. (2005). "Relationships between skin's electrical impedance and permeability in the presence of chemical enhancers." J Control Release **110**(2): 307-313.

Karande, P., A. Jain, et al. (2006). "Insights into synergistic interactions in binary mixtures of chemical permeation enhancers for transdermal drug delivery." J control Release. **110**(2): 307-313.

Katz, N. P., D. E. Shapiro, et al. (2004). "Rapid onset of cutaneous anesthesia with EMLA cream after pretreatment with a new ultrasound-emitting device." Anesth Analg. **98**(2): 371-376.

Kaushik, S., A. H. Hord, et al. (2001). "Lack of pain associated with microfabricated microneedles." Anesth Analg. **92**(2): 502-504.

Kelly, A.-M. (1998). "Does the clinically significant difference in visual analog scale pain scores vary with gender, age, or cause of pain?" Acad Emerg Med **5**(11): 1086-1090.

Kiernan, J. A. and M. L. Barr (2008). Barr's the Human Nervous System. Philadelphia, Lippincott, Williams, and Wilkins.

King, A. C., J. R. Volpicelli, et al. (1997). "Naltrexone biotransformation and incidence of subjective side effects: a preliminary study." Alcohol Clin Exp Res. **21**(5): 906-909.

Kiptoo, P. K., M. O. Hamad, et al. (2006). "Enhancement of transdermal delivery of 6-beta-naltrexol via a codrug linked to hydroxybupropion." J Control Release. **113**(2): 137-145.

Kleiber, C., M. Sorenson, et al. (2002). "Topical anesthetics for intravenous insertion in children: a randomized equivalency study." Pediatrics **110**(4): 758-761.

Kost, J., S. Mitragotri, et al. (2000). "Transdermal monitoring of glucose and other analytes using ultrasound." Nat. Med. **6**(3): 347-350.

Koutsonanos, D. G., M. del Pilar Martin, et al. (2009). "Transdermal influenza immunization with vaccine-coated microneedle arrays." PLoS One **4**(3): e4773.

Lackermeier, A., H., E. T. McAdams, et al. (1999). "*In-vivo* ac impedance spectroscopy of human skin: theory and problems in monitoring of passive percutaneous drug delivery." Ann NY Acad Sci. **873**: 197-213.

Lander, J., M. Hodgins, et al. (1996). "Determinants of success and failure of EMLA." Pain **64**(1): 89-97.

Laurent, P. E., S. Bonnet, et al. (2007). "Evaluation of the clinical performance of a new intradermal vaccine administration technique and associated delivery system." Vaccine **25**(52): 8833-8842.

Lawler, J. C., M. J. Davis, et al. (1960). "Electrical characteristics of the skin. The impedance of the surface sheath and deep tissues." J Invest Dermatol. **34**: 301-308.

Lawrence, P. F., R. M. Bell, et al. (2006). Essentials of Surgical Specialties Philadelphia, Lippincott Williams & Wilkins.

Lee, J. W., J.-H. Park, et al. (2008). "Dissolving microneedles for transdermal drug delivery." Biomaterials **29**(13): 2113-2124.

Levick, J. R. (1987). "Flow through interstitium and other fibrous matrices." Q J Exp Physiol. **72**(4): 409-438.

Levin, J. and H. I. Maibach (2005). "The correlation between transepidermal water loss and percutaneous absorption: an overview." J Control Release **103**(2): 291-299.

Licko, V. (1980). Research Monograph 28. Rockville, National Institute on Drug Abuse.

Lin, W., M. Cormier, et al. (2001). "Transdermal delivery of antisense oligonucleotides with microprojection patch (Macroflux) technology." Pharm Res **18**(12): 1789-1793.

Lynn, P. and P. Evans-Smith (2003). Lippincott's Photo Atlas of Medication Administration. Philadelphia, Lippincott Williams & Wilkins.

Lysakowski, C., L. Dumont, et al. (2003). "A needle-free jet-injection system with lidocaine for peripheral intravenous cannula insertion: a randomized controlled trial with cost-effectiveness analysis." Anesth Analg. **96**(1): 215-219.

Martanto, W., S. P. Davis, et al. (2004). "Transdermal delivery of insulin using microneedles *in-vivo*." Pharm Res **21**(6): 947-952.

Martanto, W., J. S. Moore, et al. (2006a). "Mechanism of fluid infusion during microneedle insertion and retraction." J Control Release **112**(3): 357-361.

Martanto, W., J. S. Moore, et al. (2006b). "Microinfusion using hollow microneedles." Pharm Res **23**(1): 104-113.

Matriano, J. A., M. Cormier, et al. (2002). "Macroflux microprojection array patch technology: a new and efficient approach for intracutaneous immunization." Pharm Res **19**(1): 63-70.

McAllister, D. V., P. M. Wang, et al. (2003). "Microfabricated needles for transdermal delivery of macromolecules and nanoparticles: fabrication methods and transport studies." Proc Natl Acad Sci USA **100**(24): 13755-13760.

Menon, G. K., K. R. Feingold, et al. (1992). "Lamellar body secretory response to barrier disruption." J Invest Dermatol. **98**(3): 279-289.

Migdal, M., E. Chudzynska-Pomianowska, et al. (2005). "Rapid, needle-free delivery of lidocaine for reducing the pain of venipuncture among pediatric subjects." Pediatrics **115**(4): e393-e398.

Mikszta, J., J. Alarcon, et al. (2002). "Improved genetic immunization via micromechanical disruption of skin-barrier function and targeted epidermal delivery." Nat Med **8**(4): 415-419.

Mikszta, J. and P. E. Laurent (2008). "Cutaneous delivery of prophylactic and therapeutic vaccines: historical perspective and future outlook." Expert Rev. Vaccines **7**(9): 1329-1339.

Mikszta, J. A., J. P. Dekker, et al. (2006). "Microneedle-based intradermal delivery of the anthrax recombinant protective antigen vaccine." Infect Immun **7**(12): 6806–6810.

Mikszta, J. A., M. I. Haider, et al. (2006). Microneedles for drug and vaccine delivery: when will the dream become a reality? Skin Delivery Systems: Transdermals, Dermatologicals, and Cosmetic Actives. J. J. Wille. Ames, Wiley-Blackwell**:** 309-325.

Mikszta, J. A., V. J. Sullivan, et al. (2005). "Protective immunization against inhalational anthrax: a comparison of minimally invasive delivery platforms." J Infect Dis **191**(2): 278-288.

Mitragotri, S. and J. Kost (2000). "Low-frequency sonophoresis: a noninvasive method of drug delivery and diagnostics." Biotechnol. Prog. **16**(3): 488-492.

Mitragotri, S. and J. Kost (2004). "Low-frequency sonophoresis: a review." Adv Drug Deliv Rev. **56**(5): 589-601.

Miyano, T., Y. Tobinaga, et al. (2005). "Sugar micro needles as transdermic drug delivery system." Biomed Microdevices **7**(3): 185-188.

Mollema, E. D., F. J. Snoek, et al. (2001). "Phobia of self-injecting and self-testing in insulin-treated diabetes patients: opportunities for screening." Diabet Med. **18**(8): 671-674.

Monteiro-Riviere, N. A. (1991). Comparative anatomy, physiology, and biochemistry of mammalian skin. Dermal and Ocular Toxicology: Fundamentals and Methods D. W. Hobson. Boca Raton, CRC Press.

Nair, V., O. Pillai, et al. (1999). "Transdermal iontophoresis. Part I: basic principles and considerations." Methods Find Exp Clin Pharmacol. **21**(2): 139-151.

Nir, Y., A. Paz, et al. (2003). "Fear of injections in young adults: prevalence and associations." Am J Trop Med Hyg. **68**(3): 341-344.

Nordquist, L., N. Roxhed, et al. (2007). "Novel microneedle patches for active insulin delivery are efficient in maintaining glycaemic control: an initial comparison with subcutaneous administration." Pharm Res. **24**(7): 1381-1388.

Oh, J.-H., H.-H. Park, et al. (2008). "Influence of the delivery systems using a microneedle array on the permeation of a hydrophilic molecule, calcein." Eur J Pharm Biopharm. **69**(3): 1040-1045.

Padmanabhan, R., J. B. Phipps, et al. (2008). ALZA transdermal drug delivery technologies. Modified-Release Drug Delivery Technology. M. J. Rathbone, J. Hadgraft, M. S. Roberts and M. E. Lane. New York, Informa Healthcare.

Pagliaro, L. A. and A. M. Pagliaro (1998). Psychologists' Psychotropic Drug Reference. Philadelphia, Brunner/Mazel.

Palastanga, N., D. Field, et al. (2006). Anatomy and Human Movement. London, Elsevier.

Park EJ, Werner J, et al. (2007). "Ultrasound mediated transdermal insulin delivery in pigs using a lightweight transducer." Pharm Res **24**(7): 1396-1401.

Park, J. H., M. G. Allen, et al. (2005). "Biodegradable polymer microneedles: fabrication, mechanics and transdermal drug delivery." J Control Release **104**(1): 51-66.

Park, J. H., M. G. Allen, et al. (2006). "Polymer microneedles for controlled-release drug delivery." Pharm Res **23**(5): 1008-1018.

Pettis, R. J., N. G. Harvey, et al. (2002). Method for Altering Drug Pharmacokinetics Based on Medical Delivery Platform. US 2002/0095134 A1. United States.

Pillai, O., V. Nair, et al. (1999). "Transdermal iontophoresis. Part II: peptide and protein delivery." Methods Find Exp Clin Pharmacol. **21**(3): 229-240.

Pliquett, U. and M. R. Prausnitz (2000). Electrical impedance spectroscopy for rapid and non-invasive analysis of skin electroporation. Electrochemotherapy, Electrogenetherapy, and Transdermal Drug Delivery. M. J. Jaroszeski, R. Heller and R. Gilbert. Totowa, Humana Press**:** 377-406.

Prausnitz, M. R. (2001). "Overcoming skin's barrier: the search for effective and user-friendly drug delivery." Diabetes Technol Ther. **3**(2): 233-236.

Prausnitz, M. R. (2004). "Microneedles for transdermal drug delivery." Adv Drug Deliv Rev. **56**(5): 581-587.

Prausnitz, M. R. (2005). Assessment of microneedles for transdermal drug delivery. Percutaneous Absorption: Drugs-Cosmetics-Mechanisms-Methodology. R. L. Bronaugh and H. I. Maibach. Boca Raton, Taylor & Francis.

Prausnitz, M. R., E. R. Edelman, et al. (1995). "Transdermal delivery of heparin by skin electroporation." Biotechnology (N Y) **13**(11): 1205-1209.

Prausnitz, M. R., H. S. Gill, et al. (2008). Microneedles for drug delivery. Modified Release Drug Delivery M. J. Rathbone, J. Hadgraft, J. S. Roberts and M. E. Lane. New York, Informa Healthcare**:** 295-309.

Prausnitz, M. R. and R. Langer (2008). "Trandermal drug delivery." Nat Biotech **26**(11): 1261-1268.

Prausnitz, M. R., J. A. Mikszta, et al. (2006). Microneedles. Percutaneous Penetration Enhancers. H. I. Maibach and E. W. Smith. Boac Raton, CRC Press**:** 239-256.

Prausnitz, M. R., S. Mitragotri, et al. (2004). "Current status and future potential of transdermal drug delivery." Nat Rev Drug Discov **3**(2): 115-124.

Proksch, E., K. R. Feingold, et al. (1991). "Barrier function regulates epidermal DNA synthesis." J Clin Invest. **87**(5): 1668-1673.

Reed, M. L. and W.-K. Lye (2004). "Microsystems for drug and gene delivery." Proc IEEE **92**(1): 56-75.

Roberts, M. S. and Y. G. Anissimov (2005). Mathematical models in percutaneous absorption. Percutaneous Absorption: Drugs-Cosmetics-Mechanisms-Methodology. R. L. Bronaugh and H. I. Maibach. Boca Raton, Taylor & Francis**:** 878.

Rook, A., T. Burns, et al. (2004). Rook's Textbook of Dermatology. Malden, Blackwell Publishing.

Schaefer, H. and T. E. Redelmeier (1996). Skin Barrier: Principles of Percutaneous Absorption. Basel, Karger.

Seehra, G. P. and F. H. Silver (2006). "Viscoelastic properties of acid- and alkaline-treated human dermis: a correlation between total surface charge and elastic modulus." Skin Res Technol. **12**(3): 190-198.

Sivamani, R. K., B. Stoeber, et al. (2005). "Clinical microneedle injection of methyl nicotinate: stratum corneum penetration." Skin Res Technol **11**(2): 152-156.

Smith, A. and E. Tomlinson (2008). The passport system: a new transdermal patch for water-soluble drugs, proteins, and carbohydrates. Modified Release Drug Delivery M. J. Rathbone, J. Hadgraft, J. S. Roberts and M. E. Lane. New York, Informa Healthcare**:** 417-425.

Springhouse (2005). Portable LPN: The All-in-One Reference for Practical Nurses. Philadelphia, Lippincott Williams & Wilkins.

Stoeber, B. and D. Liepmann (2000a). Two-dimensional arrays of out-of-plane needles. Proceedings from The 2000 International Mechanical Engineering Congress & Exposition. Orlando, FL. **2:** 355-359.

Stoeber, B. and D. Liepmann (2000b). Fluid injection through out-of-plane microneedles. Microtechnologies in Medicine and Biology, 1st Annual International Conference. Lyon, France, IEEE**:** 224-228.

Sullivan, S. P., N. Murthy, et al. (2008). "Minimally invasive protein delivery with rapidly dissolving polymer microneedles." Adv. Mater. **20**(5): 933-938.

Swarbrick, J. and J. C. Boylan, Eds. (2002). Encyclopedia of Pharmaceutical Technology. New York, Marcel Dekker.

Swartz, M. A. and M. E. Fleury (2007). "Interstitial flow and its effects in soft tissues." Annu. Rev. Biomed. Eng. **9**: 229-256.

Tang, H., S. Mitragotri, et al. (2001). "Theoretical description of transdermal transport of hydrophilic permeants: application to low-frequency sonophoresis." J Pharm Sci **90**(5): 545-568.

Teo, M. A. L., C. Shearwood, et al. (2005). "*In-vitro* and *in-vivo* characterization of MEMS microneedles." Biomed Microdevices. **7**(1): 47-52.

Tezel, A., S. Paliwal, et al. (2005). "Low-frequency ultrasound as a transcutaneous immunization adjuvant." Vaccine **23**(29): 3800-3807

Tezel, A., A. Sens, et al. (2003). "Description of transdermal transport of hydrophilic solutes during low-frequency sonophoresis based on a modified porous pathway model." J Pharm Sci **92**(2): 381-393.

Todd, K. H., K. G. Funk, et al. (1996). "Clinical significance of reported changes in pain severity." Ann Emerg Med. **27**(4): 485-489.

Trajanoskil, Z., L. Schaupp, et al. (1996). Interstitial fluid sampling using open flow microperfusion of subcutaneous adipose tissue. 18th Annual International Conference of the IEEE: Engineering in Medicine and Biology Society. Amsterdam, Netherlands. **1:** 87-88.

Turncliff, R. Z., J. L. Dunbar, et al. (2005). "Pharmacokinetics of long-acting naltrexone in subjects with mild to moderate hepatic impairment." J Clin Pharmacol. **45**(11): 1259-1267.

Tyagi, P. (2002). "Insulin delivery system: present trends and the future direction." Indian J. Pharmacol. **34**(6): 379-389.

Vaddi, H. K., M. O. Hamad, et al. (2005). "Human skin permeation of branched-chain 3–O-alkyl ester and carbonate prodrugs of naltrexone." Pharm Res. **22**(5): 758-765.

Valiveti, S., B. N. Nalluri, et al. (2004). "Development and validation of a liquid chromatography-mass spectrometry method for the quantitation of naltrexone and 6beta-naltrexol in guinea pig plasma." J Chromatogr B Analyt Technol Biomed Life Sci. **810**(2): 259-267.

Van Damme, P., F. Oosterhuis-Kafeja, et al. (2009). "Safety and efficacy of a novel microneedle device for dose sparing intradermal influenza vaccination in healthy adults." Vaccine **27**(3): 454-459.

Verebey, K., J. Volavka, et al. (1976). "Naltrexone: disposition, metabolism, and effects after acute and chronic dosing." Clin Pharmacol Ther. **20**(3): 315-328.

Wall, M. E., D. R. Brine, et al. (1981). "Naltrexone disposition in man after subcutaneous administration. ." Drug Metab Dispos. **9**(4): 369–375.

Wallace, M. S., B. Ridgeway, et al. (2001). "Topical delivery of lidocaine in healthy volunteers by electroporation, electroincorporation, or iontophoresis: An evaluation of skin anesthesia." Reg Anesth Pain Med. **26**(3): 229-238.

Wang, P. M., M. Cornwell, et al. (2006). "Precise microinjection into skin using hollow microneedles." J Invest Dermatol. **126**(5): 1080–1087.

Wang, P. M., M. Cornwell, et al. (2005). "Minimally invasive extraction of dermal interstitial fluid for glucose monitoring using microneedles." Diabetes Technol Ther. **7**(1): 131-141

Warner, R. R., Y. L. Boissy, et al. (1999). "Water disrupts stratum corenum lipid lamellae: damage is similar to surfactants." J Invest Dermatol. **113**(6): 960-966.

Warrell, D. A., T. M. Cox, et al., Eds. (2005). Oxford Textbook of Medicine. Oxford, Oxford University Press.

Washington, N., C. Washington, et al. (2001). Physiological Pharmaceutics: Barriers to Drug Absorption New York, Taylor and Francis.

Webb, K. E. (2006). "Use of insulin pumps for diabetes management." Medsurg Nursing **15**(2): 61-94.

Wermeling, D. P., S. L. Banks, et al. (2008). "Microneedles permit transdermal delivery of a skin-impermeant medication to humans." Proc Natl Acad Sci USA **105**(6): 2058-2063.

Wertz, P. W. and B. B. Michniak (2004). Hydration and lipids. Bioengineering of The Skin : Water and Stratum Corneum. J. W. Fluhr, P. Elsner, E. Berardesca and H. I. Maibach. Boca Raton, CRC Press**:** 359-368.

Widera, G., J. Johnson, et al. (2006). "Effect of delivery parameters on immunization to ovalbumin following intracutaneous administration by a coated microneedle array patch system." Vaccine **24**(10): 1653-1664.

Williams, A. C. (2003). Transdermal and Topical Drug Delivery: From Theory To Clinical Practice. London, Pharmaceutical Press.

Williams, A. C. and B. W. Barry (2004). "Penetration enhancers." Adv Drug Deliv Rev. **56**(5): 603-618.

Wong, D. L. and B. C.M. (1988). "Pain in children: comparison of assessment scales." Pediatr Nurs **14**(1): 9-17.

Wu, J., J. Chappelow, et al. (1998). "Defects generated in human stratum corneum specimens by ultrasound." Ultrasound Med Biol. **24**(5): 705-710.

Xie, Y., B. Xu, et al. (2005). "Controlled transdermal delivery of model drug compounds by MEMS microneedle array." Nanomedicine **1**(2): 184-190.

Yamamoto, T. and Y. Yamamoto (1976a). "Electrical properties of the epidermal stratum corneum." Med Biol Eng. **14**(2): 151-158.

Yamamoto, T. and Y. Yamamoto (1976b). "Dielectric constant and resistivity of epidermal stratum corneum." Med Biol Eng. **14**(5): 494-500.

Young, K. D. (2007). "What's new in topical anesthesia." Clin Ped Emerg Med **8**(4): 232-239.

Zambanini, A., R. B. Newson, et al. (1999). "Injection related anxiety in insulin-treated diabetes " Diabetes Res Clin Pract **46**(3): 239-246

Zempsky, W. T. (2008). Iontophoresis for local anesthesia. Anesthesia and Analgesia in Dermatologic Surgery. M. Harahap and A. R. Abadir. New York, Informa**:** 163-170.

Zempsky, W. T. (2008). "Pharmacologic approaches for reducing venous access pain in children." Pediatrics **122**(Supplement 3): S140-S153.

Zempsky, W. T., K. J. S. Anand, et al. (1998). "Lidocaine iontophoresis for topical anesthesia before intravenous line placement in children." J Pediatr. **132**(6): 1061-1063.

Zempsky, W. T., J. Sullivan, et al. (2004). "Evaluation of a low-dose lidocaine iontophoresis system for topical anesthesia in adults and children: a randomized, controlled trial." Clin Ther. **26**(7): 1110-1119.

Zhu, Q., V. G. Zarnitsyn, et al. (2009). "Immunization by vaccine-coated microneedle arrays protects against lethal influenza virus challenge." Proc Natl Acad Sci USA **106**(19): 7968-7973.